Doctoral Dissertation

Molecular Design of High-performance Polymers Using Unique Cinnamoyl Dimers

Takumi Noda

Supervisor: Tatsuo Kaneko

Graduate School of Advanced Science and Technology

Japan Advanced Institute of Science and Technology

[Materials Science]

March 2022

Abstract

For upcoming the sustainable society, the development of high-performance/functional biobased polymer materials has attracted interest from researchers. Cinnamoyl photodimers, which are derived from cinnamic acids by photo-assisted [2+2] cycloaddition, have high potentials to be used as monomers for the high-performance/functional polymers due to structural characteristics such as rigid structure, unique bending angles, chirality, and photodegradable cyclobutane. However, though cinnamoyl dimers have many interesting properties, only a few cinnamoyl dimer-based polymers were reported and the effects of cinnamoyl dimer moiety on the corresponding properties of polymers are not clear enough. In this thesis, the author describes effects of cinnamoyl dimer unit in polymer backbone on polymer properties through the developments of high-performance/functional polymers from unique cinnamoyl dimers.

This thesis is composed of following five chapters:

Chapter 1 describes the background and objectives of this research.

Chapter 2 describes the synthesis of mussel-mimetic photodegradable adhesive materials from 3,4-dihydroxycinnamoyl dimer (34THTA). The 34THTA was synthesized from 3,4-dihydroxycinnamate by solid-state photodimerization and then was polymerized to synthesize polyamides bearing adhesive catechol groups in the side chain. As a result, obtained copolyamide exhibited good adhesive properties of ~7 MPa for stainless steel substrate. In addition, the cyclobutanes in polymer backbone were cleaved by ultraviolet light irradiation. The results described in this chapter provide insights into the molecular design of eco-friendly, high-performance adhesive materials with photodegradability.

Chapter 3 describes the selective synthesis and polymerization of *β*-, and *δ*-type 4-aminocinnamoyl photodimers. In the solid-state photodimerization of 4-aminocinnamic acid derivatives, selective synthesis of each isomeric dimers was achieved by controlling molecular arrangements in the crystal. Density functional theory (DFT) calculations revealed that the *β*- and *δ*-type photodimers possessed unique bending angles of 70° and 101°, respectively. In addition, each obtained dimers were modified to diamine and dicarboxylic acid monomers then was used for the synthesis of polyamides. The present study provides a synthetic method for isomeric 4-aminocinnamoyl dimers, which have potential for high-performance and/or functional polymers based on the unique cinnamoyl dimer skeleton.

Chapter 4 describes the synthesis of soluble biobased polyimides from isomeric 4-aminocinnamoyl photodimer-based diamines with unique bending angles. The *β*-, and *δ*-type diamines, which were synthesized in chapter 3, were polymerized with tetracarboxylic acid dianhydrides to produce soluble polyimides. As a result, *δ*-type dimer-based polyimides exhibited high thermostability and good solubility in organic solvents such as chloroform owing to its rigid and bending structure. The results described in this chapter showed the diamine with an angle of 101°, similar to *δ*-type, had a suitable structure to provide solubility to the obtained polyimides. The present study provides insights into the molecular design of high-performance soluble polymers by focusing on the bending angles of the polymer chains.

Chapter 5 summarizes the syntheses and evaluation of high-performance/functional polymers using unique cinnamoyl dimers as the overall conclusions of this thesis. This research is mainly focused on the effects of cyclobutane rings in polymer backbone. since the cyclobutane rings are easily obtained by [2+2] cycloaddition of olefins, the obtained insights would be possible to expand other polymer systems including olefin structures.

Keywords: Biobased polymers, Polyamide, Polyimide, Cinnamic acid, Photodimerization, Cyclobutane.

Acknowledgement

The study presented in this dissertation has been performed under the direction of *Professor Tatsuo Kaneko*, Japan Advanced Institute of Science and Technology (JAIST), from 2019 to 2022. The author would like to express his deepest gratitude to his supervisor *Professor Tatsuo Kaneko* for his supervision, valuable guidance, kind encouragement, and support during this work.

The author would like to extend his appreciation to the committee members of this dissertation: his second supervisor *Professor Toshiaki Taniike*, *Professor Kazuaki Matsumura*, *Professor Kenzo Fujimoto* at JAIST and *Professor Tomoki Ogoshi* from Kyoto University.

The author is deeply grateful to *Assistant Professor Kenji Takada* for his excellent guidance and kind encouragement. This work would never have performed without his great supporting. In addition, the author would like to express his appreciation to *Dr. Hongrong Yin* for his valuable suggestion.

The author thanks all of members of Kaneko laboratory. In addition, the author would like to give his special thanks to *Takuma Iwasaki* and *Takumi Sato* for their contributions to this dissertation work.

The author is also grateful to the "JST SPRING, Grant Number JPMJSP2102" during 2021-2022.

Finally, the author would like to express his deep gratitude to his family for their understanding, support, and encouragement throughout his study in JAIST.

March 2022

Takumi Noda

Contents

Chapter 1

General Introduction

1.1 Biobased Polymers

In modern society, many kinds of polymer materials are used for our life. With the modernization and economic development, the mass production of the plastic materials is increasing year by year. In 2015, the mass production of polymer materials was estimated ~380 metric tons.[1] In addition, more than 99% of these polymers are produced from petroleum resources.[2]

For upcoming the sustainable society, Sustainable Development Goals (SDGs) was adopted by all member states of the United Nations in 2015. Biobased polymers, which are produced from biomass resources such as plants, animals, and microorganism-metabolized materials, are considered to one of the effective approaches to achieve these goals.[3,4] Biobased polymers can be divide three classifications;[5] (a) polymers which are directly obtained from nature, such as cellulose, chitin, collagen, and lignin. (b) polymers which are produced by microbial fermentation, such as polyhydroxybutyrate, and polyhydrxyalkanoate, and (c) polymers which are synthetically produced from biobased monomers, such as poly(lactic acid). Numerous studies regarding to these polymers have been conducted.[6–12] Hence, the development of biobased polymer materials has attracted interest from researchers in polymer chemistry field, as well as industrial fields in recent years (Figure 1-1).

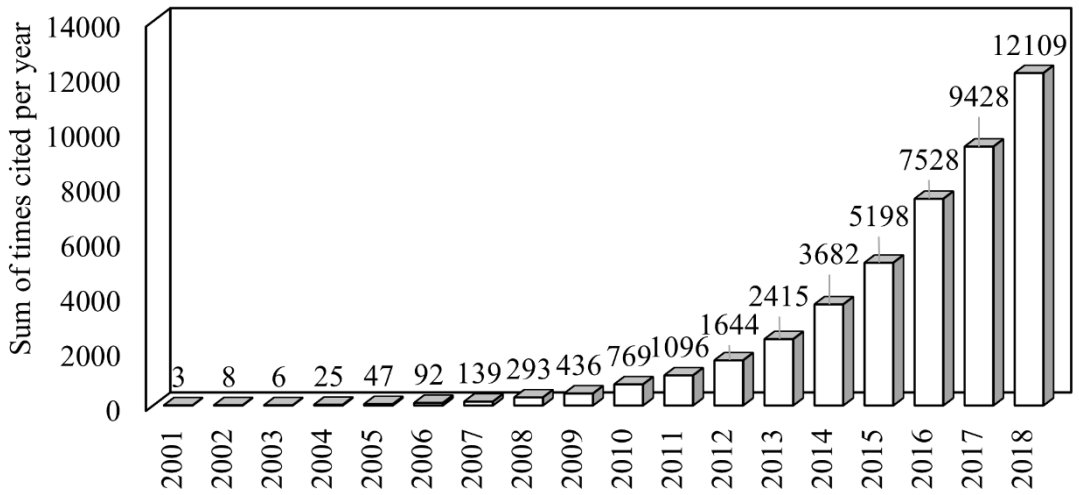

Figure 1-1. Citation number of publications about biobased polymer in recent years.[13]

1.2 Synthetic Biobased polymers

To expand applications of biobased polymers for various fields, control of physicochemical properties is required. In the case of naturally occurred biobased polymers and their modified derivatives, these materials have a limit for controlling their properties because their basic chemical structure cannot be changed significantly. On the other hand, synthetic biobased polymers have an advantage that the molecular structure can be designed in monomer unit, indicating that polymer materials with desired properties can be tailored. Therefore, numerous studies regarding to synthetic biobased polymers including conventional biobased polymers such as poly(lactic acid),[14,15] poly(butylene succinate),[16,17] and poly(trimethylene terephthalate),[18,19] have been widely investigated (Figure 1-2). With a growing interest in biobased polymers, researchers also

focus on not only polymer syntheses but also monomer syntheses from biomass resources to develop novel biobased polymers.[20,21] In recent years, high-performance biobased polymers such as polybenzimidazoles,[22] and poly(ether ketone)s[23] are developed from aromatic biobased monomers. These polymers exhibited excellent physical properties compared to common high-performance polymers derived from petroleum resources. Thus, development of novel biobased polymers and their precursors is important tasks for upcoming sustainable society.

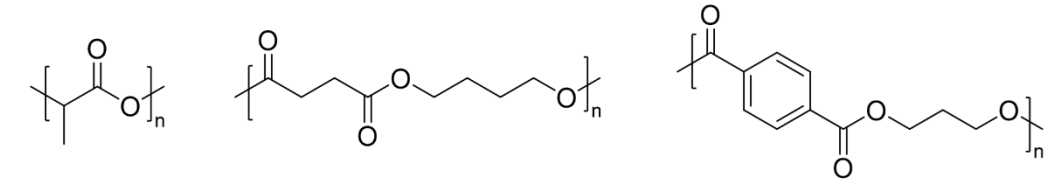

poly(lactic acid) poly(butylene succinate) poly(trimethylene terephthalate)

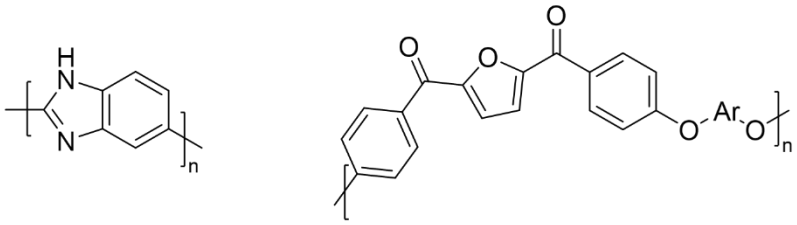

polybenzimidazoles poly(ether ketone)s

Figure 1-2. Molecular structures of typical conventional synthetic biobased polymers and recently developed high-performance biobased polymers.

1.3 Cinnamic Acids

Cinnamic acids, which are widely found in plants, are well known as one of the phenylpropanoids. Naturally occurring cinnamic acids are produced from *L*-phenylalanine catalyzed by *L*-phenylalanine ammonia-lyase[24]. In recent years, these cinnamic acids and their derivatives have been used in various field such as cosmetics,[25,26] medicines,[27,28] flavors,[29] food additives,[30,31] and intermediate of organic syntheses (Figure 1-3).[32,33] Several kinds of cinnamic acids can be produced from renewable resources by synthetical and/or biological approaches. For example, 4-hydroxy-3-methoxycinnamic acid is industrially produced by hydrolysis of *γ*-oryzanol from rice bran.[34] 3,4-Dihydroxycinnamic acid can be obtained from plant resources such as kraft pulp and sweet potato by microbial fermentation.[35,36] Thus, cinnamic acids have been attracted interest as one of the useful materials from biomass resources for upcoming sustainable society.

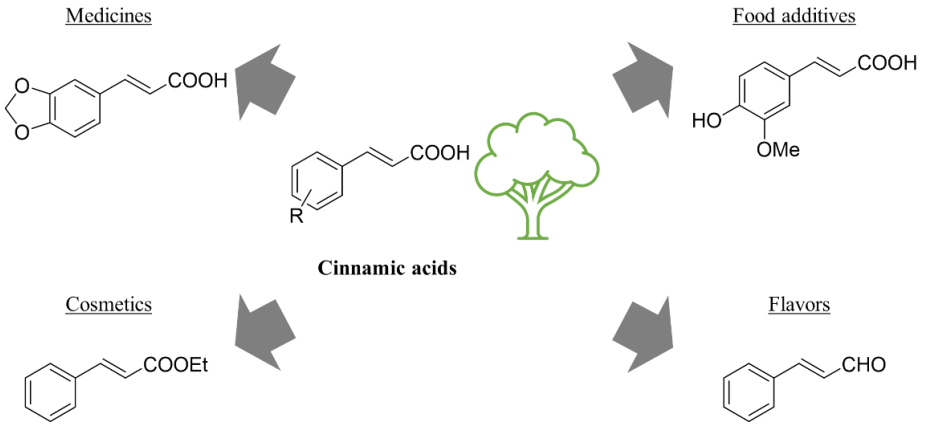

Figure 1-3. Typical applications of cinnamic acids and their derivatives.

1.3.1 Photoreactions of Cinnamic Acids

Cinnamic acids show photoreactivity since these compounds have photoreactive double bond in molecular structure. When the light with specific wavelength for photoreaction is irradiated to cinnamic acids, two kinds of photoreactions can be occurred: *cis-trans* isomerization and photodimerization.

Cis-trans isomerization:

Cis-trans isomerization of olefin compounds is well known as one of the important photoreactions. Numerous studies regarding to *cis-trans* isomerization of olefin compounds such as azobenzenes, and stilbenes have been conducted.[37–39] Since cinnamic acids have 1,2-disubstituted olefin structure, they can also exist in two kinds of geometric isomers, *cis*- and *trans*- isomers. [40] The *cis-trans* isomerization, that is torsion around the double bond, is proceeded via excited state which is caused by light irradiation with corresponding wavelength (Scheme 1-1).[41]

Scheme 1-1. *Cis-trans* Isomerization of Cinnamic Acid

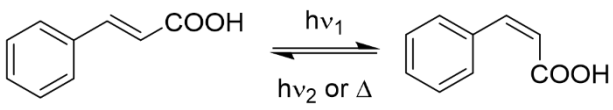

trans-type *cis*-type

Photodimerization:

From the first found in 1877, photo-induced [2+2] cycloaddition of olefin compounds have been widely studied by researchers over a century.[42–45] This reaction is proceeded by addition of olefin molecules in excited state which was generated by photo irradiation, to other olefin molecules (Scheme 1-2).[42] Cinnamic acids can also undergo dimerization by photo irradiation and afford two kinds of cinnamoyl photodimers, truxillic acids and truxinic acids[46] (Figure 1-4a). There are eleven isomers in the products of photodimerization of cinnamic acids (Figure 1-4b).[47] In nature, cinnamoyl photodimers are also existed in plants. For example, several kinds of isomeric truxillines which are produced by sunlight-assisted [2+2] cycloaddition of *cis*- and/or *trans*- cinnamoyl cocaine in plant tissues, are found in *Erythroxylum* species.[47–49] To synthesize such isomeric cinnamoyl photodimers under laboratory conditions, ultraviolet light-assisted [2+2] cycloaddition of cinnamic acid derivatives including nature-derived cinnamic acids such as cinnamic acid, 4-hydroxycinnamic acid, 4-hydroxy-3-methoxycinnamic acid, and 3,5-dimethoxy-4-hydroxycinnamic acid derivatives, have been widely conducted.[50–52] Synthetic methods of cinnamoyl photodimers can be mainly divided into two types: solution photodimerization and solid-state photodimerization.

Scheme 1-2. Formation of Olefin Photodimers via Excited State by Photo-induced Dimerization.

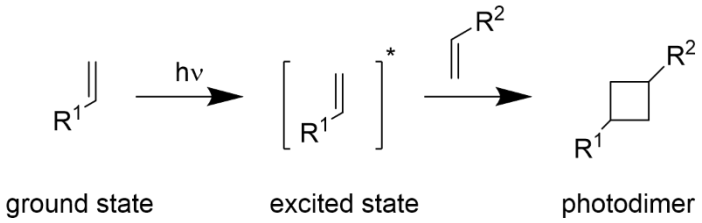

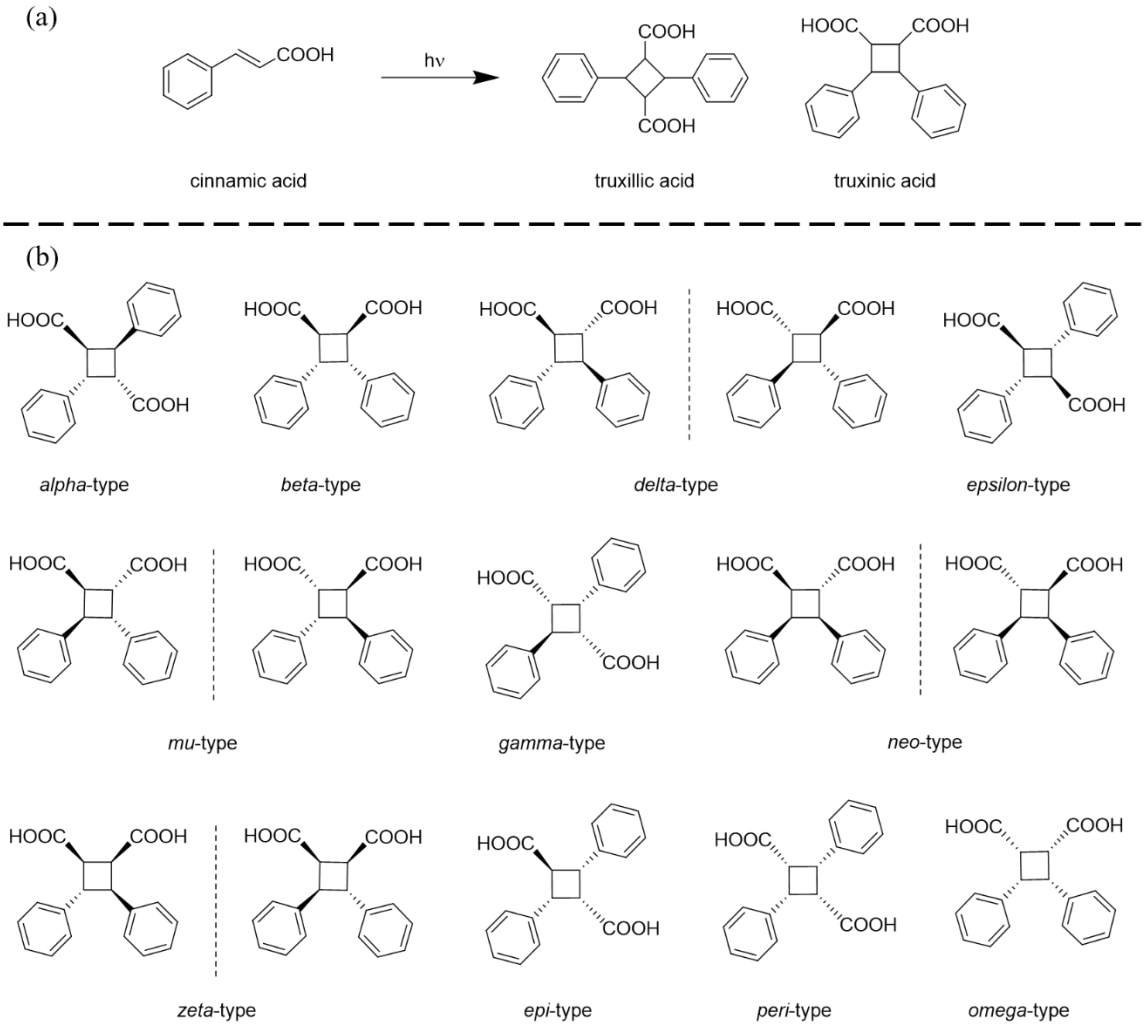

Figure 1-4. (a) Photodimerization of cinnamic acid and (b) molecular structure of isomeric cinnamoyl photodimes.

For photodimerization, two double bonds of adjacent cinnamic acid molecules in excited and ground state need to be close. In the solution photodimerization method, the photodimerization afford mixture of isomeric photodimers because cinnamic acid molecules have free movement in solution. To selectively synthesize certain isomer by solution photodimerization method, numerous studies have been conducted. One of the strategies to selectively synthesize isomeric photodimers in solution is restricting of molecular mobility and assisting molecular assemble by addition of salts,[53] host molecules,[54–56] or metal species[57] to form complexes (Figure 1-5). However, selective synthesis of photodimers by solution photodimerization method is difficult because undesired isomers and *cis*-cinnamic acids can be formed simultaneously as minor product.

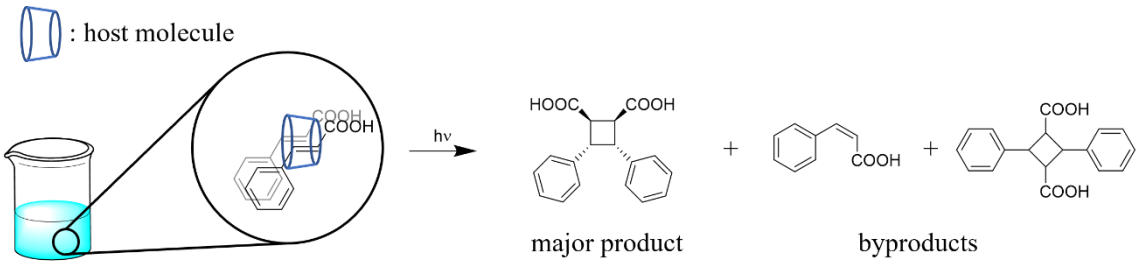

Figure 1-5. Typical examples of selective synthesis of cinnamoyl photodimers by solution photodimerization method.

On the other hand, solid-state photodimerization method is well known as one of the topochemical reactions, and only afford specific product. The structure of products depends on the arrangement of cinnamic acid molecules in the crystals since the photoreaction in crystalline state proceed with minimal molecular movement[58–60] (Figure 1-6). To proceed solid-state photodimerization, two double bonds of cinnamic acid molecules in the crystals need to be close. Schmidt and co-workers have widely studied solid-state photodimerization and found that the distance between two double bonds was closer within 4.2 Å to occur photodimerization,[58,59] Hence, solid-state photodimerization method is prefer to selective synthesis of cinnamyl dimers. To selectively synthesize isomeric photodimers, numerous studies regarding to method for controlling molecular packing in the crystals have been reported.[46,56,61,62]

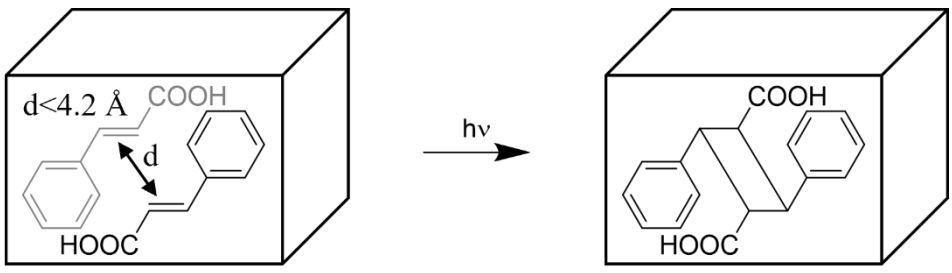

Figure 1-6. Schematic illustration of solid-state photodimerization of cinnamic acid.

1.3.2 Structural Characteristics of Cinnamoyl Dimers for High-performance/functional Polymers

Molecular design of polymers and their precursors is one of the important factors to develop polymer materials with desired properties. The cinnamoyl photodimers have important structural characteristics such as rigid structure, unique bending angles, chirality, and photo-degradable cyclobutane (Figure 1-7). From above structural characteristics, cinnamoyl photodimers are candidate as building block for high-performance and/or functional polymers.

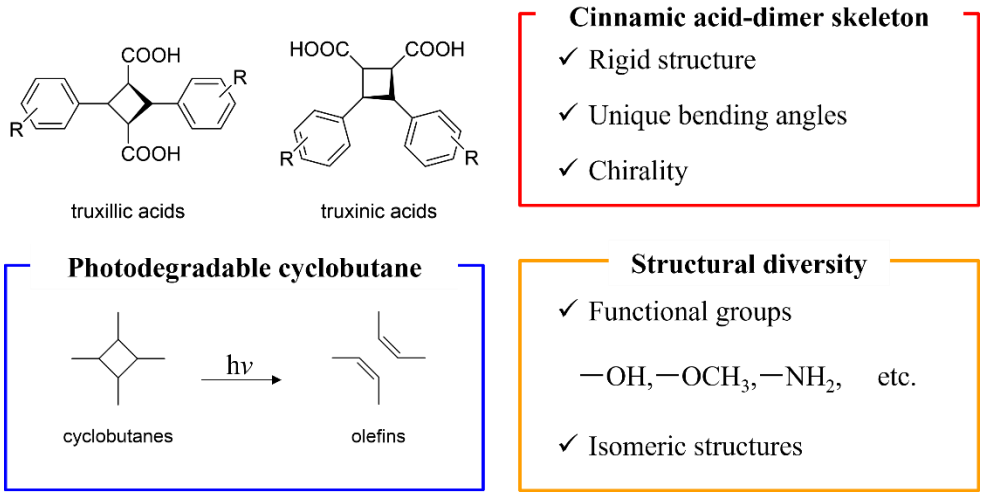

Figure 1-7. Structural characteristics of cinnamoyl photodimers.

Rigid structure:

The cinnamoyl photodimers are composed by rigid aromatic and aliphatic ring structure, benzene ring and cyclobutane ring. These rigid structures are effective in the improvement of thermal properties such as glass transition temperature, resulting in high thermal stability. In addition, these rigid structures can enhance mechanical strength of polymer materials. Thus, cinnamoyl photodimers could be a suitable candidate for syntheses of high-performance polymers.

Unique bending angle:

It is known that physicochemical properties of polymer materials such as solubility,[63–65] gas permeability[66–68], thermal properties,[69,70] and mechanical properties[71] are affected by bending structure in the polymer backbone. Since the cyclobutane ring has strain structure, bending structure with unique bending angles depended on spatial arrangement around cyclobutane ring can be introduced in polymer backbone by using cinnamoyl photodimers as monomers.

Chirality:

Optically active polymers show specific functions owing to their chirality and are used for various applications such as enantioselective separation,[72,73] and asymmetric catalysts.[74,75] Some of cinnamoyl photodimers such as *delta*-, *mu*-, *neo*-, and *zeta*- type show chirality. Hence when optically active photodimers are used as monomers for optically active polymer syntheses, specific functions can be expected.

Photodegradable cyclobutane:

The cyclobutane ring can be cleaved by ultraviolet light irradiation.[76,77] Thus, cinnamoyl dimer-based polymers can be expected to develop degradable polymer materials.

Structural diversity:

Naturally occurred cinnamic acids have various functional groups such as hydroxy, methoxy, and amino groups. These functional groups are possible to modify other functional groups by chemical modification. In addition, since the cinnamoyl photodimers have isomers as mentioned above, various kinds of polymers can be expected by using cinnamoyl dimers as monomers.

1.3.3 Cinnamoyl Dimer-based Polymers

As mentioned above, cinnamoyl dimers can be expected to apply for the syntheses of high-performance/functional polymers based on their unique structural characteristics. The photodimerization of the cinnamic acid and their derivatives have been used for photoreactive polymer syntheses, however most of studies used cinnamic acid moiety for photoreactive cross-linkage point at side chain.[78–80] Hence, studies regarding to cinnamoyl photodimer units in polymer backbone are rarely conducted.

Saigo et al. reported polyamides which were synthesized from aliphatic/aromatic diamines and optically active coumarin dimer having μ-type cinnamoyl dimer structure (Scheme 1-3).[81–83] They also investigated chiral recognition abilities of synthesized polyamides based on monomer chirality. As a result, some of polyamides with longer methylene unit, m=5–10, exhibited good chiral recognition ability for several racemates, indicated that these kinds of materials had a potential to apply chiral stationary phase for high-performance liquid chromatography.

Scheme 1-3. Synthesis of Optically Active Coumarin Dimer-based Polyamides

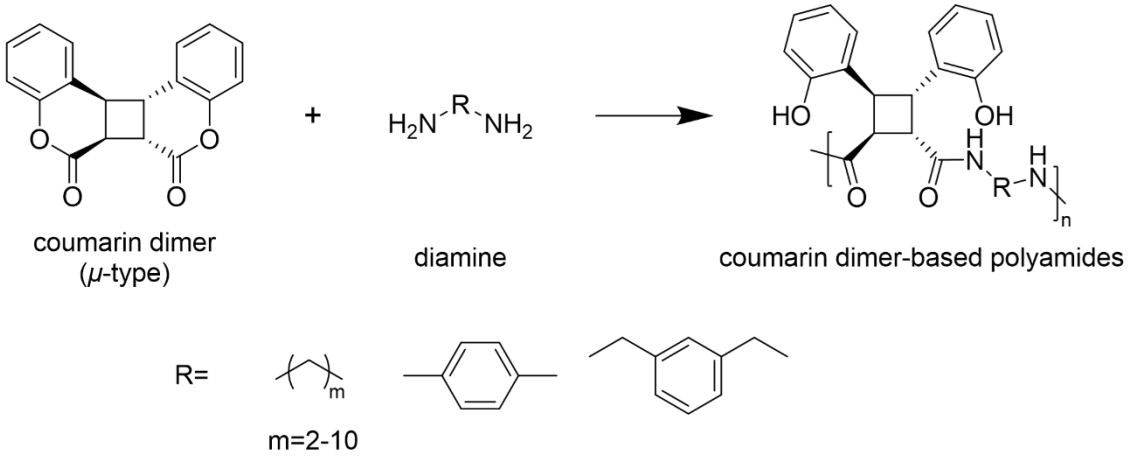

Kaneko et al. reported *α*-type 4-aminocinnamoyl photodimer-based high-performance polymers such as polyamide and polyimides (Figure 1-8). The polyamide which was synthesized from *α*-type 4-aminocinnamoyl photodimer-based diamine and dicarboxylic acid monomers exhibited much higher mechanical strength than conventional transparent polymers such as polycarbonate.[84] The polyimides synthesized from methyl 4-aminocinamate photodimer and tetracarboxylic acid anhydrides, showed good transparency and high thermal stability based on the cinnamoyl dimer skeleton.[85,86] In addition, when the methyl esters in the polyimide side chain were modified into carboxylic acid metal salt, polyimides were easily dissolved to water with high solubility.[87]

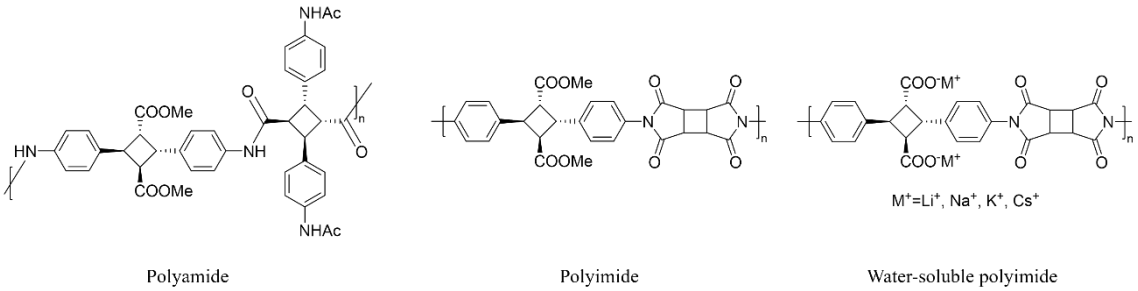

Figure 1-8. Molecular structure of representative α-type 4-aminocinnamoyl photodimer-based high-performance polymers.

Thus, cinnamoyl photodimers have been applied for high-performance and/or functional polymers, however few studies regarding to cinnamoyl photodimer-based polymers are presented, and effects of cinnamoyl photodimers on polymer properties are still not clear enough.

1.4 Objectives and Outline of the Thesis

Development of biobased polymer materials are important tasks for upcoming sustainable society. In recent years, various kinds of biobased polymers including naturally occurred polymers and synthetic polymers from biomass resources have been developed. However, compared to conventional petroleum-based polymers, performance of biobased polymers is not high enough, resulting in limited use of biobased polymers. To expand application of biobased polymers, high performance and/or functional biobased polymers are deeply required.

Cinnamic acids, one of the important intermediates from biomass resources, have been used for various applications including high-performance polymers. The cinnamic acids afford isomeric photodimers, truxillic acids, and truxinic acids by ultraviolet light irradiation. These photodimers have unique structural characteristics for high-performance and/or functional polymers such as rigid structure, unique bending angles, chirality, and photodegradable cyclobutane. However, since few studies about cinnamoyl photodimer-based polymers are presented, effects of cinnamoyl photodimers on polymer properties are not clear enough.

Based on above information, the objective of this thesis is clarification the effects of cinnamoyl dimer unit in polymer backbone on polymer properties through the developments of high-performance/functional polymers from unique cinnamoyl dimers (Figure 1-9). This research would provide insights into the molecular design of high-performance and/or functional polymers by focusing on the unique cinnamoyl dimer structures.

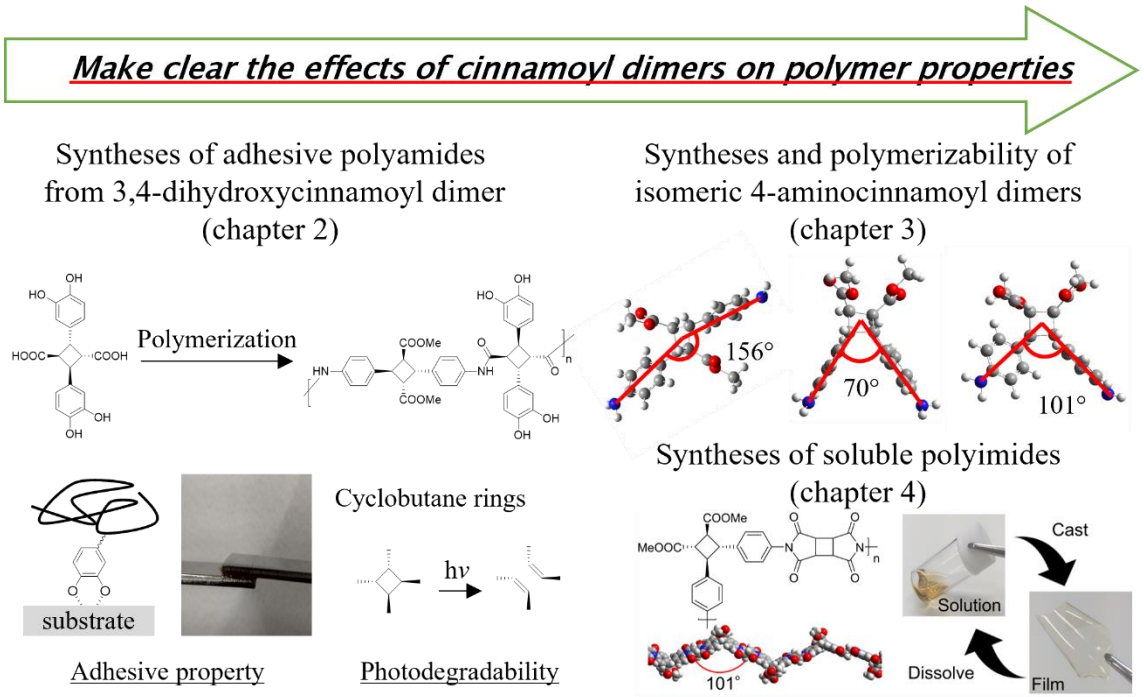

Figure 1-9. Objectives and outline of this research.

The outline of this thesis is as follows:

Chapter 2 describes the synthesis of photodegradable adhesive materials from 3,4-dihydroxycinnamoyl dimer (34THTA). The 34THTA was synthesized from methyl 3,4-dihydroxycinnamate by solid-state photodimerization and further hydrolysis of methyl esters. The obtained 34THTA was copolymerized with adipic acid and *α*-type 4-aminocinnamoyl dimer-based diamine (*α*ATA-Me). As a result, the obtained copolyamide exhibited good adhesive properties of ~7 MPa for stainless steel substrate. In addition, polyamide synthesized from 34THTA and *α*ATA-Me exhibited photodegradability by ultraviolet light irradiation.

Chapter 3 describes the synthesis and polymerization of *α*-, *β*-, and *δ*-type 4-aminocinnamoyl photodimers. The *β*- and *δ*-type photodimers were prepared from modified 4-nitrocinnamic acid derivatives, methyl 4-nitrocinnamate and *N*-hydroxysuccinimide 4-nitrocinnamate, respectively via solid-state photodimerization. Density functional theory (DFT) calculations revealed that the *β*- and *δ*-type photodimers possessed unique bending angles of 70° and 101°, respectively. The obtained photodimers were modified into diamines and dicarboxylic acid for polyamide syntheses.

Chapter 4 describes the synthesis of soluble biobased polyimides from isomeric 4-aminocinnamoyl photodimer-based diamines with unique bending angles. The *β*-, and *δ*-type diamines were polymerized with tetracarboxylic acid dianhydrides to produce soluble polyimides via chemical imidization. As a result, *δ*-type dimer-based polyimides exhibited high thermostability and good solubility in organic solvents owing to its rigid and bending structure.

Chapter 5 summarizes the syntheses and evaluation of high-performance/functional polymers using unique cinnamoyl dimers as the overall conclusions of this thesis.

1.5 References and Notes

(1) Geyer, R.; Jambeck, J. R.; Law, K. L. Production, Use, and Fate of All Plastics Ever Made. *Sci. Adv.* **2017**, *3* (7), 25–29. https://doi.org/10.1126/sciadv.1700782.

(2) Babu, R. P.; O'Connor, K.; Seeram, R. Current Progress on Bio-Based Polymers and Their Future Trends. *Prog. Biomater.* **2013**, *2* (1), 8. https://doi.org/10.1186/2194-0517-2-8.

(3) Jang, W. D.; Hwang, J. H.; Kim, H. U.; Ryu, J. Y.; Lee, S. Y. Bacterial Cellulose as an Example Product for Sustainable Production and Consumption. *Microb. Biotechnol.* **2017**, *10* (5), 1181–1185. https://doi.org/10.1111/1751-7915.12744.

(4) RameshKumar, S.; Shaiju, P.; O'Connor, K. E.; P, R. B. Bio-Based and Biodegradable Polymers - State-of-the-Art, Challenges and Emerging Trends. *Curr. Opin. Green Sustain. Chem.* **2020**, *21*, 75–81. https://doi.org/10.1016/j.cogsc.2019.12.005.

(5) Wang, S.; Chen, W.; Xiang, H.; Yang, J.; Zhou, Z.; Zhu, M. Modification and Potential Application of Short-Chain-Length Polyhydroxyalkanoate (SCL-PHA). *Polymers (Basel).* **2016**, *8* (8). https://doi.org/10.3390/polym8080273.

(6) Shahidi, F.; Arachchi, J. K. V.; Jeon, Y. J. Food Applications of Chitin and Chitosans. *Trends Food Sci. Technol.* **1999**, *10* (2), 37–51.

https://doi.org/10.1016/S0924-2244(99)00017-5.

(7) Petrasovits, L. A.; Purnell, M. P.; Nielsen, L. K.; Brumbley, S. M. Production of Polyhydroxybutyrate in Sugarcane. *Plant Biotechnol. J.* **2007**, *5* (1), 162–172. https://doi.org/10.1111/j.1467-7652.2006.00229.x.

(8) Doyle, C.; Tanner, E. T.; Bonfield, W. In Vitro and in Vivo Evaluation of Polyhydroxybutyrate and of Polyhydroxybutyrate Reinforced with Hydroxyapatite. *Biomaterials* **1991**, *12* (9), 841–847. https://doi.org/10.1016/0142-9612(91)90072-I.

(9) Nechyporchuk, O.; Belgacem, M. N.; Bras, J. Production of Cellulose Nanofibrils: A Review of Recent Advances. *Ind. Crops Prod.* **2016**, *93*, 2–25. https://doi.org/10.1016/j.indcrop.2016.02.016.

(10) Van Der Rest, M.; Garrone, R. Collagen Family of Proteins. *FASEB J.* **1991**, *5* (13), 2814–2823. https://doi.org/10.1096/fasebj.5.13.1916105.

(11) Adler, E. Lignin Chemistry-Past, Present and Future. *Wood Sci. Technol.* **1977**, *11* (3), 169–218. https://doi.org/10.1007/BF00365615.

(12) Garlotta, D. A Literature Review of Poly(Lactic Acid). *J. Polym. Environ.* **2001**, *9* (2), 63–84. https://doi.org/10.1023/A:1020200822435.

(13) Web of science, Citation report about “biobased polymer”.

http://apps.webofknowledge.com/WOS_GeneralSearch_input.do?product=WOS&search_mode=GeneralSearch&SID=D6sR9py2gT8EkY5RMaR&preferencesSaved.

(14) Tsuji, H. Poly(Lactide) Stereocomplexes: Formation, Structure, Properties, Degradation, and Applications. *Macromol. Biosci.* **2005**, *5* (7), 569–597. https://doi.org/10.1002/mabi.200500062.

(15) Kimura, Y. Molecular, Structural, and Material Design of Bio-Based Polymers. *Polym. J.* **2009**, *41* (10), 797–807. https://doi.org/10.1295/polymj.PJ2009154.

(16) Gigli, M.; Fabbri, M.; Lotti, N.; Gamberini, R.; Rimini, B.; Munari, A. Poly(Butylene Succinate)-Based Polyesters for Biomedical Applications: A Review in Memory of Our Beloved Colleague and Friend Dr. Lara Finelli. *Eur. Polym. J.* **2016**, *75*, 431–460. https://doi.org/10.1016/j.eurpolymj.2016.01.016.

(17) Hwang, S. Y.; Yoo, E. S.; Im, S. S. The Synthesis of Copolymers, Blends and Composites Based on Poly(Butylene Succinate). *Polym. J.* **2012**, *44* (12), 1179–1190. https://doi.org/10.1038/pj.2012.157.

(18) Myllytie, P.; Misra, M.; Mohanty, A. K. Carbonized Lignin as Sustainable Filler in Biobased Poly(Trimethylene Terephthalate) Polymer for Injection Molding Applications. *ACS Sustain. Chem. Eng.* **2016**, *4* (1), 102–110.

https://doi.org/10.1021/acssuschemeng.5b00796.

(19) Álvarez-Chávez, C. R.; Edwards, S.; Moure-Eraso, R.; Geiser, K. Sustainability of Bio-Based Plastics: General Comparative Analysis and Recommendations for Improvement. *J. Clean. Prod.* **2012**, *23* (1), 47–56. https://doi.org/10.1016/j.jclepro.2011.10.003.

(20) Rosatella, A. A.; Simeonov, S. P.; Frade, R. F. M.; Afonso, C. A. M. 5-Hydroxymethylfurfural (HMF) as a Building Block Platform: Biological Properties, Synthesis and Synthetic Applications. *Green Chem.* **2011**, *13* (4), 754–793. https://doi.org/10.1039/c0gc00401d.

(21) Birajdar, M. S.; Joo, H.; Koh, W. G.; Park, H. Natural Bio-Based Monomers for Biomedical Applications: A Review. *Biomater. Res.* **2021**, *25* (1), 1–14. https://doi.org/10.1186/s40824-021-00208-8.

(22) Nag, A.; Ali, M. A.; Kawaguchi, H.; Saito, S.; Kawasaki, Y.; Miyazaki, S.; Kawamoto, H.; Adi, D. T. N.; Yoshihara, K.; Masuo, S.; Katsuyama, Y.; Kondo, A.; Ogino, C.; Takaya, N.; Kaneko, T.; Ohnishi, Y. Ultrahigh Thermoresistant Lightweight Bioplastics Developed from Fermentation Products of Cellulosic Feedstock. *Adv. Sustain. Syst.* **2021**, *5* (1), 2000193. https://doi.org/10.1002/adsu.202000193.

(23) Kanetaka, Y.; Yamazaki, S.; Kimura, K. Preparation of Poly(Ether Ketone)s Derived from 2,5-Furandicarboxylic Acid via Nucleophilic Aromatic Substitution Polymerization. *J. Polym. Sci. Part A Polym. Chem.* **2016**, *54* (19), 3094–3101. https://doi.org/10.1002/pola.28193.

(24) Yamada, S.; Nabe, K.; Izuo, N. Production of L-Phenylalanine from Trans-Cinnamic Acid with Rhodotorula Glutinis Containing L-Phenylalanine Ammonia-Lyase Activity. *Appl. Environ. Microbiol.* **1981**, *42* (5), 773–778. https://doi.org/10.1128/aem.42.5.773-778.1981.

(25) Li, Y.; Tang, L.; Ma, X.; Wang, X.; Zhou, W.; Bai, D. Synthesis and Characterization of Zn-Ti Layered Double Hydroxide Intercalated with Cinnamic Acid for Cosmetic Application. *J. Phys. Chem. Solids* **2017**, *107* (March), 62–67. https://doi.org/10.1016/j.jpcs.2017.02.018.

(26) Gunia-Krzyżak, A.; Słoczyńska, K.; Popiół, J.; Koczurkiewicz, P.; Marona, H.; Pękala, E. Cinnamic Acid Derivatives in Cosmetics: Current Use and Future Prospects. *Int. J. Cosmet. Sci.* **2018**, *40* (4), 356–366. https://doi.org/10.1111/ics.12471.

(27) Ruwizhi, N.; Aderibigbe, B. A. Cinnamic Acid Derivatives and Their Biological Efficacy. *Int. J. Mol. Sci.* **2020**, *21* (16), 1–36.

https://doi.org/10.3390/ijms21165712.

(28) Karamac, M.; Koleva, L.; Kancheva, V. D.; Amarowicz, R. The Structure-Antioxidant Activity Relationship of Ferulates. *Molecules* **2017**, *22* (4), 15–19. https://doi.org/10.3390/molecules22040527.

(29) Letizia, C. S.; Cocchiara, J.; Lapczynski, A.; Lalko, J.; Api, A. M. Fragrance Material Review on Cinnamic Acid. *Food Chem. Toxicol.* **2005**, *43* (6), 925–943. https://doi.org/10.1016/j.fct.2004.09.015.

(30) Zhang, Z.; Qin, G.; Li, B.; Tian, S. Effect of Cinnamic Acid for Controlling Gray Mold on Table Grape and Its Possible Mechanisms of Action. *Curr. Microbiol.* **2015**, *71* (3), 396–402. https://doi.org/10.1007/s00284-015-0863-1.

(31) Kumar, N.; Pruthi, V. Potential Applications of Ferulic Acid from Natural Sources. *Biotechnol. Reports* **2014**, *4* (1), 86–93. https://doi.org/10.1016/j.btre.2014.09.002.

(32) Nomura, E.; Noda, T.; Gomi, D.; Mori, H. Substituent Effect on the Formation of Arylindanes by Dimerization of Ferulic Acid and Its Related Compounds. *ACS Omega* **2018**, *3* (10), 12746–12753. https://doi.org/10.1021/acsomega.8b01953.

(33) Gallage, N. J.; Hansen, E. H.; Kannangara, R.; Olsen, C. E.; Motawia, M. S.; Jørgensen, K.; Holme, I.; Hebelstrup, K.; Grisoni, M.; Møller, B. L. Vanillin

Formation from Ferulic Acid in Vanilla Planifolia Is Catalysed by a Single Enzyme. *Nat. Commun.* **2014**, *5* (May). https://doi.org/10.1038/ncomms5037.

(34) Taniguchi, H.; Nomura, E.; Tsuno, T.; Minami, S.; Kato, K.; Hayashi, C. Method of Manufacturing Ferulic Acid. U.S. patent 5288902A, 1994.

(35) Kawaguchi, H.; Katsuyama, Y.; Danyao, D.; Kahar, P.; Nakamura-Tsuruta, S.; Teramura, H.; Wakai, K.; Yoshihara, K.; Minami, H.; Ogino, C.; Ohnishi, Y.; Kondo, A. Caffeic Acid Production by Simultaneous Saccharification and Fermentation of Kraft Pulp Using Recombinant Escherichia Coli. *Appl. Microbiol. Biotechnol.* **2017**, *101* (13), 5279–5290. https://doi.org/10.1007/s00253-017-8270-0.

(36) Takenaka, M.; Nanayama, K.; Isobe, S.; Murata, M. Changes in Caffeic Acid Derivatives in Sweet Potato (Ipomoea Batatas L.) during Cooking and Processing. *Biosci. Biotechnol. Biochem.* **2006**, *70* (1), 172–177. https://doi.org/10.1271/bbb.70.172.

(37) Hammond, G. S.; Saltiel, J.; Lamola, A. A.; Turro, N. J.; Bradshaw, J. S.; Cowan, D. O.; Counsell, R. C.; Vogt, V.; Dalton, C. Mechanisms of Photochemical Reactions in Solution. XXII.1 Photochemical Cis-Trans Isomerization. *J. Am. Chem. Soc.* **1964**, *86* (16), 3197–3217. https://doi.org/10.1021/ja01070a002.

(38) Yamashita, S.; Ono, H.; Toyama, O. The Cis-Trans Photoisomerization of Azobenzene . *Bull. Chem. Soc. Jpn.* **1962**, *35* (11), 1849–1853. https://doi.org/10.1246/bcsj.35.1849.

(39) Taoda, H.; Hayakawa, K.; Kawase, K.; Yamakita, H. Photochemical Conversion and Storage of Solar Energy by Azobenzene. *J. Chem. Eng. Japan* **1987**, *20* (3), 265–270. https://doi.org/10.1252/jcej.20.265.

(40) Salum, M. L.; Erra-Balsells, R. High Purity Cis-Cinnamic Acid Preparation for Studying Physiological Role of Trans-Cinnamic and Cis-Cinnamic Acids in Higher Plants. *Environ. Control Biol.* **2013**, *51* (1), 1–10. https://doi.org/10.2525/ecb.51.1.

(41) Hocking, M. B. Photochemical and Thermal Isomerizations of Cis - and Trans - Cinnamic Acids, and Their Photostationary State . *Can. J. Chem.* **1969**, *47* (24), 4567–4576. https://doi.org/10.1139/v69-757.

(42) Poplata, S.; Tröster, A.; Zou, Y. Q.; Bach, T. Recent Advances in the Synthesis of Cyclobutanes by Olefin [2 +2] Photocycloaddition Reactions. *Chem. Rev.* **2016**, *116* (17), 9748–9815. https://doi.org/10.1021/acs.chemrev.5b00723.

(43) Crimmins, M. T. Synthetic Applications of Intramolecular Enone-Olefin Photocycloadditions. *Chem. Rev.* **1988**, *88* (8), 1453–1473.

https://doi.org/10.1021/cr00090a002.

(44) Arnold, D. R.; Du, X. The Photochemical Nucleophile-Olefin Combination, Aromatic Substitution Reaction: Methanol-.Alpha.- and .Beta.-Pinene, 1,4-Dicyanobenzene. The Photo-NOCAS Reaction. Part 3. *J. Am. Chem. Soc.* **1989**, *111* (19), 7666–7667. https://doi.org/10.1021/ja00201a085.

(45) Poplata, S.; Bach, T. Enantioselective Intermolecular [2+2] Photocycloaddition Reaction of Cyclic Enones and Its Application in a Synthesis of (-)-Grandisol. *J. Am. Chem. Soc.* **2018**, *140* (9), 3228–3231. https://doi.org/10.1021/jacs.8b01011.

(46) Bernstein, H. I.; Quimby, W. C. The Photochemical Dimerization of Trans-Cinnamic Acid 1. *J. Am. Chem. Soc.* **1943**, *65* (10), 1845–1846. https://doi.org/10.1021/ja01250a016.

(47) Mallette, J. R.; Casale, J. F. Rapid Determination of the Isomeric Truxillines in Illicit Cocaine via Capillary Gas Chromatography/Flame Ionization Detection and Their Use and Implication in the Determination of Cocaine Origin and Trafficking Routes. *J. Chromatogr. A* **2014**, *1364*, 234–240. https://doi.org/10.1016/j.chroma.2014.08.072.

(48) Lydon, J.; Casale, J. F.; Kong, H.; Sullivan, J. H.; Daughtry, C. S. T.; Bailey, B. The Effects of Ambient Solar UV Radiation on Alkaloid Production by

Erythroxylum Novogranatense Var. Novogranatense. *Photochem. Photobiol.* **2009**, *85* (5), 1156–1161. https://doi.org/10.1111/j.1751-1097.2009.00562.x.

(49) Moore, J. M.; Casale, J. F.; Cooper, D. A. Comparative Determination of Total Isomeric Truxillines in Illicit, Refined, South American Cocaine Hydrochloride Using Capillary Gas Chromatography-Electron Capture Detection. *J. Chromatogr. A* **1996**, *756* (1–2), 193–201. https://doi.org/10.1016/S0021-9673(96)00651-6.

(50) Russell, W. R.; Hanley, A. B.; Burkitt, M. J.; Chesson, A. Effect of Substitution on the 2+2 Cycloaddition Reaction of Phenylpropanoids. *Bioorg. Chem.* **1999**, *27* (5), 339–350. https://doi.org/10.1006/bioo.1999.1143.

(51) Gießel, J. M.; Kohlmann, T.; Zeitz, T.; Kluge, R.; Csuk, R. Synthesis of Sinapine and Its Unprecedented Ruthenium-Catalyzed [2+2] Photodimerization. *Mediterr. J. Chem.* **2019**, *9* (4), 258–265. https://doi.org/10.13171/mjc941911051057rc.

(52) Maeda, H.; Nishimura, K.; Yokoyama, A.; Sugimoto, A.; Mizuno, K.; Hosoda, A.; Nomura, E.; Taniguchi, H. Intramolecular [2+2] Photocycloaddition and Cycloreversion of Ferulic Acid Derivatives. *Rapid Commun. Photoscience* **2015**, *4* (1), 12–15. https://doi.org/10.5857/RCP.2015.4.1.12.

(53) Nakamura, T.; Takagi, K.; Sawaki, Y. Photodimerization of Trans -Cinnamic

Acid in a Bilayer of Dimethyldioctadecylammonium Bromide. *Bull. Chem. Soc. Jpn.* **1998**, *71* (4), 909–914. https://doi.org/10.1246/bcsj.71.909.

(54) UEKAMA, K.; OTAGIRI, M.; KANIE, Y.; TANAKA, S.; IKEDA, K. Inclusion Complexes of Cinnamic Acids with Cyclodextrins. Mode of Inclusion in Aqueous Solution. *Chem. Pharm. Bull.* **1975**, *23* (7), 1421–1430. https://doi.org/10.1248/cpb.23.1421.

(55) Karthikeyan, S.; Ramamurthy, V. Templating Photodimerization of Trans-Cinnamic Acid Esters with a Water-Soluble Pd Nanocage. *J. Org. Chem.* **2007**, *72* (2), 452–458. https://doi.org/10.1021/jo0617722.

(56) Pattabiraman, M.; Kaanumalle, L. S.; Natarajan, A.; Ramamurthy, V. Regioselective Photodimerization of Cinnamic Acids in Water: Templation with Cucurbiturils. *Langmuir* **2006**, *22* (18), 7605–7609. https://doi.org/10.1021/la061215a.

(57) Rivera, J. M.; Silva-Brenes, D. A Photoresponsive Supramolecular G-Quadruplex. *Org. Lett.* **2013**, *15* (10), 2350–2353. https://doi.org/10.1021/ol400610x.

(58) Schmidt, G. M. J. Photodimerization in the Solid State. *Pure Appl. Chem.* **1971**, *27* (4), 647–678. https://doi.org/10.1351/pac197127040647.

(59) Sonoda, Y. Solid-State [2+2] Photodimerization and Photopolymerization of α,ω-Diarylpolyene Monomers: Effective Utilization of Noncovalent Intermolecular Interactions in Crystals. *Molecules* **2011**, *16* (1), 119–148. https://doi.org/10.3390/molecules16010119.

(60) Enkelmann, V.; Wegner, G.; Novak, K.; Wagener, K. B. Single-Crystal-to-Single-Crystal Photodimerization of Cinnamic Acid. *J. Am. Chem. Soc.* **1993**, *115* (22), 10390–10391. https://doi.org/10.1021/ja00075a077.

(61) D'Agostino, S.; Taddei, P.; Boanini, E.; Braga, D.; Grepioni, F. Photo- vs Mechano-Induced Polymorphism and Single Crystal to Single Crystal [2 + 2] Photoreactivity in a Bromide Salt of 4-Amino-Cinnamic Acid. *Cryst. Growth Des.* **2017**, *17* (9), 4491–4495. https://doi.org/10.1021/acs.cgd.7b00415.

(62) Nakanishi, F.; Nakanishi, H.; Tsuchiya, M.; Hasegawa, M. Water-Participation in the Crystalline-State Photodimerization of Cinnamic Acid Derivatives. A New Type of Organic Photoreaction. *Bull. Chem. Soc. Jpn.* **1976**, *49* (11), 3096–3099. https://doi.org/10.1246/bcsj.49.3096.

(63) Ding, M. Isomeric Polyimides. *Prog. Polym. Sci.* **2007**, *32* (6), 623–668. https://doi.org/10.1016/j.progpolymsci.2007.01.007.

(64) Mi, Z.; Wang, S.; Hou, Z.; Liu, Z.; Jin, S.; Wang, X.; Wang, D.; Zhao, X.;

Zhang, Y.; Zhou, H.; Chen, C. Soluble Polyimides Bearing (Cis, Trans)-Hydrogenated Bisphenol A and (Trans, Trans)-Hydrogenated Bisphenol A Moieties: Synthesis, Properties and the Conformational Effect. *Polymers (Basel).* **2019**, *11* (5), 854. https://doi.org/10.3390/polym11050854.

(65) Hsiao, S. H.; Chen, Y. J. Structure-Property Study of Polyimides Derived from PMDA and BPDA Dianhydrides with Structurally Different Diamines. *Eur. Polym. J.* **2002**, *38* (4), 815–828. https://doi.org/10.1016/S0014-3057(01)00229-4.

(66) Park, J. Y.; Paul, D. R. Correlation and Prediction of Gas Permeability in Glassy Polymer Membrane Materials via a Modified Free Volume Based Group Contribution Method. *J. Memb. Sci.* **1997**, *125* (1), 23–39. https://doi.org/10.1016/S0376-7388(96)00061-0.

(67) Coleman, M. R.; Koros, W. J. Isomeric Polyimides Based on Fluorinated Dianhydrides and Diamines for Gas Separation Applications. *J. Memb. Sci.* **1990**, *50* (3), 285–297. https://doi.org/10.1016/S0376-7388(00)80626-2.

(68) Aitken, C. L.; Koros, W. J.; Paul, D. R. Effect of Structural Symmetry on Gas Transport Properties of Polysulfones. *Macromolecules* **1992**, *25* (13), 3424–3434. https://doi.org/10.1021/ma00039a018.

(69) Fang, X.; Yang, Z.; Zhang, S.; Gao, L.; Ding, M. Polyimides Derived from Mellophanic Dianhydride. *Macromolecules* **2002**, *35* (23), 8708–8717. https://doi.org/10.1021/ma0204610.

(70) Dingemans, T. J.; Mendes, E.; Hinkley, J. J.; Weiser, E. S.; StClair, T. L. Poly(Ether Imide)s from Diamines with Para-, Meta-, and Ortho-Arylene Substitutions: Synthesis, Characterization, and Liquid Crystalline Properties. *Macromolecules* **2008**, *41* (7), 2474–2483. https://doi.org/10.1021/ma8000324.

(71) Jassal, M.; Ghosh, S. Aramid Fibres - An Overview. *Indian J. Fibre Text. Res.* **2002**, *27* (3), 290–306.

(72) Shen, J.; Okamoto, Y. Efficient Separation of Enantiomers Using Stereoregular Chiral Polymers. *Chem. Rev.* **2016**, *116* (3), 1094–1138. https://doi.org/10.1021/acs.chemrev.5b00317.

(73) Okamoto, Y.; Nakano, T. Asymmetric Polymerization. *Chem. Rev.* **1994**, *94* (2), 349–372. https://doi.org/10.1021/cr00026a004.

(74) Itsuno, S.; Paul, D. K.; Salam, M. A.; Haraguchi, N. Main-Chain Ionic Chiral Polymers: Synthesis of Optically Active Quaternary Ammonium Sulfonate Polymers and Their Application in Asymmetric Catalysis. *J. Am. Chem. Soc.* **2010**, *132* (9), 2864–2865. https://doi.org/10.1021/ja909972d.

(75) Haraguchi, N.; Kiyono, H.; Takemura, Y.; Itsuno, S. Design of Main-Chain Polymers of Chiral Imidazolidinone for Asymmetric Organocatalysis Application. *Chem. Commun.* **2012**, *48* (33), 4011–4013. https://doi.org/10.1039/c2cc18115k.

(76) Yonezawa, N.; Kubo, M.; Saigo, K.; Hasegawa, M. Solvent- and Wavelength-Dependence of the Photocleavage of the Cyclobutane Ring in N , N ′-Dibutyl- c -3, c -4-Bis(2-Hydroxyphenyl)- r -1, c -2-Cyclobutanedicarboxamide. *Bull. Chem. Soc. Jpn.* **1988**, *61* (3), 1005–1007. https://doi.org/10.1246/bcsj.61.1005.

(77) Bieniek, N.; Inacker, S.; Kim, H.-C.; Hampp, N. Cyclobutane-Cleavage of Anti-Head-to-Head Coumarin and Quinolinone Homo- and Cross-Dimers via Single- and Two-Photon-Absorption Photochemistry. *J. Photochem. Photobiol. A Chem.* **2021**, *414* (April), 113286. https://doi.org/10.1016/j.jphotochem.2021.113286.

(78) Kawatsuki, N.; Matsushita, H.; Kondo, M. Photoinduced Cooperative Reorientation of Photoreactive Liquid Crystalline Copolymer Films Comprised of Cinnamic Acid and Phenylbenzoate Side Groups. *J. Photopolym. Sci. Technol.* **2012**, *25* (3), 303–308. https://doi.org/10.2494/photopolymer.25.303.

(79) Schelkle, K. M.; Bender, M.; Beck, S.; Jeltsch, K. F.; Stolz, S.; Zimmermann, J.; Weitz, R. T.; Pucci, A.; Müllen, K.; Hamburger, M.; Bunz, U. H. F. Photo-Cross-

Linkable Polymeric Optoelectronics Based on the [2 + 2] Cycloaddition Reaction of Cinnamic Acid. *Macromolecules* **2016**, *49* (5), 1518–1522. https://doi.org/10.1021/acs.macromol.5b02407.

(80) Sierocka, M.; Łyk, B.; Pączkowski, J.; Zakrzewski, A.; Wrzyszczyński, A. Light-Sensitive Epoxy-Based Resins: Synthesis, Light-Sensitivity, Spectro-Sensitivity and Sensitization. *Polym. Photochem.* **1984**, *4* (3), 207–222. https://doi.org/10.1016/0144-2880(84)90062-9.

(81) Saigo, K.; Nakamura, M.; Suzuki, Y.; Fang, L.; Hasegawa, M. Synthesis and Properties of Polyamides Having Anti Head-to-Head Umbelliferone Dimer as a Component. *Macromolecules* **1990**, *23* (16), 3722–3729. https://doi.org/10.1021/ma00218a002.

(82) Hayashi, K.; Saigo, K.; Shiwaku, T.; Fujioka, K.; Sukegawa, M.; Chen, Y.; Yonezawa, N.; Hasegawa, M.; Hashimoto, T. Optically Active Polyamides Consisting of Anti Head-to-Head Coumarin Dimer and a,w-Alkanediamine. Odd-Even Discrimination in Chiral Recognition Ability Depending on the Methylene Number of the Diamine Component and Correlation between the Ability and Crys. *Macromolecules* **1990**, *23* (11), 2830–2836. https://doi.org/10.1021/ma00213a002.

(83) Saigo, K.; Chen, Y.; Yonezawa, N.; Tachibana, K.; Kanoe, T.; Hasegawa, M. NEW CHIRAL STATIONARY PHASES FOR OPTICAL RESOLUTION. OPTICALLY ACTIVE POLYAMIDES HAVING (−)- ANTI HEAD-TO-HEAD COUMARIN DIMER COMPONENT. *Chem. Lett.* **1985**, *14* (12), 1891–1894. https://doi.org/10.1246/cl.1985.1891.

(84) Tateyama, S.; Masuo, S.; Suvannasara, P.; Oka, Y.; Miyazato, A.; Yasaki, K.; Teerawatananond, T.; Muangsin, N.; Zhou, S.; Kawasaki, Y.; Zhu, L.; Zhou, Z.; Takaya, N.; Kaneko, T. Ultrastrong, Transparent Polytruxillamides Derived from Microbial Photodimers. *Macromolecules* **2016**, *49* (9), 3336–3342. https://doi.org/10.1021/acs.macromol.6b00220.

(85) Suvannasara, P.; Tateyama, S.; Miyasato, A.; Matsumura, K.; Shimoda, T.; Ito, T.; Yamagata, Y.; Fujita, T.; Takaya, N.; Kaneko, T. Biobased Polyimides from 4-Aminocinnamic Acid Photodimer. *Macromolecules* **2014**, *47* (5), 1586–1593. https://doi.org/10.1021/ma402499m.

(86) Dwivedi, S.; Kaneko, T. Molecular Design of Soluble Biopolyimide with High Rigidity. *Polymers (Basel).* **2018**, *10* (4), 1–8. https://doi.org/10.3390/polym10040368.

(87) Dwivedi, S.; Nag, A.; Sakamoto, S.; Funahashi, Y.; Harimoto, T.; Takada, K.;

Kaneko, T. High-Temperature Resistant Water-Soluble Polymers Derived from Exotic Amino Acids. *RSC Adv.* **2020**, *10* (62), 38069–38074. https://doi.org/10.1039/d0ra06620f.

Chapter 2

Syntheses of Photodegradable Adhesive Polyamides from 3,4-dihydroxycinnamoyl Dimer

2. 1 Introduction

In nature, mussels can adhere to organic/inorganic surfaces by using adhesive proteins.[1–3] According to studies of adhesion mechanism of mussels, catechol groups in the adhesive proteins have an important role for the strong adhesion preperties.[4] In recent years, to develop adhesive materials with strong adhesive property, numerous studies regarding to mussel-mimetic adhesive materials containing catechol groups have been conducted.[5–8] However, since most of the reported mussel-mimetic adhesive materials are composed of aliphatic moieties, thermal and mechanical properties of these materials are limited.

3,4-Dihydroxycinnamic acid (34DHCA), one of the plant-derived cinnamic acid derivatives, has been considered as useful component for the synthesis of high-performance biobased polymers due to its rigid aromatic structure.[9–11] In addition, since 34DHCA has a catechol group, application for the adhesive materials are also conducted.[12,13] For example, Kaneko et al. reported hyper-branched polyesters synthesized from 34DHCA. The polyesters exhibited good thermostability over 150 °C and strong adhesive property based on catechol groups in chain ends.[14,15] Thus, the 34DHCA component is considered that one of the suitable candidate for high-performance adhesive materials.

Since 34DHCA have photoreactive double bond, photo-assisted dimerization can be expected. Because of useful characteristics of 3,4-dihydroxycinnamoyl dimer (34THTA) such as rigid molecular structure, two catechol groups, and photodegradable cyclobutane, 34THTA have high potentials for high-performance, photodegradable polymer materials. However, studies regarding to 34THTA-based polymers have not been conducted yet.

In this chapter, the author focused on 34THTA to be used as dicarboxylic acid monomer for the synthesis of adhesive polyamides (Scheme 2-1). To develop high-performance photodegradable 34THTA-based adhesive polyamides, truxillic acid-type photodimer, such as α-type, is suitable candidate because (a) the rigid α-type cinnamoyl dimer skeleton could lead high mechanical strength of polymers,[16] and (b) the photo-assisted cleavage of cyclobutane rings could easily induce main chain scission, indicating good photodegradability. In addition, these adhesive polyamides with 34THTA components were expected to exhibit excellent heat resistance based on the rigid cinnamoyl dimer skeleton, and strong adhesive property based on the catechol groups in side chain, respectively. Furthermore, since 34DHCA is produced from bio-derived resources, these polyamides are expected to contribute to a sustainable society as high-performance and eco-friendly materials.

Scheme 2-1. Synthesis of Adhesive Polyamide from 34THTA and Diamine Monomer

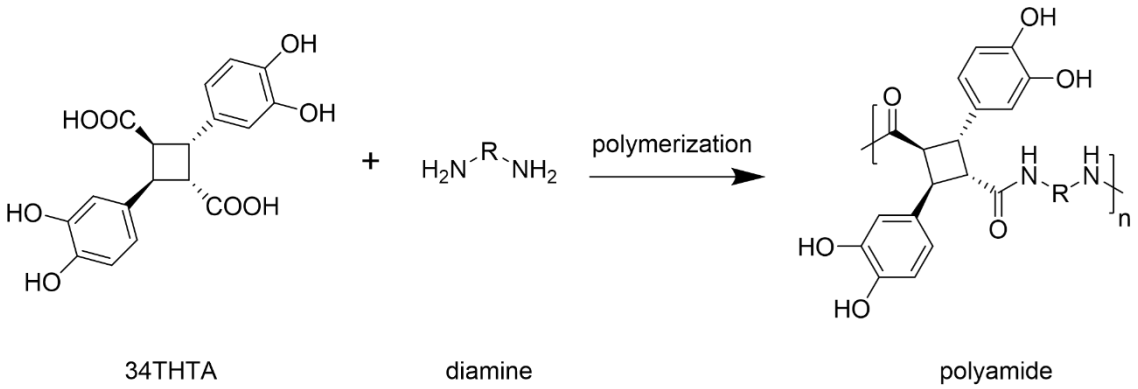

34THTA diamine polyamide

2.2 Experimental Section

Materials. Hexane (>95.0%), chloroform (>99.0%), tetrahydrofuran (THF, >99.5%), methanol (>99.8%), acetone (>99.0%), ethyl acetate (>99.5%), dimethyl sulfoxide (DMSO, >99.0%), *N*,*N*-dimethylformamide (DMF, >99.5%), *N*,*N*-dimethylacetamide (DMAc, >99.0%), sulfuric acid (96.0%), hydrochloric acid (35.0–37.0%), sodium hydroxide (>97.0%), and pyridine (>99.5%) were purchased from Kanto Chemicals Co., Inc. 4-Aminocinnamic acid (4ACA, >98.0%), cinnamic acid (>98.0%), adipic acid (AA, >99.0%), ethylenediamine anhydrous (EDA, >97.0%), hexamethylenediamine (HMDA, >99.0%), decamethylenediamine (DMDA, >98.0%), and triphenyl phosphite (>97.0%) were purchased from Tokyo Kasei Kogyo Co., Ltd. Calcium hydride (>80.0%) and 1-methyl-2-pyrrolidone (NMP, >99.0%) were purchased from FUJIFILM Wako Pure Chemical Corporation. 3,4-Dihydroxycinnamic acid (34DHCA) was purchased from Tateyama Kasei, Co. Ltd. Magnesium sulfate (>99.0%) was purchased from Sigma-Aldrich Co., Ltd. DMAc and pyridine were distilled from CaH_2 prior to their use. HMDA and DMDA were distilled prior to their use. The *α*-type 4-aminocinnamyl dimer-based diamine (*α*ATA-Me), and *α*-truxillic acid (TA) were synthesized by an analogous to method described in previously reported literatures.[16–18] All other chemicals were purchased from available suppliers and used without purification.

Characterization. The ^{1}H (400 MHz) and ^{13}C NMR (100 MHz) spectra were recorded on a Bruker AVANCE 400 instrument using DMSO-d_6 as the solvent. Size exclusion chromatography (SEC) measurements of the obtained polyimides were performed at 40 °C using a JASCO GPC-101 system equipped with two Shodex KD-806M columns (linear, 8 mm × 300 mm) using 0.01 M LiBr in DMF at the flow rate of 1.0 mL min^{-1}. The number-average molecular weight (M_n) and dispersity (M_w/M_n) of the polymers were determined by the RI based on poly(methyl methacrylate) (PMMA) standards. Thermogravimetric analysis (TGA) and differential scanning calorimetry (DSC) were carried out on Hitachi High-Tech Corporation, STA7200 and Seiko Instruments SII, X-DSC7000T, respectively, at a heating rate of 10 °C min^{-1} under a nitrogen atmosphere. TGA and DSC measurements were carried out over the range of 25−800 °C, and 25−210 °C, respectively. Thermomechanical analysis (TMA) was carried out on Hitachi TMA7100C (tensile mode) from 50 to 210 °C with a heating rate of 5 °C min^{-1} under a nitrogen atmosphere. The contact angle was measured using a Kyowa Interface Science, Drop-Master DM 300. The tensile measurements were carried out at an elongation speed of 0.5 mm min^{-1} on a tensiometer, the Instron 3365 with a load cell (5 kN), at room temperature. The solubility of the polyamides was evaluated at room temperature in various polar (protic and aprotic) and nonpolar solvents and strong acids with a

concentration 2 mg mL^{-1}.

Synthesis of Methyl 3,4-Dihydroxycinnamate (34DHCA-Me). To a solution of 34DHCA (40.0 g, 0.22 mol) in methanol (500 mL), sulfuric acid (1.20 mL, 3.75 mmol) was added dropwise at 0 °C. The reaction mixture was stirred for 17 h at reflux temperature then was cooled to room temperature. After evaporating the solvent, the products were extracted using ethyl acetate, and the extract was first washed with water, then water saturated with sodium bicarbonate, and finally with water again. The organic portion was dried over $MgSO_4$. After evaporating the solvent, the product was dried under reduced pressure to give 34DHCA-Me as a brown solid. Yield, 30.7 g (72%). ^{1}H NMR spectrum is shown in Figure 2-1. ^{1}H NMR (400 MHz, DMSO-d_6): δ (ppm) 3.70 (s, 3H, CH_3), 6.29 (d, 1H, J = 15.9 Hz, CH=CH), 6.78 (d, 1H, J = 8.1 Hz, ArH), 7.02 (dd, 1H, J = 8.3 and 2.1 Hz, ArH), 7.08 (d, 1H, J = 2.1 Hz, ArH),7.51 (d, 1H, J = 16.0 Hz, Ar-C*H*=CH), 9.38 (brs, 2H, OH). ^{13}C NMR (100 MHz, DMSO-d_6): δ (ppm) 51.2, 113.7, 114.8, 115.8, 121.5, 125.5, 145.2, 145.6, 148.5 167.1.

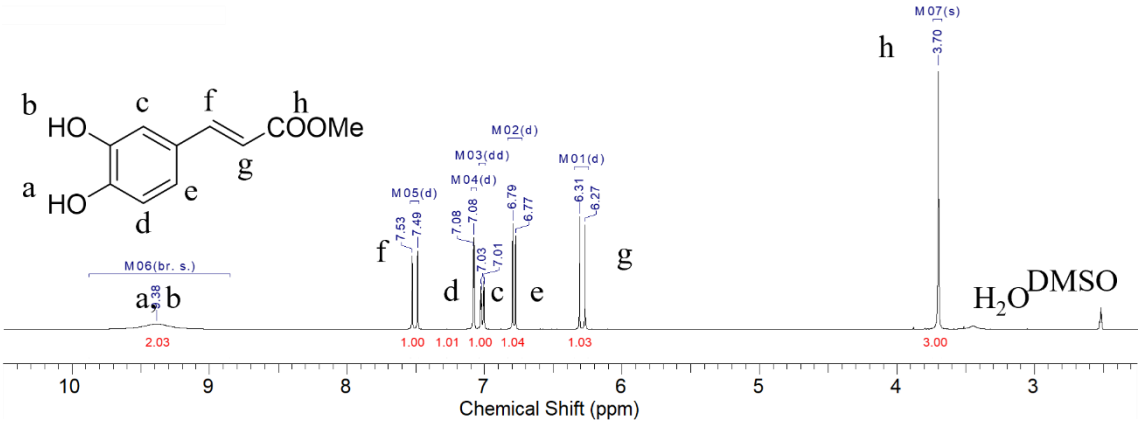

Figure 2-1. ^{1}H NMR spectrum (400 MHz, DMSO-d_6) of 34DHCA-Me.

Synthesis of Dimethyl 3,3′,4,4′-Tetrahydroxy-*α*-truxillate (34THTA-Me). The powder of 34DHCA-Me (20.0 g, 103 mmol) was dispersed in hexane (1 L) under magnetic agitation at room temperature and then irradiated with ultraviolet light by a high-pressure mercury lamp (Omni Cure S1500, EXFO Photonic Solutions Inc., lamp spectra are shown in Figure 2-2) for 24 h to induce [2+2] photocycloaddition. After the reaction, the precipitates were filtered and then dried under reduced pressure to give 34THTA-Me as a white solid. Yield, 19.0 g (95%). ^{1}H NMR spectrum is shown in Figure 2-3. ^{1}H NMR (400 MHz, DMSO-d_6): δ (ppm) 3.30 (s, 6H, CH_3), 3.70 (dd, 2H, J = 10.3, 7.2 Hz, CH), 4.08 (dd, 2H, J = 10.3, 7.2 Hz, CH), 6.53 (dd, 2H, J = 8.1, 2.1 Hz, ArH), 6.64 (s, 2H, ArH), 6.65 (d, 2H, J = 6.5 Hz, ArH), 8.82 (brs, 4H, OH). ^{13}C NMR (100 MHz, DMSO-d_6), δ (ppm) 40.5, 46.4, 51.2, 114.8, 115.3, 118.1, 129.6, 144.1, 144.9, 172.0.

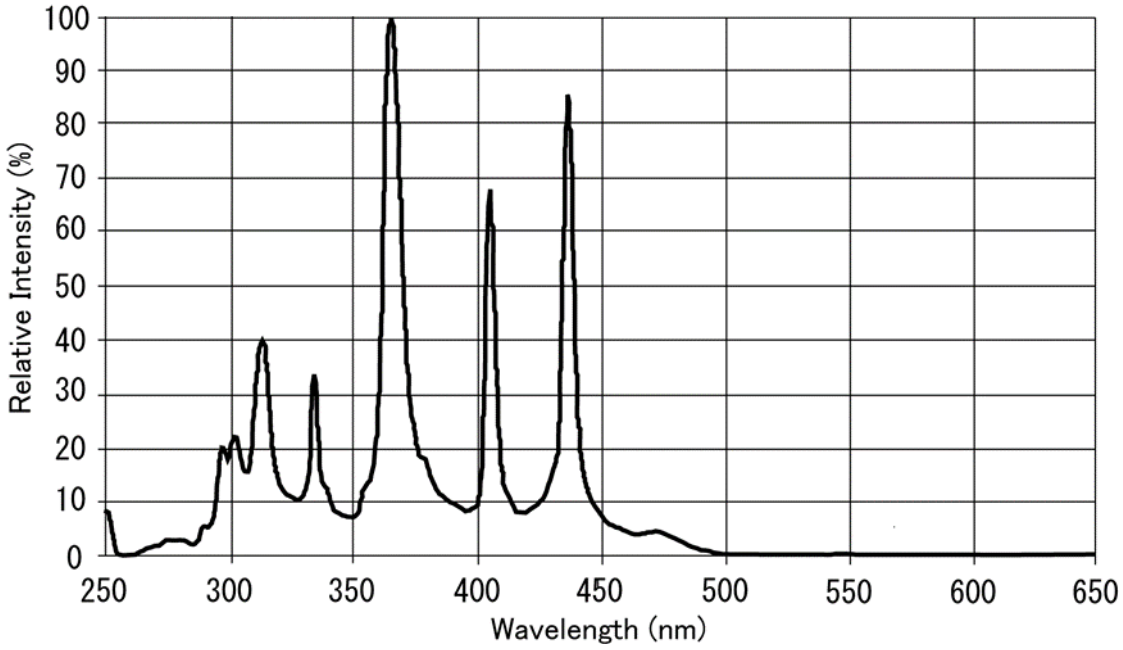

Figure 2-2. Lamp spectra of Omni Cure S1500.

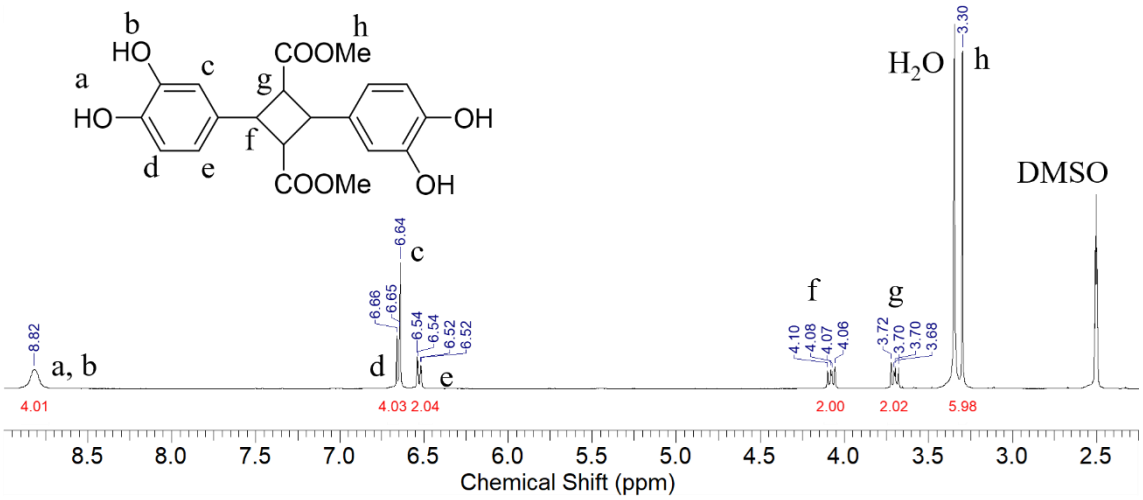

Figure 2-3. ^{1}H NMR spectrum (400 MHz, DMSO-d_6) of 34THTA-Me.

Synthesis of 3,3′,4,4′-Tetrahydroxy-*α*-truxillic Acid (34THTA). To a 2 M aqueous solution of sodium hydroxide (75 mL), 34THTA-Me (19.0 g, 48.9 mmol) was added. The reaction mixture was stirred at 60 °C for 15 h under a nitrogen atmosphere then was cooled to room temperature. The reaction mixture was acidified with concentrated hydrochloric acid then was extracted using ethyl acetate, and the extract was washed with water. The organic portion was dried over $MgSO_4$. After evaporating the solvent, the product was dried under reduced pressure to give 34THTA as a white solid. Yield, 9.36 g (53%). ^{1}H NMR spectrum is shown in Figure 2-4. ^{1}H NMR (400 MHz, DMSO-d_6) : δ (ppm) 3.56 (dd, 2H, J = 10.4, 7.2 Hz, CH), 4.01 (dd, 2H, J = 10.2, 7.3 Hz, CH), 6.55 (dd, 2H, J = 8.2, 2.1 Hz, ArH), 6.64–6.68 (m, 4H, ArH), 8.71 (s, 2H, OH), 8.79 (s, 2H, OH), 11.96 (brs, 2H, COOH). ^{13}C NMR (100 MHz, DMSO-d_6), δ (ppm) 40.5, 46.8, 115.0, 115.3, 118.4, 130.3, 144.0, 144.9, 173.1.

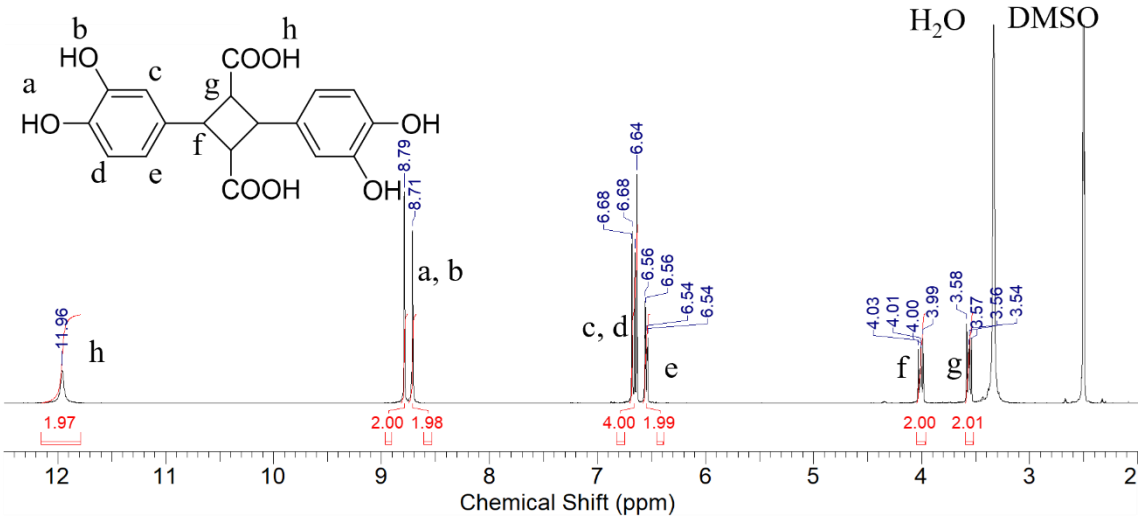

Figure 2-4. ^{1}H NMR spectrum (400 MHz, DMSO-d_6) of 34THTA.

Synthesis of Polyamides from 34THTA and Aliphatic Diamines. A typical polymerization procedure is as follows. To 34THTA (382 mg, 1.06 mmol) and EDA (63.7 mg, 1.06 mmol) placed in a flask under nitrogen atmosphere, DMAc (2.0 mL), triphenyl phosphite (0.71 mL, 2.71 mmol), and pyridine (0.97 mL, 12.0 mmol) ware added. After the reaction mixture was stirred for 24 hours at 60 °C, the reaction mixture was added into methanol (300 mL) to precipitate the polymer. The formed precipitates were filtered then were dried under reduced pressure to give PA-EDA as a light-yellow powder. Yield, 331 mg (81%). Other polyamides from 34THTA and aliphatic diamines such as HMDA and DMDA were synthesized following above methods. Yield, PA-HMDA (90%), PA-DMDA (80%).

Synthesis of Polyamide and Copolyamides from 34THTA, AA, and *α*ATA-Me. A typical polymerization procedure is as follows. To 34THTA (270 mg, 0.75 mmol), AA (36.5 mg, 0.25 mmol), and *α*ATA-Me (354 mg, 1.00 mmol) placed in a flask under nitrogen atmosphere, DMAc (3.0 mL), triphenyl phosphite (0.60 mL, 2.30 mmol), and pyridine (0.97 mL, 12.0 mmol) ware added. After the reaction mixture was stirred for 3 hours at 60 °C, the reaction mixture was added dropwise into methanol (300 mL) to precipitate the polymer. The formed precipitates were filtered then were dried under reduced pressure to give coPA-1 as a white fibril. Yield, 652 mg (96%). Other polyamide

and copolyamides with different charge ratio were synthesized following above methods. Yield, PA-*α*ATA-Me (92%). coPA-2 (94%), and coPA-3 (85%).

Synthesis of Copolyamide from TA, AA, and *α*ATA-Me. To TA (74 mg, 0.25 mmol), AA (110 mg, 0.75 mmol), and *α*ATA-Me (354 mg, 1.00 mmol) placed in a flask under nitrogen atmosphere, DMAc (3.0 mL), triphenyl phosphite (0.60 mL, 2.30 mmol), and pyridine (0.97 mL, 12.0 mmol) ware added. After the reaction mixture was stirred for 3 hours at 60 °C, the reaction mixture was added dropwise into methanol (300 mL) to precipitate the polymer. The formed precipitates were filtered then were dried under reduced pressure to give coPA-TA as a white fibril. Yield, 501 mg (94%).

Film Preparation of Synthesized Polyamides. The polyamide was dissolved in small amount of DMAc then was cast onto a glass plate to obtain a polyimide film.

Preparation of Test Piece Glued by Polyamides for Adhesion Test. Stainless steel (SUS304) and aluminum substrates were purchased from Standard-testpiece Co. Ltd and used as received. Both substrates were 100 mm long, 25 mm wide and 2 mm thick. The bonding area was 12.5 mm long and 25 mm wide. The polyamide film was melted between two substrates at 160 °C and 10 MPa for 5 min using hot press. The bonded test pieces were cooled to room temperate and then were kept under atmospheric conditions.

2.3 Results and Discussion

2.3.1 Synthesis of 3,4-Dihydroxycinnamoyl Dimer, 34THTA

To synthesize 34THTA by solid-state photodimeization, chemical modification of 34DHCA was required because 34DHCA was inert to photodimerization in crystalline state. 34DHCA-Me, which was easily derived from 34DHCA by methyl esterification, was selected for solid-state photodimerization based on previously reported literature regarding to synthesis of 34THTA derivative.[19] For the synthesis of 34THTA-Me, the photodimerization of 34DHCA-Me was carried out in the crystalline-state with ultraviolet light irradiation. From ^{1}H NMR measurement, the olefin signals of the 34DHCA-Me at 6.29 and 7.51 ppm disappeared, while the cyclobutane signals of the objective products, 34THTA-Me, appeared at 3.70 and 4.08 ppm (Figure 2-3). After 99% conversion was achieved monitored by NMR, the suspended crystals were collected. The 34THTA-Me was then converted into 34THTA by a simple hydrolysis and further acidification (Scheme 2-2). The molecular structure of the 34DHCA-Me, 34THTA-Me, and 34THTA were identified by NMR spectroscopy (Figure 2-1, 2-3, 2-4).

Scheme 2-2. Synthetic Route of the 34THTA

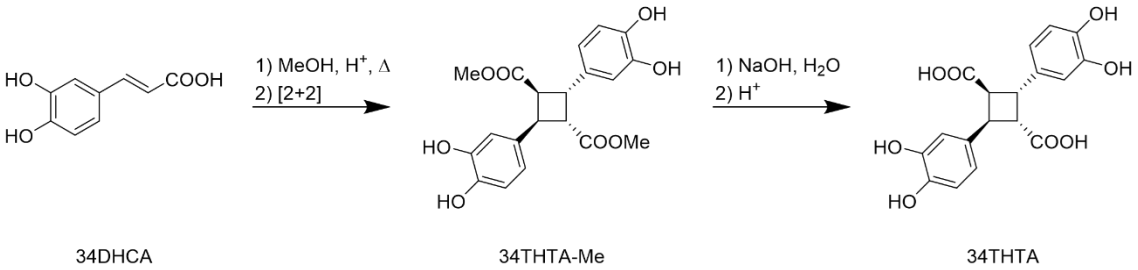

34DHCA 34THTA-Me 34THTA

2.3.2 Synthesis of 34THTA-based Adhesive Polyamides and Copolyamides

34THTA-based polyamides and copolyamides (PAs and coPAs) were synthesized by a conventional polymerization process using pyridine and tripheylphosphite (Scheme 2-3). When the 34THTA was polycondensed with aliphatic diamine (e.g., EDA and DMDA), the polyamides were precipitated during the polymerization process, presumably due to high reactivity of aliphatic diamines. On the other hand, PA-*α*ATA-Me synthesized from two kinds of *α*-type cinnamoyl dimers, 34THTA and *α*ATA-Me, exhibited good solubility in DMAc during polymerization (Scheme 2-3a). Thus, *α*ATA-Me was used as diamine component for further study on 34THTA-based adhesive materials by copolymerization.

Scheme 2-3. Synthetic Route of the (a) PAs from 34THTA and Aliphatic/aromatic Diamine, (b) CoPAs from 34THTA, *α*ATA-Me, and AA, (c) CoPA from TA, *α*ATA-Me, and AA

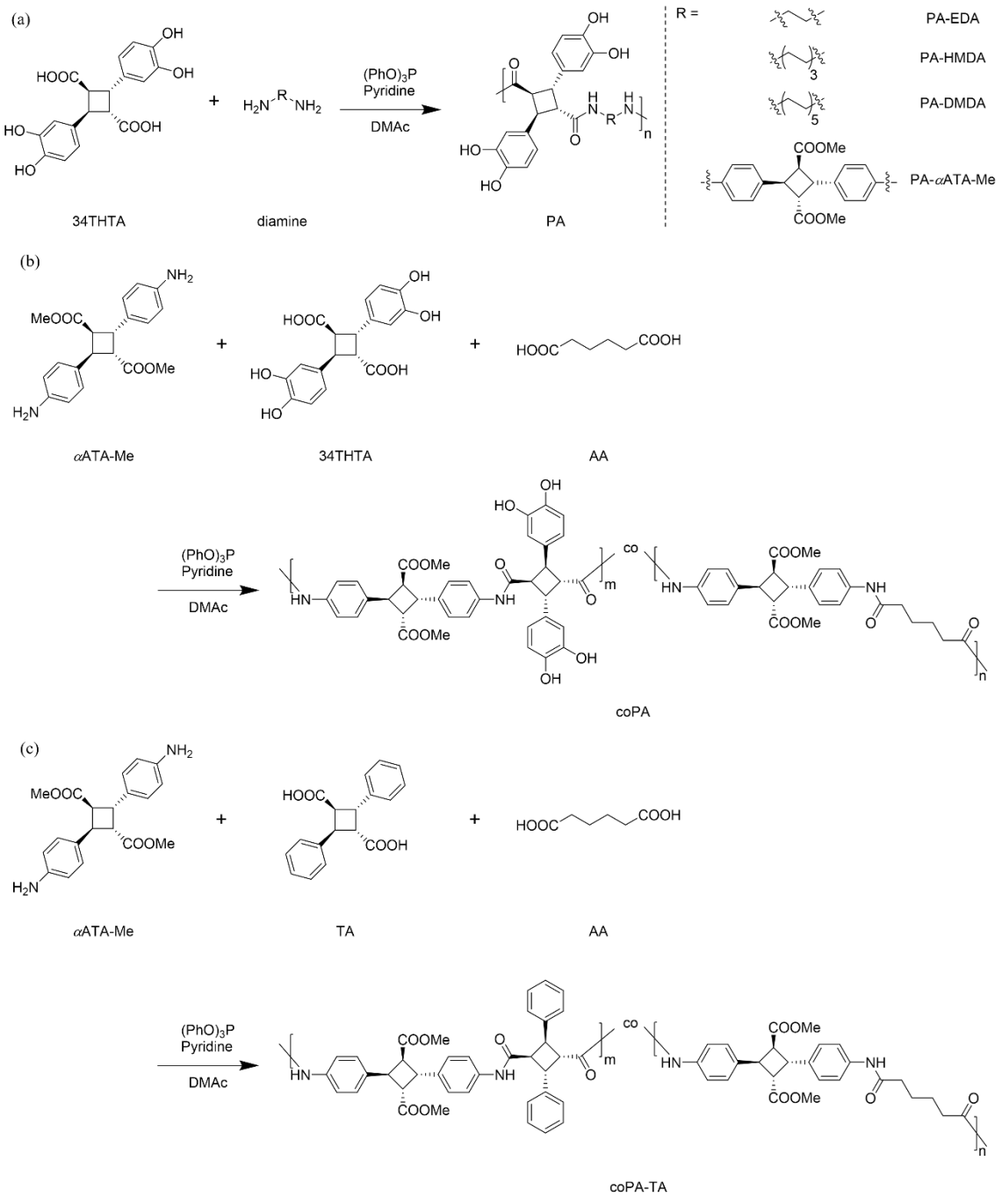

The PA-*α*ATA-Me had a rigid ring-connected backbone, which may cause hard and brittle properties. To improve flexibility of 34THTA-based polyamides, copolymerization with flexible aliphatic dicarboxylic acid, AA, which is well-known as monomers for nylon 6,6, was carried out (Scheme 2-3b). In addition, to evaluate adhesive properties based on catechol groups, coPA-TA without catechol groups was synthesized from *α*ATA-Me, AA, and TA instead of 34THTA for comparison (Scheme 2-3c).

The ^{1}H NMR spectra of synthesized PA-*α*ATA-Me and coPAs showed the main chain proton signals for amide, aromatics, cyclobutanes, and aliphatic chains at ~9.8 ppm, 7.6–7.1 ppm, 4.2–3.8 ppm and 2.4–1.6 ppm respectively (Figure 2-5). In addition, the proton signals at ~8.6 ppm and 6.7–6.5 ppm were assigned as hydroxy groups and aromatics in side chain, respectively. The NMR spectroscopy results clearly indicated that the expected PA and coPAs were synthesized.

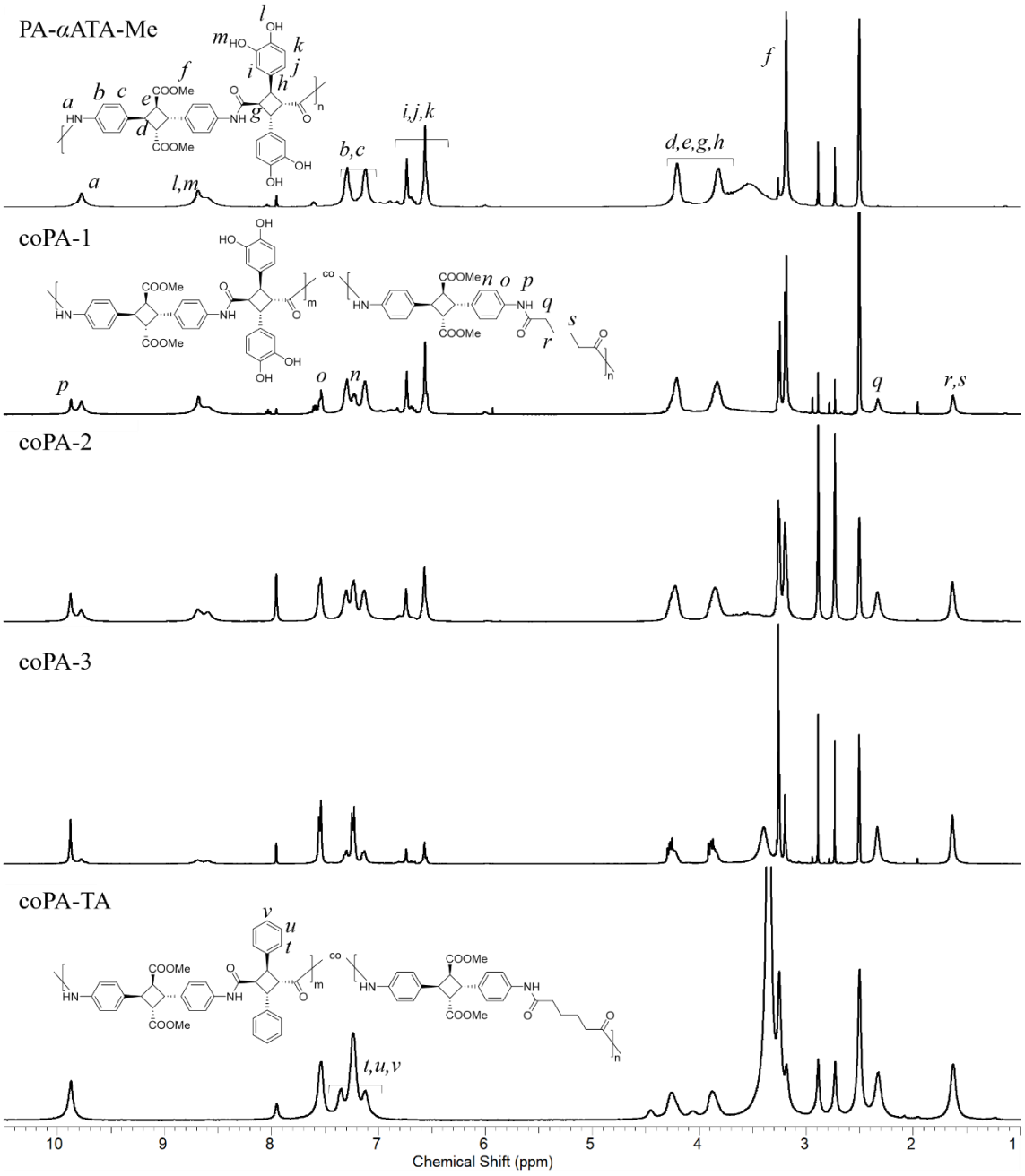

Figure 2-5. ^{1}H NMR spectra (400 MHz, DMSO-d_6) of synthesized PA-αATA-Me and coPAs.

The number-average molecular weight (M_n), weight-average molecular weight (M_w), and molecular weight distribution (M_w/M_n) of the synthesized PA-αATA-Me and coPAs were determined by SEC measurements (Table 2-1, SEC traces are shown in Figure 2-6). The synthesized PA-αATA-Me and coPAs showed M_ws ranging from 50000 to 544000 and M_w/M_n ranging from 3.10 to 9.79. In the case of long polymerization time, these polyamides were easily formed gels with the increasing molecular weight. To avoid such gelation, the polymerization was stopped before beginning of the gelation, resulted in wide range of M_w/M_n.

Table 2-1. Molecular weights of the synthesized polyamides and copolyamides[a]

polyamide	[αATA-Me]$_0$/[34THTA]$_0$/[AA]$_0$/[TA]$_0$	M_n	M_w	M_w/M_n
PA-αATA-Me	1/1/0/0	20000	76000	3.93
coPA-1	1/0.75/0.25/0	11000	50000	4.56
coPA-2	1/0.5/0.5/0	47000	460000	9.79
coPA-3	1/0.25/0.75/0	30000	93000	3.10
coPA-TA	1/0/0.75/0.25	81000	544000	6.73

[a] The weight-average molecular weight, M_w, the number-average molecular weight, M_n, and the molecular weight distribution, M_w/M_n, of polyimides were determined by SEC; eluent, 0.01 M LiBr in DMF; flow rate, 1.0 mL min^{-1}; standards, PMMA standards.

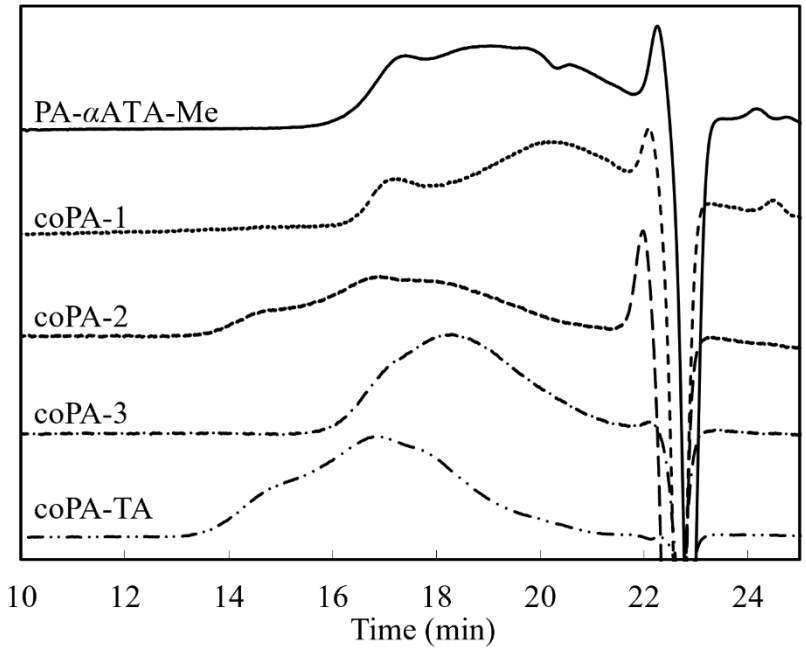

Figure 2-6. SEC traces of the synthesized polyamides (solvent, 0.01 M LiBr in DMF; flow rate, 1.0 mL min^{-1}).

The weight loss temperature (5% weight loss temperature, T_{d5}, and 10% weight loss temperature, T_{d10}) and glass transition temperature (T_g) of the synthesized polyamides were evaluated by TGA (Figure 2-7) and DSC (Figure 2-8), respectively. From Table 2-2, the synthesized polyamides exhibited high stability against thermal degradation of T_{d5} and T_{d10} values ranging 295 to 350 °C and 335 to 365 °C, respectively. In the case of coPA-3 and coPA-TA, the T_g was observed in 195 and 185 ºC, respectively. On the other hand, T_g of other polyamides was not determined. This DSC results indicated that the T_g was decreased because the flexibility of polymer chains was improved with increasing AA composition.

Table 2-2. Thermal properties of the synthesized polyamides

polyamide	[αATA-Me]$_0$/[34THTA]$_0$/[AA]$_0$/[TA]$_0$	T_{d5} (ºC)[a]	T_{d10} (ºC)[a]	T_g (ºC)[b]
PA-αATA-Me	1/1/0/0	295	335	ND
coPA-1	1/0.75/0.25/0	330	355	ND
coPA-2	1/0.5/0.5/0	315	345	ND
coPA-3	1/0.25/0.75/0	315	340	195
coPA-TA	1/0/0.75/0.25	350	365	185

[a] 5% weight loss temperature, T_{d5}, and 10% weight loss temperature, T_{d10}, were obtained from TGA curve scanned at a heating rate of 10 ˚C min^{-1} under a nitrogen atmosphere. [b] Glass transition temperature, T_g, was measured by DSC thermogram scanned at a heating rate of 10 ˚C min^{-1} under a nitrogen atmosphere. ND refers to not determined.

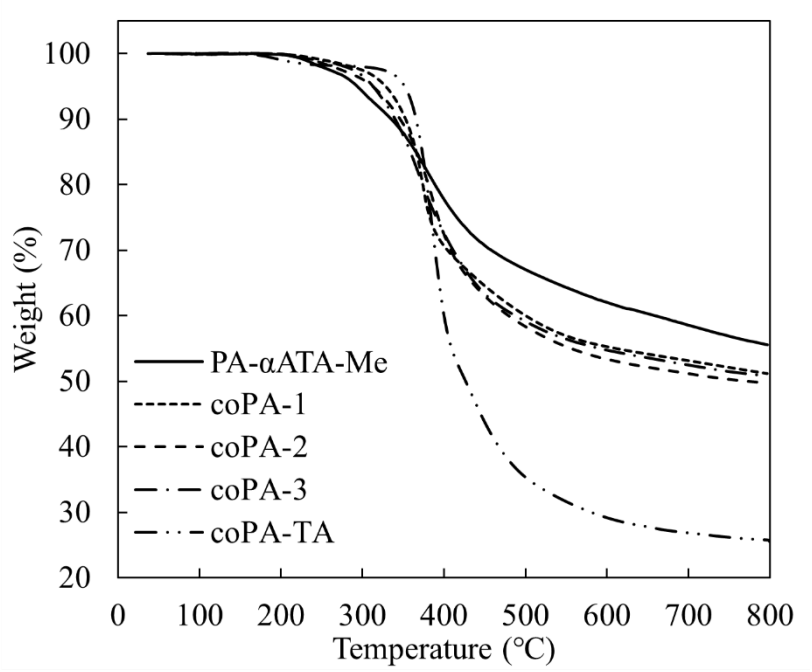

Figure 2-7. TGA curves of synthesized polyamides.

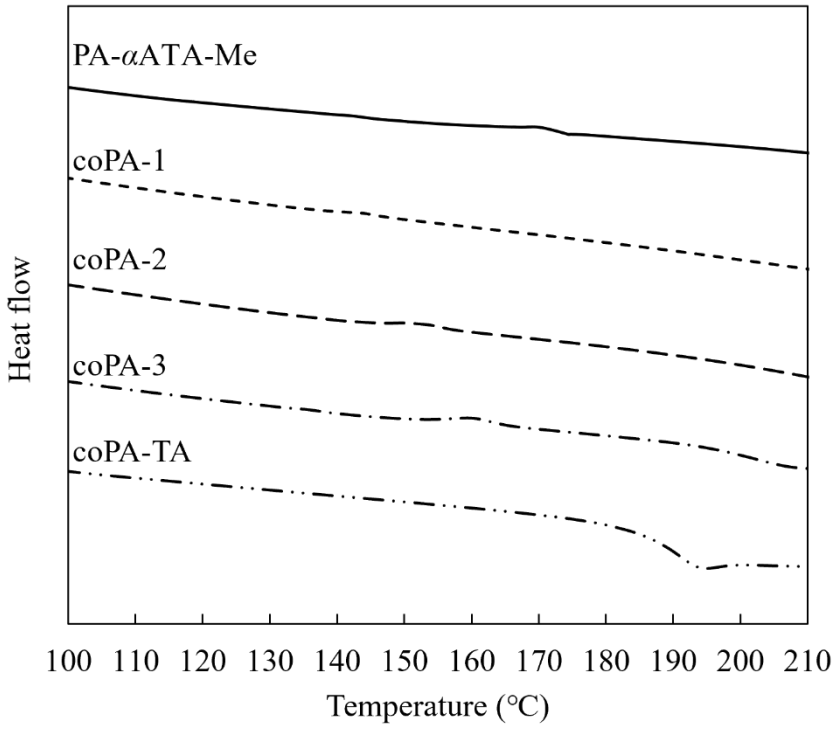

Figure 2-8. DSC curves of synthesized polyamides.

2.3.3 Solubility Test of Synthesized Polyamides

The solubility of the synthesized polyamides was evaluated by dissolving them in four groups of solvents: (1) nonpolar solvents such as hexane; (2) polar aprotic solvents such as DMF, DMAc, NMP, DMSO, THF, and chloroform; (3) polar protic solvents such as distilled water, and methanol; and (4) strong acids such as concentrated sulfuric acid (Table 2-3). All polyamides were soluble in the DMF, DMAc, NMP, DMSO, and sulfuric acid. However, these solvents were unsuitable to use as adhesive solution due to low volatility and toxicity.[20]

Table 2-3. Solubility of the Synthesized Polyamides[a]

solvent	PA-αATA-Me	coPA-1	coPA-2	coPA-3	coPA-TA
n-hexane	−	−	−	−	−
chloroform	−	−	−	−	−
water	−	−	−	−	−
methanol	−	−	−	−	−
tetrahydrofuran	−	−	−	−	−
N,N-dimethylformamide	+	+	+	+	+
N,N-dimethylacetamide	+	+	+	+	+
N-methyl-2-pyrrolidone	+	+	+	+	+
dimethyl sulfoxide	+	+	+	+	+
conc. sulfuric acid	+	+	+	+	+

[a] The solubility was evaluated under the condition of 2 mg-polyamide/1 mL-solvent at 25 °C. + refers to soluble, and − refers to insoluble.

2.3.4 Film Preparation of the Synthesized Polyamides

The polyamide films were prepared by solution casting on glass plates after dissolution in DMAc. As a result, films for all the synthesized polyamides were fabricated with high transparency (Figure 2-9).

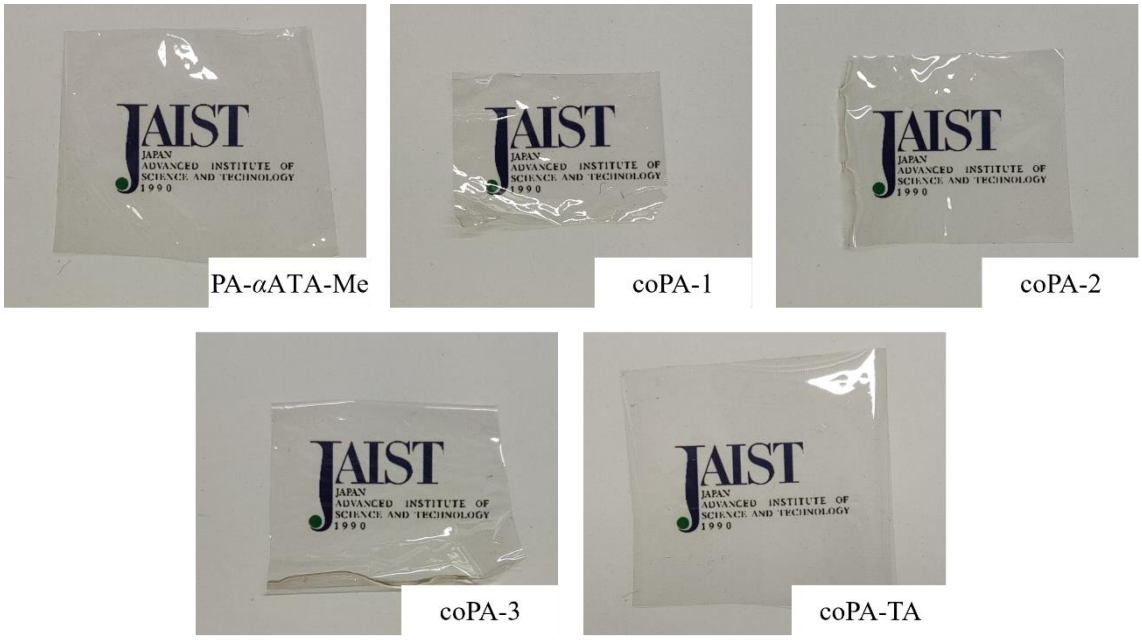

Figure 2-9. Appearance of polyamide films casted over DMAc.

The mechanical properties of the polyamide films were evaluated by a tensile tester to determine their Young's modulus, tensile strength at break, and elongation at break (Table 2-4, stress−strain curves are shown in Figure 2-10). The polyamide films exhibited Young's modulus, tensile strength, and elongation at break in the range of 0.6–1.0 GPa, 15–53 MPa, and 5.2–13.1%, respectively. In particular, the coPAs showed a

tendency to increase elongation at break with increasing AA composition, indicating that toughness of polyamides was enhanced.

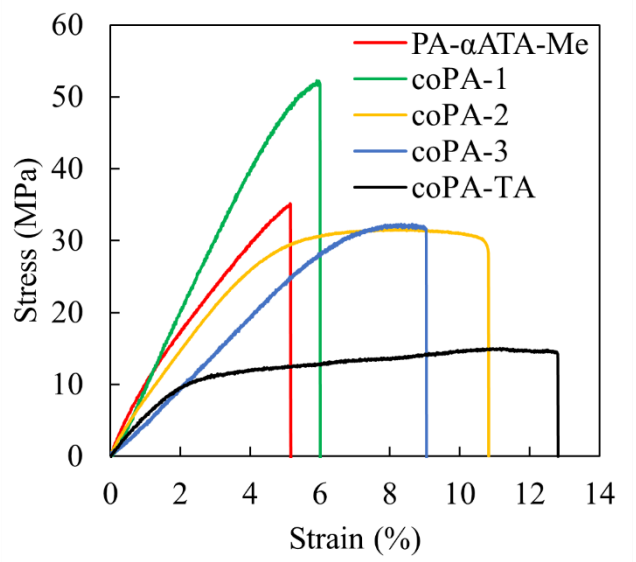

Figure 2-10. Stress-strain curves of polyamide films.

The contact angle of the polyamide films was evaluated by sessile drop method (Table 2-4). The contact angle of the polyamide films was in the range of 72–86˚. With the increasing AA composition in the 34THTA-based coPAs, the contact angle was increased due to increasing hydrophobic aliphatic chain component. The contact angle of coPA-3 bearing catechol groups was 86, which was larger than the coPA-TA without the catechol groups. This is because the 34THTA unit was minor component in the coPA-3, and thus, there was no effect on the contact angle.

Table 2-4. Mechanical properties, contact angle and softening temperature of the polyamide films

polyamide	$[\alpha ATA\text{-}Me]_0/[34THTA]_0/[AA]_0/[TA]_0$	Young's modulus[a] (GPa)	tensile strength[a] (MPa)	elongation at break[a] (%)	contact angle (º)	T_s[b] (ºC)
PA-αATA-Me	1/1/0/0	0.9 ± 0.1	35 ± 0.8	5.2 ± 0.5	72	127
coPA-1	1/0.75/0.25/0	1.0 ± 0.2	53 ± 3.8	7.3 ± 0.7	78	111
coPA-2	1/0.5/0.5/0	1.0 ± 0.1	34 ± 1.5	9.7 ± 3.4	79	115
coPA-3	1/0.25/0.75/0	0.6 ± 0.1	35 ± 1.6	10.5 ± 2.3	86	117
coPA-TA	1/0/0.75/0.25	0.7 ± 0.1	15 ± 0.3	13.1 ± 0.3	79	110

[a] Young's modulus, tensile strength, and elongation at break were obtained from a tensiometer at room temperature. [b] Softening temperature, T_s was obtained from TMA curve scanned at a heating rate of 5 °C min^{-1} under a nitrogen atmosphere.

The softening temperature (T_s) of the polyamide films was evaluated by TMA (Table 2-4, TMA curves are shown in Figure 2-11). All of the coPAs exhibited similar T_s values ranging from 110 to 117 ºC. This result indicated that the ratio of the AA component has negligible effects on T_s of the synthesized polyamide films. On the other hand, the PA-*α*ATA-Me without AA component showed slightly higher T_s value of 127 ºC. In addition, the PA-*α*ATA-Me film was shrunk with temperature increasing. This is because orientation of the rigid PA-*α*ATA-Me chains was eliminated by thermal treatment.

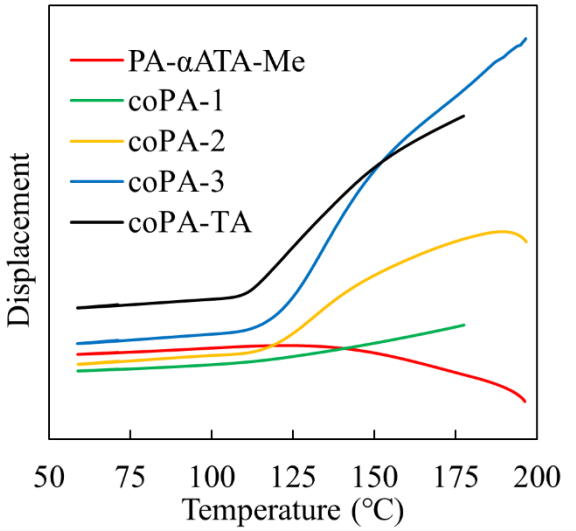

Figure 2-11. TMA curves of polyamide films.

2.3.5 Adhesive Test of the Synthesized Polyamides

To evaluate adhesive property of synthesized 34THTA-based polyamides, tensile test of the two kinds of substrates which were glued by each 34THTA-based polyamide, was carried out. The bonded substrates were pulled in opposite directions to evaluate adhesive shear strength for each substrate (Table 2-5, stress−strain curves are shown in Figure 2-12). For comparison, coPA-TA, which was synthesized from TA instead of 34THTA, was also evaluated to clarify effect of catechol groups. From Table 2-5, adhesive shear strength of synthesized 34THTA-based polyamides for stainless steel and aluminum substrates were ranged in 2.5–7.1 MPa and 1.6–5.3 MPa, respectively. In particular, coPA-3 exhibited adhesive shear strength of 7.1 MPa for stainless steel substrate. This value was matched to expected performance of conventional instant superglue, 2–8 MPa,[21] indicated that coPA-3 portrayed strong adhesive property. On the other hand, adhesive shear strengths of coPA-TA were ~0 MPa for each substrate. This results clearly indicated that strong adhesive property of 34THTA-based polyamides was caused by catechol groups in polymer side chain. In addition, with increasing AA composition, 34THTA-based polyamides exhibited tendency to increase adhesive shear strength. This result presumably caused by toughness of adhesive materials as mentioned above.

Table 2-5. Adhesive shear strength of the synthesized polyamides

polyamide	[αATA-Me]$_0$/[34THTA]$_0$/[AA]$_0$/[TA]$_0$	adhesive shear strength (MPa)[a]	
		stainless steel (SUS304)	aluminum
PA-αATA-Me	1/1/0/0	3.6	1.6
coPA-1	1/0.75/0.25/0	2.5	4.6
coPA-2	1/0.5/0.5/0	5.0	4.6
coPA-3	1/0.25/0.75/0	7.1	5.3
coPA-TA	1/0/0.75/0.25	0.3	0.1

[a] Adhesive shear strength was obtained from a tensiometer at room temperature.

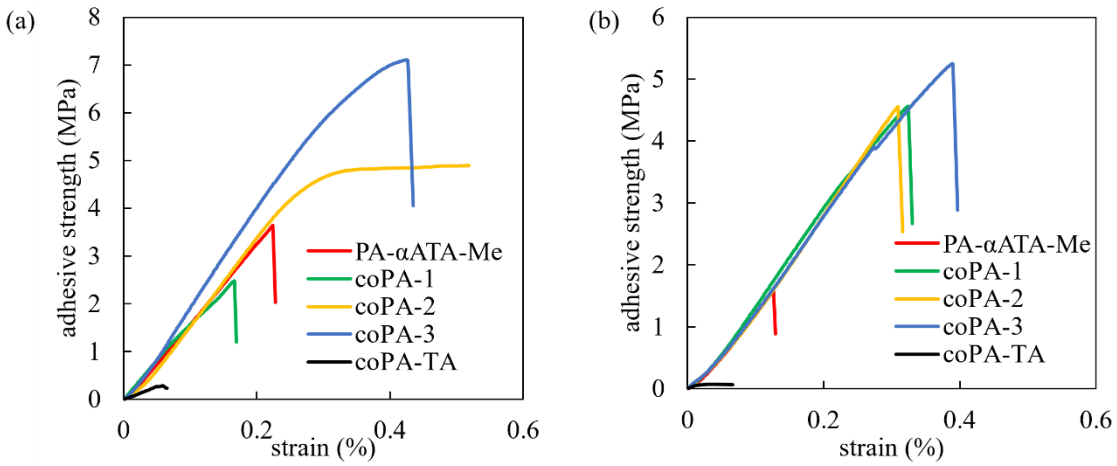

Figure 2-12. Stress−strain curves of different substrates glued by 34THTA-based polyamide films, (a) stainless steel and (b) aluminum.

The fracture surfaces of pulled specimens are shown in Figure 2-13. In the case of PA-*α*ATA-Me used as adhesive materials, fracture was occurred between adhesive and surface of the test piece (adhesion failure). This result presumably caused by shrink of the PA-*α*ATA-Me film during thermal treatment as mentioned above. On the other hand, fracture of the specimens glued by coPA-3 with flexible aliphatic components and small amount of 34THTA moieties was occurred in adhesives (cohesive failure). Hence, in the 34THTA-based polyamides, only 0.25 mole equivalent of 34THTA unit to 1 mole of diamine component was enough to adhere metal surfaces.

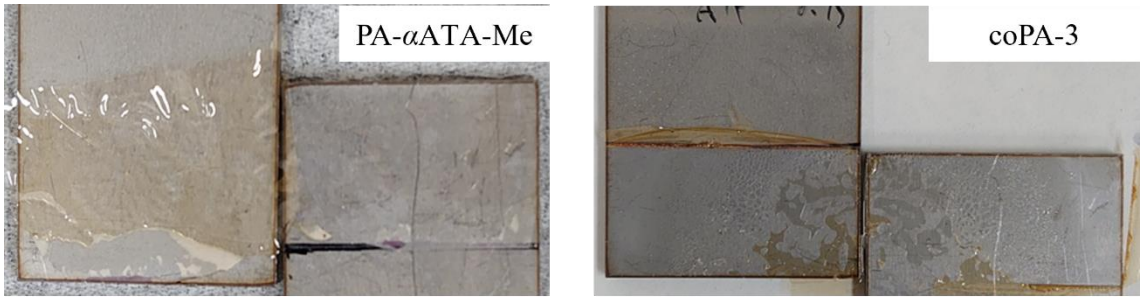

Figure 2-13. Appearance of fractured surfaces after tensile test glued by PA-*α*ATA-Me and coPA-3.

2.3.6 Photodegradability of the Synthesized Polyamide, PA-*α*ATA-Me

As mentioned above, since the 34THTA-based polyamides have photodegradable cyclobutane ring in polymer backbone, application for the degradable adhesive polymer materials is expected. To evaluate photodegradability of PA-*α*ATA-Me which synthesized from two kinds of cinnamoyl dimers, 34THTA and *α*ATA-Me, ultraviolet light with a main wavelength of 254 nm was irradiated to PA-*α*ATA-Me (Scheme 2-4). The photodegradation was monitored by ^{1}H NMR spectroscopy (Figure 2-14). With the increase of irradiation time, broad signals around 7.4–6.5 ppm and 4.3–3.8 ppm, assigned as aromatics and cyclobutanes of PA-*α*ATA-Me, respectively, became weaker. In addition, new signals of degradation products were appeared around 10 ppm and 7.7–6.5 ppm, assigned as amide, aromatics and double bonds, respectively. This NMR study clearly indicated that cleavage of cyclobutane rings was proceeded by ultraviolet light irradiation. Thus, 34THTA-based polyamides including PA-*α*ATA-Me showed potential to use high-performance photodegradable adhesives.

Scheme 2-4. Photodegradation of PA-*α*ATA-Me

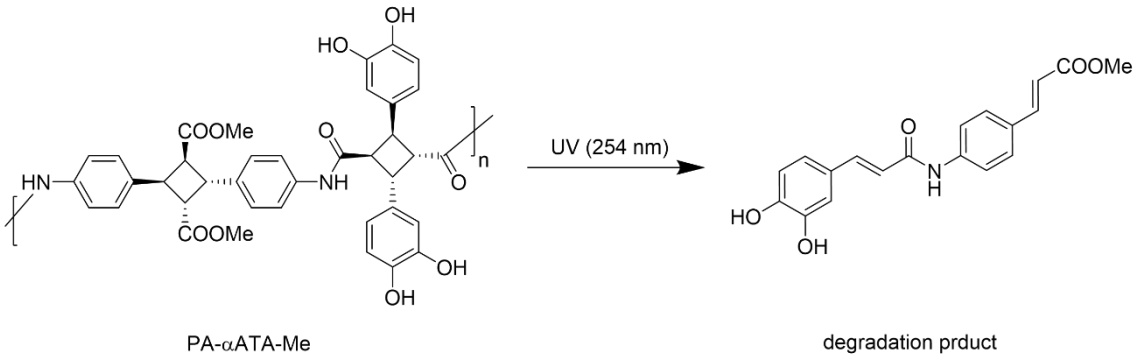

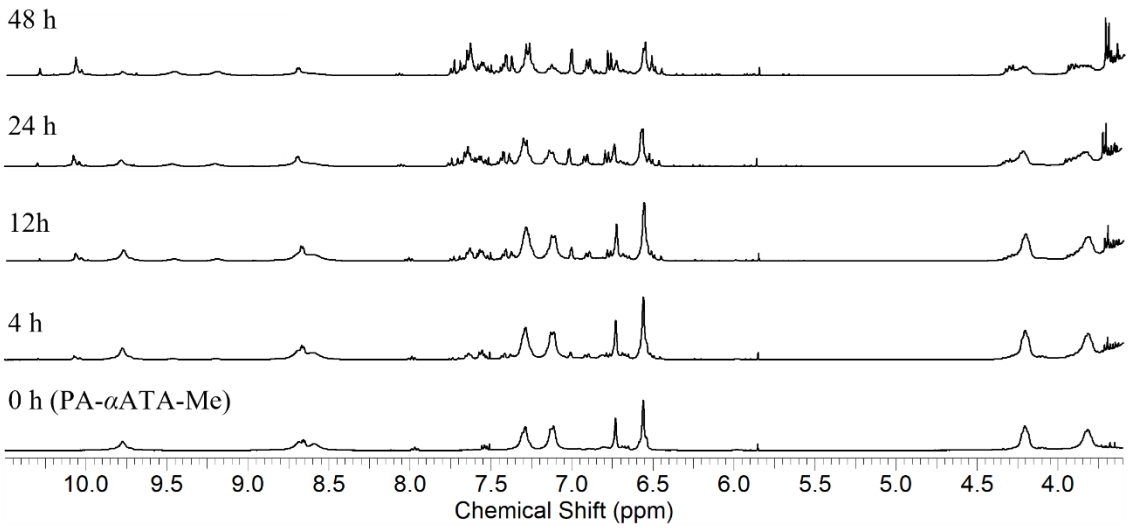

Figure 2-14. Change of ^{1}H NMR spectra (400 MHz, DMSO-d_6) of PA-*α*ATA-Me by ultraviolet light irradiation.

2.4 Conclusions

34THTA was synthesized from 34DHCA-Me by solid-state photodimerization and further hydrolysis of methyl esters. The obtained dimer was polymerized with aliphatic/aromatic diamines and AA to synthesize adhesive polyamides. All of the obtained 34THTA-based polyamides showed high thermostability, with T_{d10} of ~355 °C, and fabricated to transparent films by solution casting. From the tensile test of metal substrate glued by synthesized polyamides, copolyamide from 34THTA, *α*ATA-Me and AA, exhibited strong adhesive properties for stainless substrate of ~7 MPa, matched to conventional instant superglue. Furthermore, PA-*α*ATA-Me, synthesized from 34THTA and *α*ATA-Me, exhibited photo-induced degradation by cleavage of cyclobutane rings in the main chain. In the present study, 34THTA-based polyamides with high thermostability, strong adhesive property, and photodegradability were prepared. These properties can only be realized by rigid and photoreactive cinnamoyl dimer skeleton, which is an essential component of this study. This research provides insights into the molecular design of mussel-mimetic high-performance adhesive polymers with photodegradability.

2.5 References and Notes

(1) Lin, Q.; Gourdon, D.; Sun, C.; Holten-Andersen, N.; Anderson, T. H.; Waite, J. H.; Israelachvili, J. N. Adhesion Mechanisms of the Mussel Foot Proteins Mfp-1 and Mfp-3. *Proc. Natl. Acad. Sci. U. S. A.* **2007**, *104* (10), 3782–3786. https://doi.org/10.1073/pnas.0607852104.

(2) Waite, J. H.; Tanzer, M. L. Polyphenolic Substance of Mytilus Edulis: Novel Adhesive Containing L-Dopa and Hydroxyproline. *Science (80-.).* **1981**, *212* (4498), 1038–1040. https://doi.org/10.1126/science.212.4498.1038.

(3) Waite, J. H. Nature's Underwater Adhesive Specialist. *Int. J. Adhes. Adhes.* **1987**, *7* (1), 9–14. https://doi.org/10.1016/0143-7496(87)90048-0.

(4) Yu, M.; Hwang, J.; Deming, T. J. Role of 1-3,4-Dihydroxyphenylalanine in Mussel Adhesive Proteins. *J. Am. Chem. Soc.* **1999**, *121* (24), 5825–5826. https://doi.org/10.1021/ja990469y.

(5) North, M. A.; Del Grosso, C. A.; Wilker, J. J. High Strength Underwater Bonding with Polymer Mimics of Mussel Adhesive Proteins. *ACS Appl. Mater. Interfaces* **2017**, *9* (8), 7866–7872. https://doi.org/10.1021/acsami.7b00270.

(6) Guo, Q.; Chen, J.; Wang, J.; Zeng, H.; Yu, J. Recent Progress in Synthesis and Application of Mussel-Inspired Adhesives. *Nanoscale* **2020**, *12* (3), 1307–1324.

https://doi.org/10.1039/c9nr09780e.

(7) Lee, S. B.; González-Cabezas, C.; Kim, K. M.; Kim, K. N.; Kuroda, K. Catechol-Functionalized Synthetic Polymer as a Dental Adhesive to Contaminated Dentin Surface for a Composite Restoration. *Biomacromolecules* **2015**, *16* (8), 2265–2275. https://doi.org/10.1021/acs.biomac.5b00451.

(8) Li, Y.; Cheng, J.; Delparastan, P.; Wang, H.; Sigg, S. J.; DeFrates, K. G.; Cao, Y.; Messersmith, P. B. Molecular Design Principles of Lysine-DOPA Wet Adhesion. *Nat. Commun.* **2020**, *11* (1), 1–8. https://doi.org/10.1038/s41467-020-17597-4.

(9) Longe, L.; Garnier, G.; Saito, K. Synthesis of Lignin-Based Phenol Terminated Hyperbranched Polymer. *Molecules* **2019**, *24* (20), 1–9. https://doi.org/10.3390/molecules24203717.

(10) Ishii, D.; Iwata, T. Synthesis, Characterization and Fiber Spinning of Poly(Caffeic Acid). *J. Fiber Sci. Technol.* **2019**, *75* (11), 181–185. https://doi.org/10.2115/fiberst.2019-0021.

(11) Fonseca, A. C.; Lima, M. S.; Sousa, A. F.; Silvestre, A. J.; Coelho, J. F. J.; Serra, A. C. Cinnamic Acid Derivatives as Promising Building Blocks for Advanced Polymers: Synthesis, Properties and Applications. *Polym. Chem.* **2019**, *10* (14),

1696–1723. https://doi.org/10.1039/c9py00121b.

(12) Zhang, C.; Bai, Y.; Liu, W. Reversible Adhesives Based on Acrylate Copolymer Modified by Caffeic Acid Containing Boroxin. *J. Appl. Polym. Sci.* **2020**, *137* (20), 1–12. https://doi.org/10.1002/app.48703.

(13) Wang, S.; Kitamura, Y.; Hiraishi, N.; Taira, S.; Tsuge, A.; Kaneko, T.; Kaneko, D. Preparation of Mussel-Inspired Biopolyester Adhesive and Comparative Study of Effects of Meta- or Para-Hydroxyphenylpropionic Acid Segments on Their Properties. *Polymer (Guildf).* **2019**, *165* (September 2018), 152–162. https://doi.org/10.1016/j.polymer.2019.01.012.

(14) Kaneko, T.; Thi, T. H.; Shi, D. J.; Akashi, M. Environmentally Degradable, High-Performance Thermoplastics from Phenolic Phytomonomers. *Nat. Mater.* **2006**, *5* (12), 966–970. https://doi.org/10.1038/nmat1778.

(15) Kaneko, D.; Kinugawa, S.; Matsumoto, K.; Kaneko, T. Terminally-Catecholized Hyper-Branched Polymers with High Performance Adhesive Characteristics. *Plant Biotechnol.* **2010**, *27* (3), 293–296. https://doi.org/10.5511/plantbiotechnology.27.293.

(16) Tateyama, S.; Masuo, S.; Suvannasara, P.; Oka, Y.; Miyazato, A.; Yasaki, K.; Teerawatananond, T.; Muangsin, N.; Zhou, S.; Kawasaki, Y.; Zhu, L.; Zhou, Z.;

Takaya, N.; Kaneko, T. Ultrastrong, Transparent Polytruxillamides Derived from Microbial Photodimers. *Macromolecules* **2016**, *49* (9), 3336–3342. https://doi.org/10.1021/acs.macromol.6b00220.

(17) Suvannasara, P.; Tateyama, S.; Miyasato, A.; Matsumura, K.; Shimoda, T.; Ito, T.; Yamagata, Y.; Fujita, T.; Takaya, N.; Kaneko, T. Biobased Polyimides from 4-Aminocinnamic Acid Photodimer. *Macromolecules* **2014**, *47* (5), 1586–1593. https://doi.org/10.1021/ma402499m.

(18) Pattabiraman, M.; Kaanumalle, L. S.; Natarajan, A.; Ramamurthy, V. Regioselective Photodimerization of Cinnamic Acids in Water: Templation with Cucurbiturils. *Langmuir* **2006**, *22* (18), 7605–7609. https://doi.org/10.1021/la061215a.

(19) Wang, Z.; Flores, Q.; Guo, H.; Trevizo, R.; Zhang, X.; Wang, S. Crystal Engineering Construction of Caffeic Acid Derivatives with Potential Applications in Pharmaceuticals and Degradable Polymeric Materials. *CrystEngComm* **2020**, *22* (45), 7847–7857. https://doi.org/10.1039/d0ce01403f.

(20) Barry, C. P.; Morose, G. J.; Begin, K.; Atwater, M.; Hansen, C. J. The Identification and Screening of Lower Toxicity Solvents for Contact Adhesives. *Int. J. Adhes. Adhes.* **2017**, *78* (June), 174–181.

https://doi.org/10.1016/j.ijadhadh.2017.06.022.

(21) Kaneko, D.; Wang, S.; Matsumoto, K.; Kinugawa, S.; Yasaki, K.; Chi, D. H.; Kaneko, T. Mussel-Mimetic Strong Adhesive Resin from Bio-Base Polycoumarates. *Polym. J.* **2011**, *43* (10), 855–858. https://doi.org/10.1038/pj.2011.77.

Chapter 3

Syntheses and Polymerizability of Isomeric 4-Aminocinnamoyl Dimers with Different Bending Angles

3.1 Introduction

Physicochemical properties of polymer materials are affected by backbone architectures. Bending structure which is one of the well-known backbone architectures, affects several physicochemical properties such as solubility,[1–3] electric properties,[4] thermal properties,[5–7] and mechanical properties.[8] Various kinds of bending structures including conventional bending linkages, such as –O–, –S–, $–CH_2–$, S=O, and SO_2, have been introduced in polymer backbone to control properties. However, these bending linkages are not suitable to investigate effects of bending angles on polymer properties because polymer chains bearing these linkages are possible to take various conformations due to the high flexibility. Hence, to clarify effects of bending angles on polymer properties, rigid and fixed bending architectures are required.

A typical example of such rigid and fixed bending architecture is *meta*-, and *ortho*-substituted benzenes. When these substituted benzenes are used as building block, bending structures with angles of 60° and 120°, respectively, are introduced in polymer backbones. Among them, *meta*-substituted benzenes such as *meta*-phenylenediamine have been used for controlling polymer properties.[2,9]On the other hand, since *ortho*-substituted benzene monomers are generally difficult to polymerize due to steric hindrance, effects of acute bending angles in the main chain on polymer properties are

not investigated yet. In addition, effects of other bending angles are rarely conducted, resulted in the effects on the properties of bending angles are not clear enough.

Cinnamic acid can undergo solid-state photodimerization, a form of topochemical reaction, to afford rigid photodimers, truxillic acids and truxinic acids.[10–12] Schmidt and co-workers have reported that three types of molecular packing in the crystalline state (i.e., α-, β-, and γ-form) afford two types of isomeric cinnamoyl dimers by UV-assisted [2+2]cycloaddition; α- and β-form crystals afford α-type truxillic acid and β-type truxinic acid as cinnamoyl photodimers, respectively, while γ-form crystals are inert to photodimerization.[13–15] Since the structure of the products depends on the molecular arrangement in the crystals, it is possible to selectively synthesize stereospecific photodimers by controlling the molecular packing in the crystals of the original cinnamate derivatives. To accomplish this, researchers have attempted to control the molecular packing in the crystals by evaluating the substituent effects of cinnamic acid derivatives,[15] solvent effects, and crystallization rate.[16,17] However, since cinnamoyl crystals are generally α-form crystals, systematic studies regarding the control of molecular packing in these crystals are rarely conducted. A few studies on the photodimerization of 4-aminocinnamic acid (4ACA),which afford α-type truxillic acids, have been reported.[15,18,19] On the other hand, truxinic acid derivatives such as β- and δ-

type derivatives with bending structures are suitable candidates for the introduction of rigid bending architecture to polymer chains.

In this chapter, the author focused on isomeric 4ACA photodimers with rigid bending structures, which were selectively photodimerized from molecular packing-controlled crystals of the 4ACA derivatives by introducing substituent groups to be used as diamine and dicarboxylic acid monomers for the synthesis and evaluation of polyamides with different bending angles to clarify the effects on the properties of each angle (Scheme 3-1).

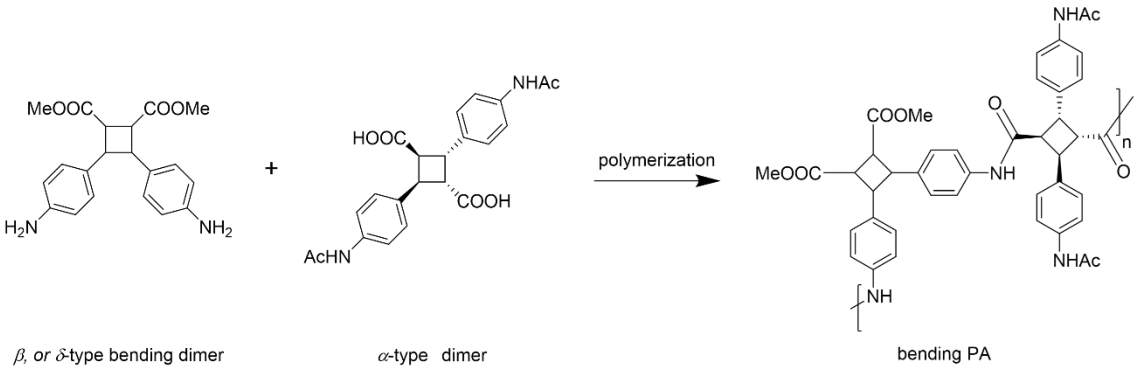

Scheme 3-1. Synthesis of Bending Polyamides from Isomeric 4-Aminocinnamoyl Dimers

3.2 Experimental Section

Materials. Hexane (>95.0%), benzene (>99.5%), toluene (>99.0%), chloroform (>99.0%), dichloromethane (>99.0%), tetrahydrofuran (THF, >99.5%), 1,4-dioxane (>99.5%), methanol (>99.8%), 2-propanol (>99.7%), acetone (>99.0%), ethyl acetate (>99.5%), dimethyl sulfoxide (DMSO, >99.0%), *N*,*N*-dimethylformamide (DMF, >99.5%), *N*,*N*-dimethylacetamide (DMAc, >99.0%), sulfuric acid (96.0%), trifluoroacetic acid (>99.0%), hydrochloric acid (35.0–37.0%), acetic anhydride (>97.0%), sodium hydroxide (>97.0%), and pyridine (>99.5%) were purchased from Kanto Chemicals Co., Inc. 4-Aminocinnamic acid (4ACA, >98.0%), 4-nitrocinnamic acid (4NCA, >99.0%), *N*-hydroxysuccinimide (NHS, >98.0%), *N*,*N*′-diisopropylcarbodiimide (DIC, >98.0%), and triphenyl phosphite (>97.0%) were purchased from Tokyo Kasei Kogyo Co., Ltd. Palladium-activated carbon (Pd 5%) and 1-methyl-2-pyrrolidone (NMP, >99.0%) were purchased from FUJIFILM Wako Pure Chemical Corporation. Ethanol (95.2–95.4%) was purchased from Japan Alcohol Trading Co., Ltd. The *α*-type 4-aminocinnamyl dimer-based diamine and dicarboxylic acid, *α*ATA-Me and *α*ATA-Ac, were synthesized by an analogous to method described in previously reported literatures.[19,20] All chemicals were purchased from available suppliers and used without purification.

Characterization. The ^{1}H (400 MHz) and ^{13}C NMR (100 MHz) spectra were recorded on a Bruker AVANCE 400 instrument using DMSO-d_6 as the solvent. X-ray diffraction data was measured on a Rigaku R-Axis RAPID diffractometer using filtered Mo Kα radiation (λ = 0.71075 Å) at 123 K (cold gas stream). Size exclusion chromatography (SEC) measurements of the obtained polyimides were performed at 40 °C using a JASCO GPC-101 system equipped with two Shodex KD-806M columns (linear, 8 mm × 300 mm) using 0.01 M LiBr in DMF at the flow rate of 1.0 mL min^{-1}. The number-average molecular weight (M_n) and dispersity (M_w/M_n) of the polymers were determined by the RI based on poly(methyl methacrylate) (PMMA) standards. Fourier transform ion cyclotron resonance mass spectrometry (FT-ICR MS) was performed using Bruker SolariX-JA. Thermogravimetric analysis (TGA) and differential scanning calorimetry (DSC) were carried out on Hitachi High-Tech Corporation, STA7200 and Seiko Instruments SII, X-DSC7000T, respectively, at a heating rate of 10 °C min^{-1} under a nitrogen atmosphere. TGA and DSC measurements were carried out over the range of 25−800 °C, and 25−250 °C, respectively. The solubility of the polyamides was evaluated at room temperature in various polar (protic and aprotic) and nonpolar solvents and strong acids with a concentration 2 mg mL^{-1}. Density functional theory (DFT) calculations were performed at the B3LYP/6-311++G(d,p) level using Gaussian 16.

Synthesis of Methyl 4-Nitrocinnamate (4NCA-Me). To a solution of 4NCA (2.00 g, 10.4 mmol) in methanol (50 mL), sulfuric acid (0.20 mL, 3.75 mmol) was added dropwise at 0 °C. The reaction mixture was stirred for 12 h at reflux temperature and then cooled to room temperature. The formed precipitates were filtered and washed with water (100 mL × 3) and then dried under reduced pressure to give 4NCA-Me as a white solid. Yield, 1.84 g (85.6%). ^{1}H NMR spectrum is shown in Figure 3-1. ^{1}H NMR (400 MHz, DMSO-d_6): δ (ppm) 3.75 (s, 3H, CH_3), 6.86 (d, 1H, J = 16.1 Hz, CH=CH), 7.76 (d, 1H, J = 16.1 Hz, Ar-C*H*=CH), 8.00 (d, 1H, J = 8.8 Hz, ArH), 8.24 (d, 1H, J = 8.8 Hz, ArH). ^{13}C NMR (100 MHz, DMSO-d_6): δ (ppm) 51.8, 122.1, 123.9, 129.5, 140.4, 142.0, 148.1, 166.2. FT-ICR MS (ESI) calcd for $C_{10}H_{10}NO_4$ $[M+H]^+$ 208.0604, found 208.0604.

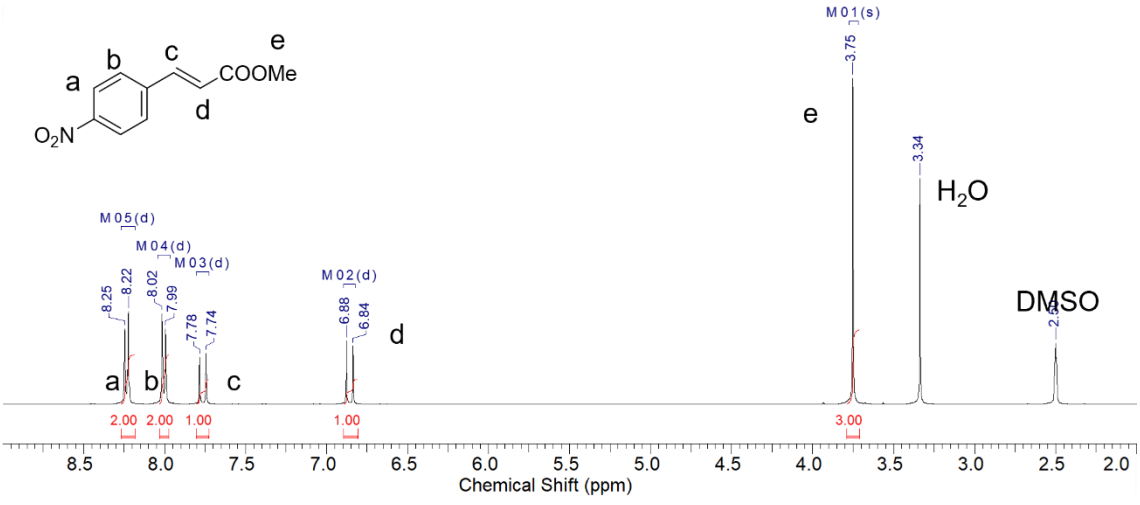

Figure 3-1. ^{1}H NMR spectrum (400 MHz, DMSO-d_6) of 4NCA-Me.

Synthesis of Dimethyl 4,4′-Dinitro-*β*-truxinate (*β*NTA-Me). The powder of 4NCA-Me (2.00 g, 9.65 mmol) was dispersed in hexane (50 mL) under magnetic agitation at room temperature and then irradiated with UV using a 250–450 nm mercury lamp for 15 h to induce [2+2] photocycloaddition. The precipitates were filtered and then dried under reduced pressure to give *β*NTA-Me as a white solid. Yield, 1.92 g (96.2%). ^{1}H NMR spectrum is shown in Figure 3-2. ^{1}H NMR (400 MHz, DMSO-d_6): δ (ppm) 3.67 (s, 6H, CH_3), 4.15–4.19 (m, 2H, CH), 4.50–4.54 (m, 2H, CH), 7.39 (d, 4H, J = 8.8 Hz, ArH), 7.97 (d, 4H, J = 8.7 Hz, ArH). ^{13}C NMR (100 MHz, DMSO-d_6), δ (ppm) 41.7, 44.3, 52.0, 123.0, 129.2, 146.0, 146.3, 172.2. FT-ICR MS (ESI) calcd for $C_{20}H_{18}N_2NaO_8$ $[M+Na]^+$ 437.0955, found 437.0949.

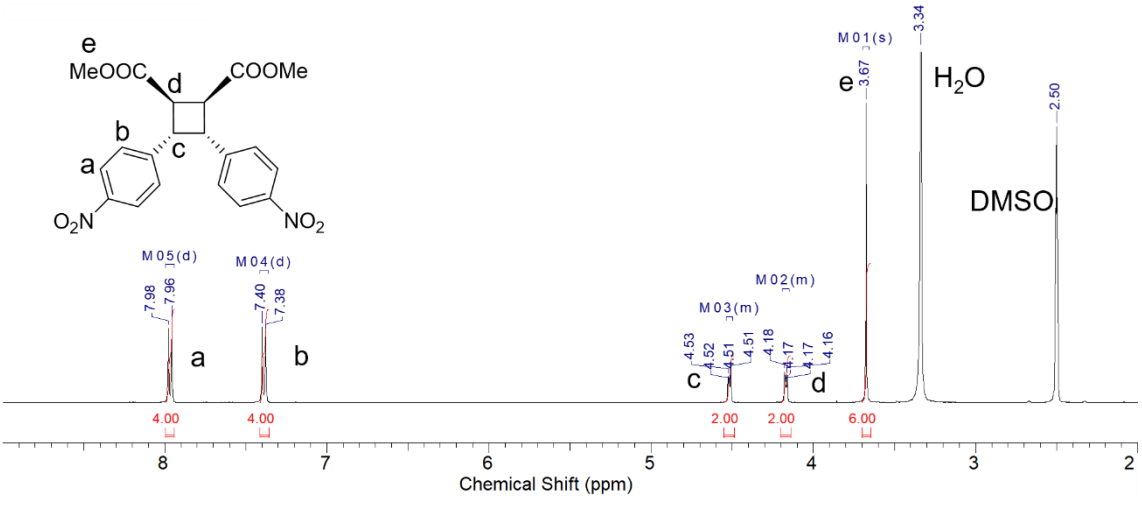

Figure 3-2. ^{1}H NMR spectrum (400 MHz, DMSO-d_6) of *β*NTA-Me.

Synthesis of Dimethyl 4,4′-Diamino-*β*-truxinate (*β*ATA-Me). To a solution of *β*NTA-Me (1.00 g, 2.41 mmol) in methanol (30 mL), palladium on carbon (0.55 g) was added. The reaction mixture was stirred at 50 °C under a hydrogen atmosphere. The reaction was monitored by ^{1}H NMR measurement. After the reaction, the reaction mixture was filtrated to remove palladium on carbon. The organic part was evaporated and dried under reduced pressure to give *β*ATA-Me as a brown solid. Yield, 0.748 g (87.5%). ^{1}H NMR spectrum is shown in Figure 3-3. ^{1}H NMR (400 MHz, DMSO-d_6) : δ (ppm) 3.61 (s, 6H, CH_3), 3.73–3.77 (m, 2H, CH), 3.91–3.95 (m, 2H, CH), 4.76 (s, 4H, NH_2), 6.29 (d, 4H, J = 8.3 Hz, ArH), 6.66 (d, 4H, J = 8.4 Hz, ArH). ^{13}C NMR (100 MHz, DMSO-d_6), δ (ppm) 42.7, 44.3, 51.6, 113.5, 126.1, 128.5, 146.5, 173.1. FT-ICR MS (ESI) calcd for $C_{20}H_{23}N_2O_4$ $[M+H]^+$ 355.1652, found 355.1649.

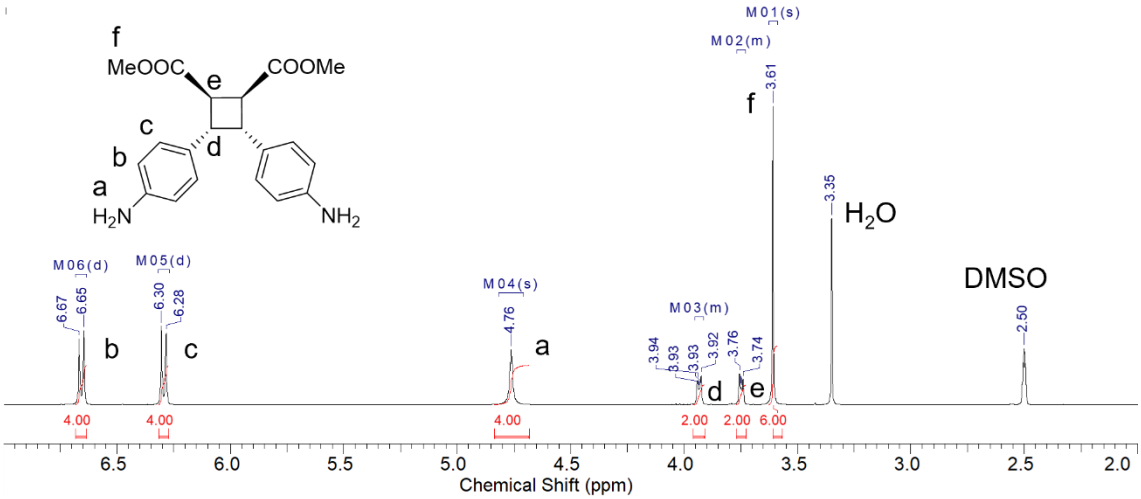

Figure 3-3. ^{1}H NMR spectrum (400 MHz, DMSO-d_6) of *β*ATA-Me.

Synthesis of 4,4'-Dinitro-*β*-truxinic Acid (*β*NTA). To a 1 M aqueous solution of sodium hydroxide (50 mL), *β*NTA-Me (4.00 g, 9.65 mmol) was added. The reaction mixture was stirred at 25 °C for 4 days. The reaction mixture was filtered to remove insoluble components. The filtrate was acidified with concentrated hydrochloric acid. The formed precipitates were collected by filtration then were dried under reduced pressure to give *β*NTA as a brown solid. Yield, 2.56 g (67.0%). ^{1}H NMR spectrum is shown in Figure 3-4. ^{1}H NMR (400 MHz, DMSO-d_6) : δ (ppm) 3.95–3.99 (m, 2H, CH), 4.46–4.48 (m, 2H, CH), 7.38 (d, 4H, J = 8.8 Hz, ArH), 7.96 (d, 4H, J = 8.8 Hz, ArH), 12.65 (brs., 2H, COOH). ^{13}C NMR (100 MHz, DMSO-d_6), δ (ppm) 42.1, 44.3, 122.9, 129.2, 145.9, 147.0, 173.4. FT-ICR MS (MALDI) calcd for $C_{18}H_{14}N_2NaO_8$ $[M+Na]^+$ 409.0642, found 409.153.

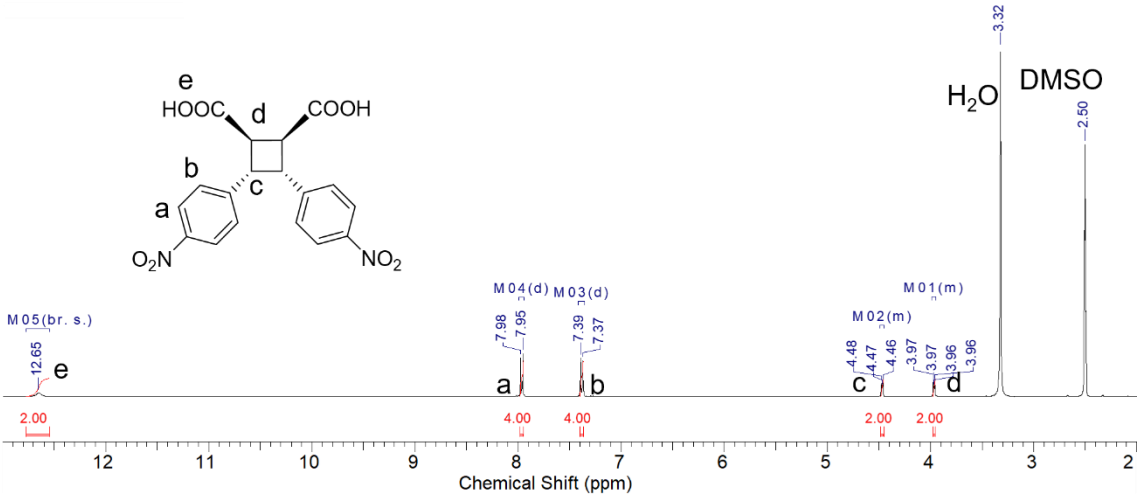

Figure 3-4. ^{1}H NMR spectrum (400 MHz, DMSO-d_6) of *β*NTA.

Synthesis of 4,4'-Diamino-*β*-truxinic Acid (*β*ATA). To a solution of *β*NTA (2.56 g, 6.62 mmol) in THF (40 mL), palladium on carbon (2.20 g) was added. The reaction mixture was stirred at 25 °C under a hydrogen atmosphere. The reaction was monitored by ^{1}H NMR measurement. After the reaction, the reaction mixture was filtered to remove palladium on carbon. The organic potion was evaporated and then was dried under reduced pressure to give *β*ATA as a white solid. Yield, 985 mg (45.5%). ^{1}H NMR spectrum is shown in Figure 3-5. ^{1}H NMR (400 MHz, DMSO-d_6) : δ (ppm) 3.52–3.60 (m, 2H, C*H*), 3.87–3.91 (m, 2H, C*H*), 4.71 (brs, 4H, NH_2), 6.29 (d, 4H, *J* = 8.4 Hz, ArH), 6.64 (d, 4H, *J* = 8.4 Hz, ArH), 12.15 (brs., 2H, COOH). ^{13}C NMR (100 MHz, DMSO-d_6), δ (ppm) 43.1, 44.2, 113.5, 126.8, 128.5, 146.3, 174.3. FT-ICR MS (MALDI) calcd for $C_{18}H_{18}N_2NaO_4$ $[M+Na]^+$ 349.1159, found 349.010.

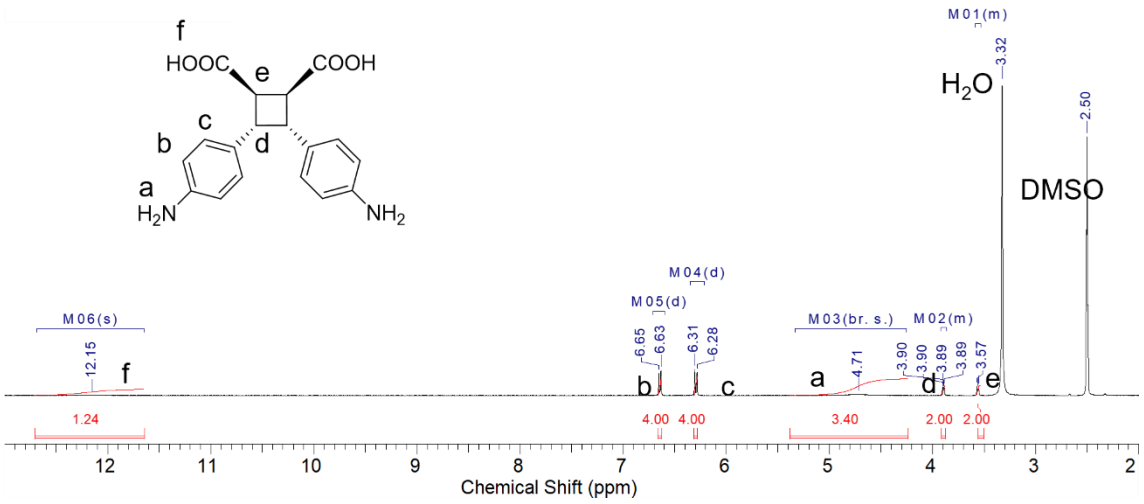

Figure 3-5. ^{1}H NMR spectrum (400 MHz, DMSO-d_6) of *β*ATA.

Synthesis of 4,4'-Diacetamide-*β*-truxinic Acid (*β*ATA-Ac). To a solution of *β*ATA (728 mg, 1.77 mmol) in THF (35 mL), acetic anhydride (2.50 mL, 22.7 mmol) was added. The reaction mixture was stirred at 50 °C for 17 h. After evaporating the solvent, the obtained products were washed with water then were dried under reduced pressure to give *β*ATA-Ac as a white solid. Yield, 805 mg (87.9%). ^{1}H NMR spectrum is shown in Figure 3-6. ^{1}H NMR (400 MHz, DMSO-d_6) : δ (ppm) 1.96 (s, 6H, CH_3), 3.72–3.75 (m, 2H, CH), 4.07–4.12 (m, 2H, CH), 6.93 (d, 4H, J = 8.6 Hz, ArH), 7.28 (d, 4H, J = 8.6 Hz, ArH), 9.72 (s, 2H, NH), 12.39 (brs., 2H, COOH) ^{13}C NMR (100 MHz, DMSO-d_6): δ (ppm) 23.9, 42.6, 44.1, 118.2, 128.1, 133.9, 137.2, 168.0, 174.0. FT-ICR MS (MALDI) calcd for $C_{22}H_{22}N_2NaO_6$ $[M+Na]^+$ 433.1370, found 433.040.

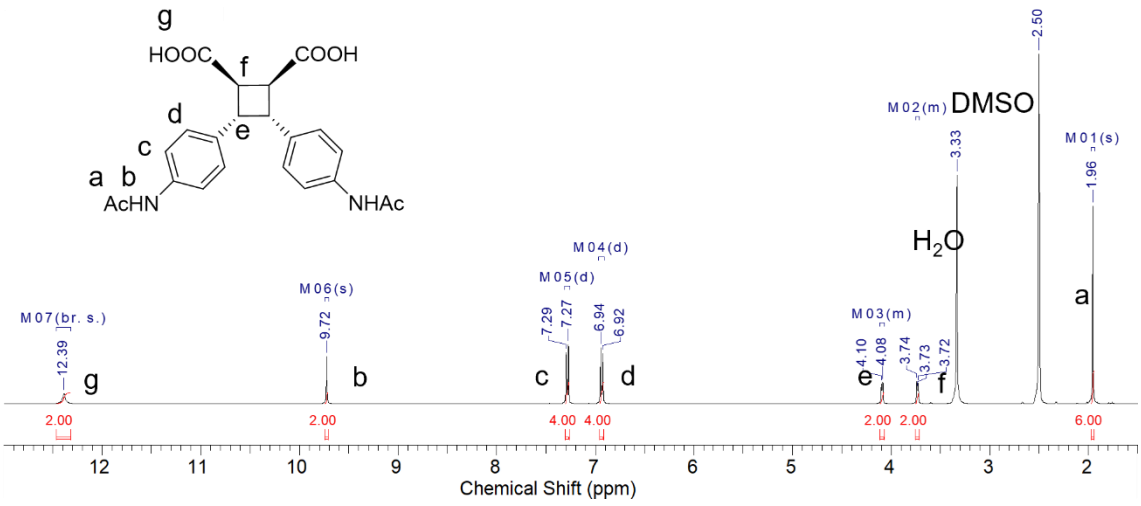

Figure 3-6. ^{1}H NMR spectrum (400 MHz, DMSO-d_6) of *β*ATA-Ac.

Synthesis of *N*-Hydroxysuccinimide 4-Nitrocinnamate (4NCA-NHS). To a solution of 4NCA (5.00 g, 25.9 mmol) and *N*-hydroxysuccinimide (4.48 g, 38.9 mmol) in 1,4-dioxane (25 mL), *N*,*N*- diisopropylcarbodiimide (6.01 mL, 38.8 mmol) was added dropwise at 0 °C. The reaction mixture was stirred overnight at reflux temperature then cooled to room temperature. The formed precipitates were filtered and washed with 2-propanol (100 mL × 3) and then dried under reduced pressure to give 4NCA-NHS as a yellow crystal. Yield, 6.33 g (84.3%). ^{1}H NMR spectrum is shown in Figure 3-7. ^{1}H NMR (400 MHz, DMSO-d_6) : δ (ppm) 2.87 (brs, 4H, CH_2), 7.24 (d, J = 16.1 Hz, 1H, CH=CH), 8.11 (d, J = 16.1 Hz, 1H, Ar-C*H*=CH), 8.13–8.17 (m, 2H, ArH), 8.27–8.32 (m, 2H, ArH). ^{13}C NMR (100 MHz, DMSO-d_6): δ (ppm) 25.5, 116.2, 124.0, 130.3, 139.5, 147.2, 148.8, 161.9, 170.3. FT-ICR MS (MALDI) calcd for $C_{13}H_{10}N_2NaO_6$ $[M+Na]^+$ 313.0431, found 312.8639.

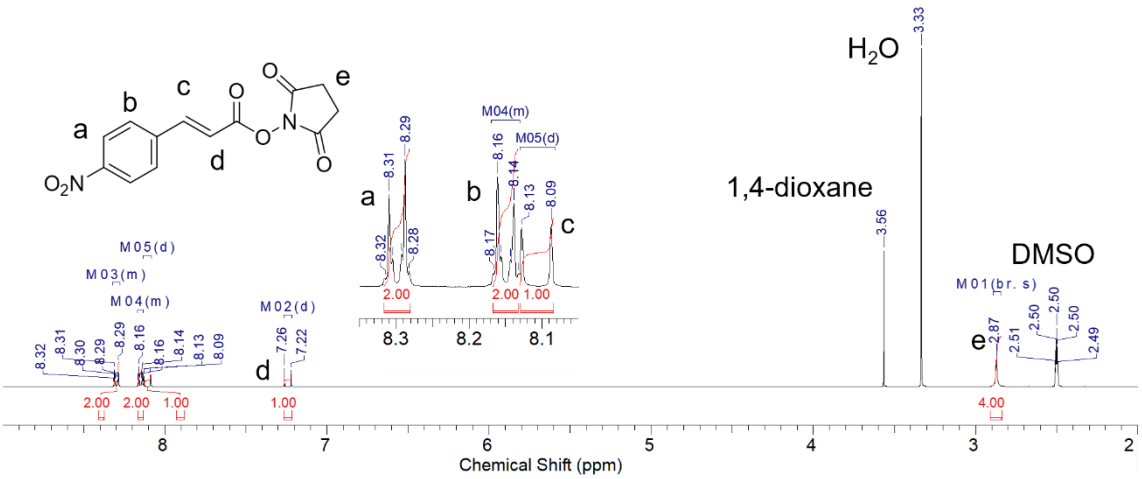

Figure 3-7. ^{1}H NMR spectrum (400 MHz, DMSO-d_6) of 4NCA-NHS.

Synthesis of Bis(*N*-hydroxysuccinimide) 4,4′-Dinitro-*δ*-truxinate (*δ*NTA-NHS). The powder of 4NCA-NHS (3.00 g, 10.3 mmol) was dispersed in benzene (45 mL) under magnetic agitation in water bath at room temperature and then irradiated with ultraviolet light by a high-pressure mercury lamp (Omni Cure S1500, EXFO Photonic Solutions Inc.) for 72 h to induce [2+2] photocycloaddition. After the reaction, the precipitates were filtered and then dried under reduced pressure to give *δ*NTA-NHS as a brown solid. Yield, 2.21 g (73.7%). ^{1}H NMR spectrum is shown in Figure 3-8. ^{1}H NMR (400 MHz, DMSO-d_6) : δ (ppm) 2.82 (brs, 8H, CH_2), 4.16–4.26 (m, 4H, CH), 7.77 (d, J = 8.8 Hz, 4H, ArH), 8.22 (d, J = 8.8 Hz, 4H, ArH). ^{13}C NMR (100 MHz, DMSO-d_6), δ (ppm) 25.5, 40.7, 47.1, 123.8, 128.9, 145.6, 147.1, 166.7, 170.0. FT-ICR MS (MALDI) calcd for $C_{26}H_{21}N_4O_{12}$ $[M+H]^+$ 581.1150, found 581.7283.

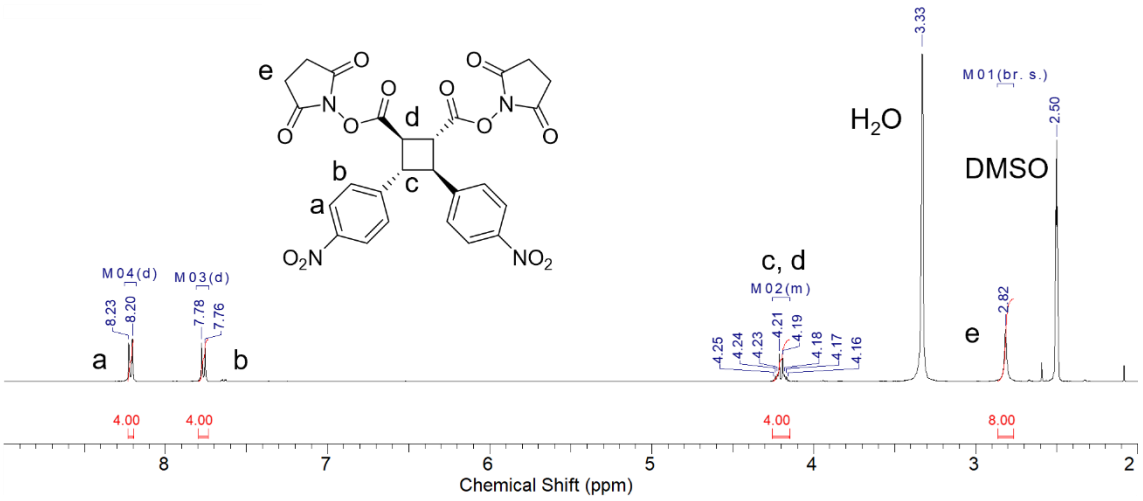

Figure 3-8. ^{1}H NMR spectrum (400 MHz, DMSO-d_6) of *δ*NTA-NHS.

Synthesis of Dimethyl 4,4′-Dinitro-*δ*-truxinate (*δ*NTA-Me). A solution of *δ*NTA-NHS (3.00 g, 5.17 mmol) in methanol (50 mL) was stirred overnight at reflux temperature and then extracted using ethyl acetate (50 mL × 3), washed with distilled water (50 mL). The organic portion was dried over anhydrous $MgSO_4$. After filtration and evaporation to remove the solvent, the residue was dissolved in dichloromethane and then filtered to remove insoluble impurities. The organic part was evaporated and dried under reduced pressure to give *δ*NTA-Me as a brown solid. Yield, 1.92 g (89.7%). ^{1}H NMR spectrum is shown in Figure 3-9. ^{1}H NMR (400 MHz, DMSO-d_6) : δ (ppm) 3.58–3.60 (m, 2H, CH), 3.67 (s, 6H, CH_3), 3.90–3.95 (m, 2H, CH), 7.64 (d, J = 8.8 Hz, 4H, ArH), 8.21 (d, J = 8.7 Hz, 4H, ArH). ^{13}C NMR (100 MHz, DMSO-d_6), δ (ppm) 43.5, 46.1, 52.1, 123.8, 128.5, 146.7, 147.9, 171.7. FT-ICR MS (ESI) calcd for $C_{20}H_{18}N_2NaO_8$ $[M+Na]^+$ 437.0955, found 437.0952.

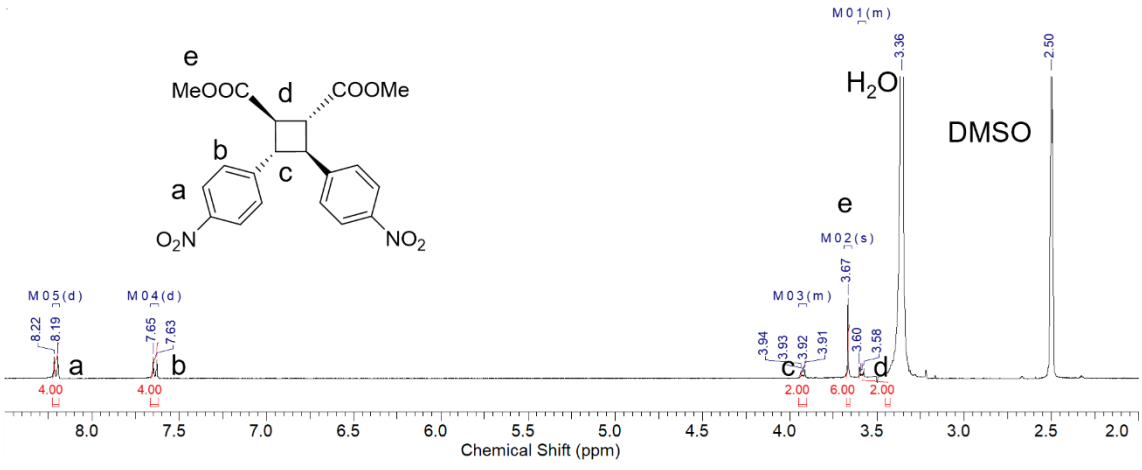

Figure 3-9. ^{1}H NMR spectrum (400 MHz, DMSO-d_6) of *δ*NTA-Me.

Synthesis of Dimethyl 4,4′-Diamino-*δ*-truxinate (*δ*ATA-Me). To a solution of *δ*NTA-Me (2.36 g, 5.70 mmol) in ethyl acetate (60 mL), palladium on carbon (0.59 g) was added. The reaction mixture was stirred at room temperature under a hydrogen atmosphere. The reaction was monitored by ^{1}H NMR measurement. After the reaction, the reaction mixture was filtrated to remove palladium on carbon. The organic part was evaporated and dried under reduced pressure to give *δ*ATA-Me as a yellow solid. Yield, 1.63 g (80.8%). ^{1}H NMR spectrum is shown in Figure 3-10. ^{1}H NMR (400 MHz, DMSO-d_6) : δ (ppm) 3.14–3.19 (m, 2H, CH), 3.26–3.30 (m, 2H, CH), 3.62 (s, 6H, CH_3), 4.99 (s, 4H, NH_2), 6.49 (d, J = 8.3 Hz, 4H, ArH), 6.90 (d, J = 8.3 Hz, 4H, ArH)). ^{13}C NMR (100 MHz, DMSO-d_6), δ (ppm) 44.3, 47.6, 51.8, 113.8, 127.4, 128.0, 147.6, 172.6. FT-ICR MS (ESI) calcd for $C_{20}H_{23}N_2O_4$ $[M+H]^+$ 355.1652, found 355.1651.

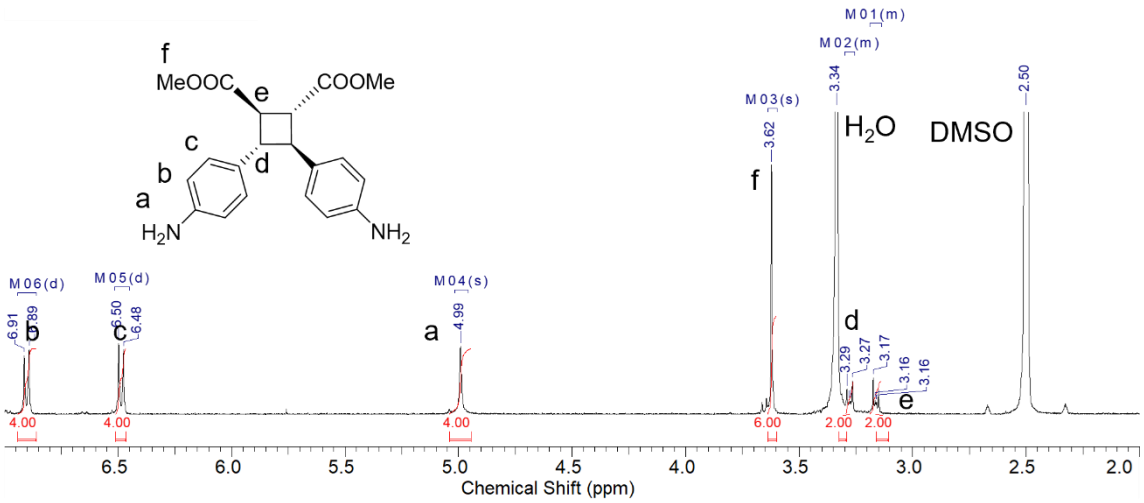

Figure 3-10. ^{1}H NMR spectrum (400 MHz, DMSO-d_6) of *δ*ATA-Me.

Synthesis of 4,4'-Dinitro-*δ*-truxinic Acid (*δ*NTA). The powder of *δ*NTA-NHS (1.86 g, 3.20 mmol) was dispersed in water (50 mL) under magnetic agitation at 25 °C. The reaction mixture was stirred at reflux temperature for 15 h then was cooled to room temperature. The formed precipitates were collected by filtration then were dried under reduced pressure to give *δ*NTA as a brown solid. Yield, 1.10 g (88.9%). ^{1}H NMR spectrum is shown in Figure 3-11. ^{1}H NMR (400 MHz, DMSO-d_6) : δ (ppm) 3.36–3.41 (m, 2H, CH), 3.85–3.90 (m, 2H, CH), 7.64 (d, 4H, J = 8.8 Hz, ArH), 8.21 (d, 4H, J = 8.8 Hz, ArH), 12.78 (brs, 2H, COOH). ^{13}C NMR (100 MHz, DMSO-d_6), δ (ppm) 44.1, 46.0, 123.8, 128.4, 146.6, 148.4, 173.0. FT-ICR MS (MALDI) calcd for $C_{18}H_{14}N_2NaO_8$ $[M+Na]^+$ 409.0642, found 409.131.

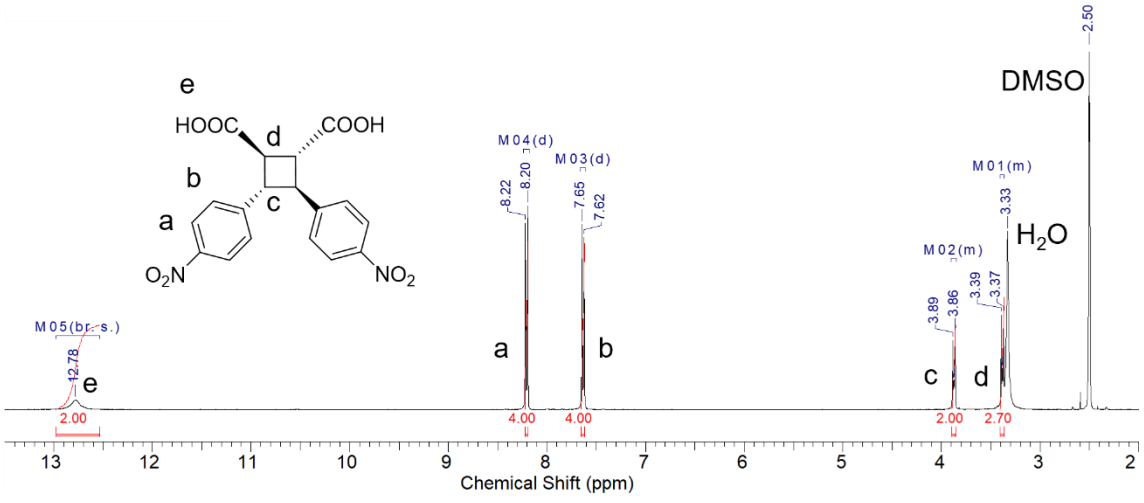

Figure 3-11. ^{1}H NMR spectrum (400 MHz, DMSO-d_6) of *δ*NTA.

Synthesis of 4,4'-Diamino-*δ*-truxinic Acid (*δ*ATA). To a solution of *δ*NTA (1.10 g, 2.85 mmol) in THF (40 mL), palladium on carbon (1.00 g) was added. The reaction mixture was stirred at 25 °C under a hydrogen atmosphere. The reaction was monitored by ^{1}H NMR measurement. After the reaction, the reaction mixture was filtered to remove palladium on carbon. The organic potion was evaporated and then was dried under reduced pressure to give *δ*ATA as a white solid. Yield, 912 mg (98.1%). ^{1}H NMR spectrum is shown in Figure 3-12. ^{1}H NMR (400 MHz, DMSO-d_6) : δ (ppm) 2.98–3.00 (m, 2H, CH), 3.22–3.25 (m, 2H, C*H*), 4.95 (brs, 4H, NH_2), 6.49 (d, 4H, J = 8.4 Hz, ArH), 6.90 (d, 4H, J = 8.4 Hz, ArH), 12.39 (brs., 2H, COOH). ^{13}C NMR (100 MHz, DMSO-d_6), δ (ppm) 44.9, 47.3, 113.8, 127.3, 128.6, 147.5, 174.0. FT-ICR MS (MALDI) calcd for $C_{18}H_{18}N_2NaO_4$ $[M+Na]^+$ 349.1159, found 348.984.

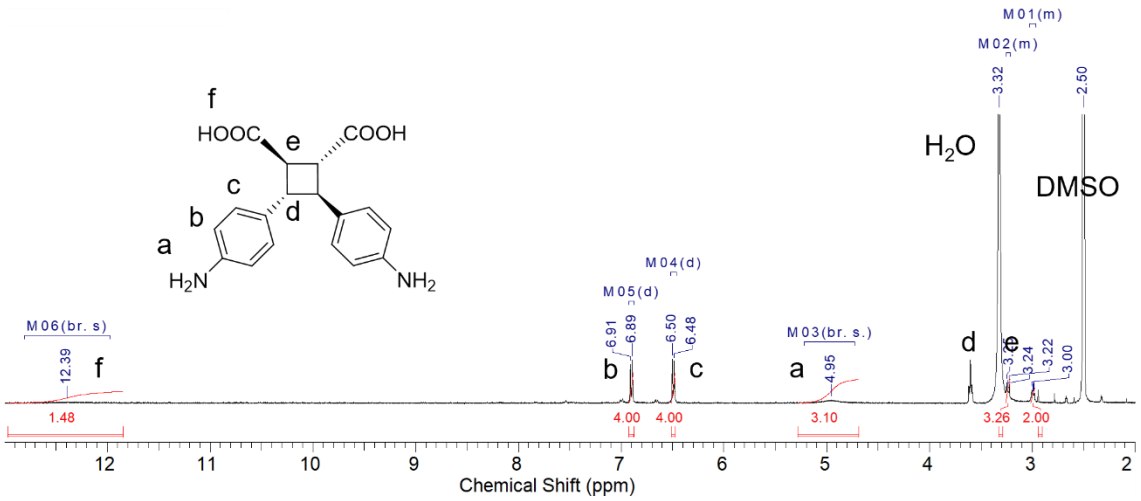

Figure 3-12. ^{1}H NMR spectrum (400 MHz, DMSO-d_6) of *δ*ATA.

Synthesis of 4,4'-Diacetamide-*δ*-truxinic Acid (*δ*ATA-Ac). To a solution of *δ*ATA (500 mg, 1.53 mmol) in THF (20 mL), acetic anhydride (1.25 mL, 11.4 mmol) was added. The reaction mixture was stirred at 50 °C for 17 h. After evaporating the solvent, the obtained products were washed with water then were dried under reduced pressure to give *δ*ATA-Ac as a yellow solid. Yield, 491 mg (78.1%). ^{1}H NMR spectrum is shown in Figure 3-13. ^{1}H NMR (400 MHz, DMSO-d_6) : δ (ppm) 2.01 (s, 6H, CH_3), 3.11–3.13 (m, 2H, CH), 3.42–3.46 (m, 2H, CH), 7.20 (d, 4H, J = 8.6 Hz, ArH), 7.50 (d, 4H, J = 8.5 Hz, ArH), 9.90 (s, 2H, NH), 12.58 (brs., 2H, COOH) ^{13}C NMR (100 MHz, DMSO-d_6): δ (ppm) 23.9, 31.0, 46.7, 119.1, 127.1, 135.9, 138.1, 168.1, 173.9. FT-ICR MS (MALDI) calcd for $C_{22}H_{22}N_2NaO_6$ $[M+Na]^+$ 433.1370, found 433.246.

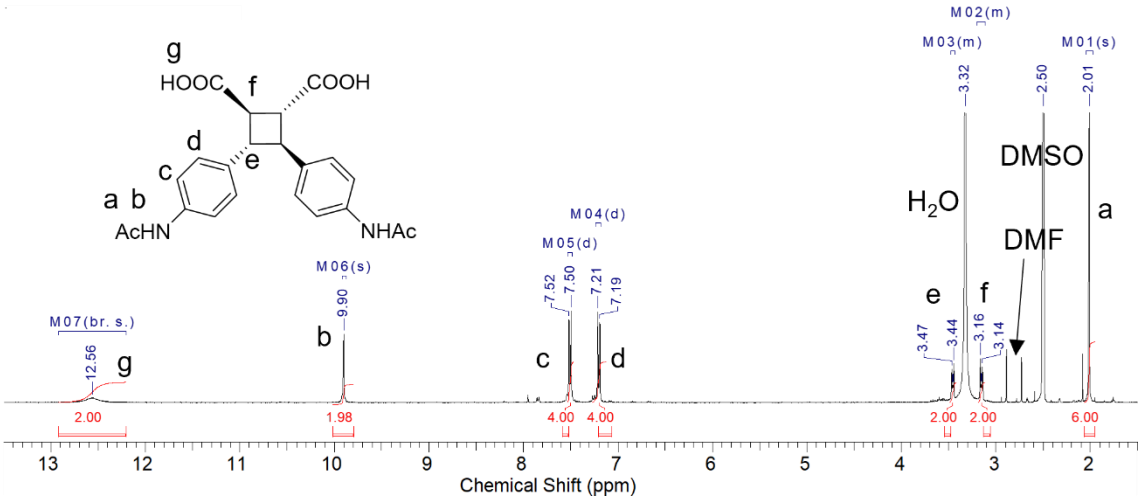

Figure 3-13. ^{1}H NMR spectrum (400 MHz, DMSO-d_6) of *δ*ATA-Ac.

Crystal Structure Analysis of *β*NTA-Me and *δ*NTA-Me. Single crystals of *β*NTA-Me and *δ*NTA-Me were recrystallized from hexane/ethyl acetate.

Crystal Data of *β*NTA-Me. M = 414.37, monoclinic, a = 10.8155(2), b = 13.1531(2), c = 13.9689(3) Å, U = 1986.31(6) Å^3, T = 123 K, space group $P2_1/c$ (no. 14), Z = 4, 33666 reflections measured, 4536 were unique (R_{int} = 0.0228) and were used in all of the calculations. The final $wR(F_2)$ was 0.1094 (all data).

Crystal Data of *δ*NTA-Me. M = 414.37, triclinic, a = 10.00584 (18), b = 13.9329 (3), c = 14.4777 (3) Å, U = 1914.56 (6) Å^3, T = 123 K, space group P-1 (no. 2), Z = 4, 33210 reflections measured, 8747 were unique (R_{int} = 0.0255) and were used in all of the calculations. The final $wR(F_2)$ was 0.0979 (all data).

Syntheses of Isomeric 4-Aminocinnamoyl Dimer-based Polyamides. A typical polymerization procedure is as follows. To *β*ATA-Me (100 mg, 0.282 mmol), and *α*ATA-Ac (116 mg, 0.282 mmol) placed in a flask under nitrogen atmosphere, NMP (0.54 mL), tripheylphosphite (0.20 mL, 0.763 mmol), and pyridine (0.27 mL, 3.39 mmol) ware added. After the reaction mixture was stirred for 24 hours at 80 °C, the reaction mixture was added into methanol (100 mL) to precipitate the polymer. The formed precipitates were filtered then were dried under reduced pressure to give *βα*-PA as a white powder. Yield,

184 mg (88%). Other polyamides from isomeric 4-aminocinnamoyl dimer-based monomers such as *α*ATA-Me, *β*ATA-Me, *δ*ATA-Me, *α*ATA-Ac, *β*ATA-Ac, and *δ*ATA-Ac were synthesized following above methods. Yield, *δα*-PA (79%), *αβ*-PA (91%), *ββ*-PA (88%), *δβ*-PA (78%), *αδ*-PA (81%), *βδ*-PA (85%), *δδ*-PA (79%).

3.3 Results and Discussion

3.3.1 Synthesis of Isomeric 4-Aminocinnamoyl Dimers

To synthesize α-type 4-aminocinnamoyl photodimers (αATA-Me), 4-aminocinnamic acid hydrochloride (4ACA-HCl) was used due to its parallel arrangement and the location of the phenyl head that is contiguous to the carboxylic acid tail.[19,20] To selectively synthesize truxinic acid esters by solid-state photodimerization, 4NCA esters were used because the photodimerization of 4NCA afforded 4,4′-dinitro-β-truxinic acid[22], presumably owing to the parallel arrangement, where the carboxylic acid tails were contiguous (Figure 3-14a and Scheme 3-2). For the synthesis of βATA-Me, the photodimerization of 4NCA-Me, which was easily derived from biobased 4ACA, was carried out in the solid state with ultraviolet irradiation for conversion into βNTA-Me. From ^{1}H NMR spectrum, the olefin signals of the 4NCA-Me at 6.86 and 7.76 ppm disappeared, while the cyclobutane signals of the objective products, βNTA-Me, appeared at 4.15–4.19 and 4.50–4.54 ppm. Monitored by NMR, after 99% conversion was achieved, the suspended crystals were collected by filtration. Molecular structures of obtained photodimers were identified by single-crystal X-ray diffraction analysis (Figure 3-15). The βNTA-Me was then converted into βATA-Me by a simple reduction process using hydrogen gas in the present of palladium carbon, as confirmed by NMR

spectroscopy.

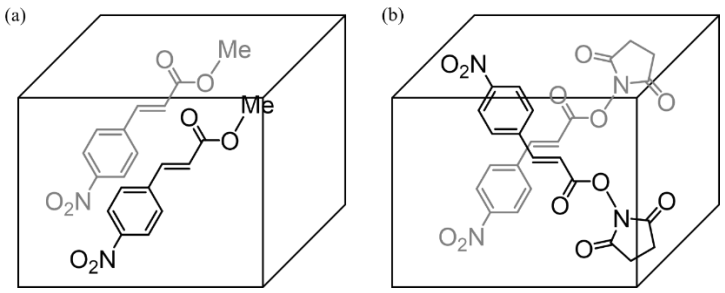

Figure 3-14. Schematic illustrations of molecular arrangement in crystals for solid-state photodimerization, (a) 4NCA-Me, and (b) 4NCA-NHS.

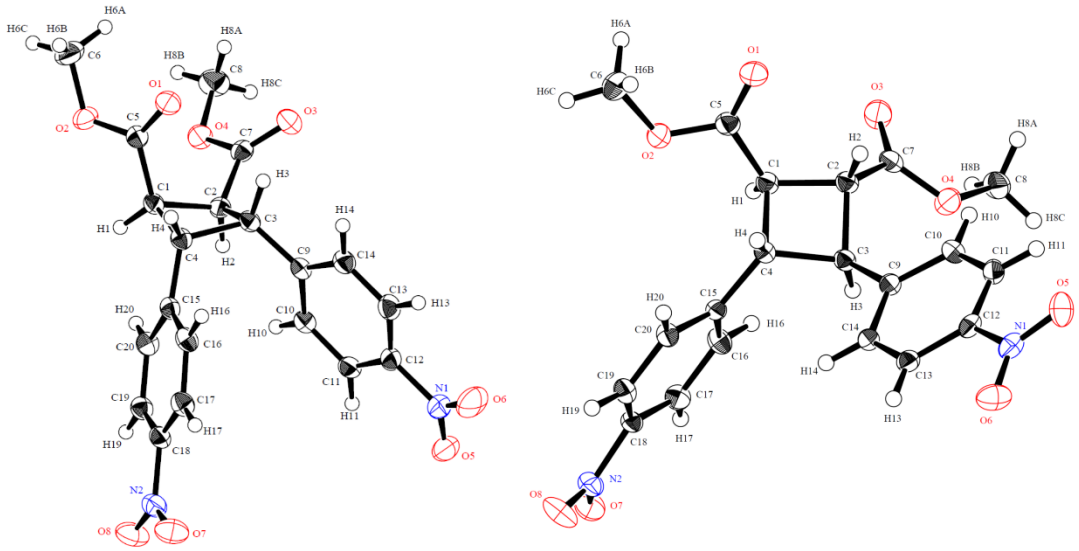

Figure 3-15. ORTEP drawing of *β*NTA-Me (left) and *δ*NTA-Me (right).

Scheme 3-2. Synthetic Route of the Isomeric 4-Aminocinnamoyl Dimer-based Monomers and Polyamides

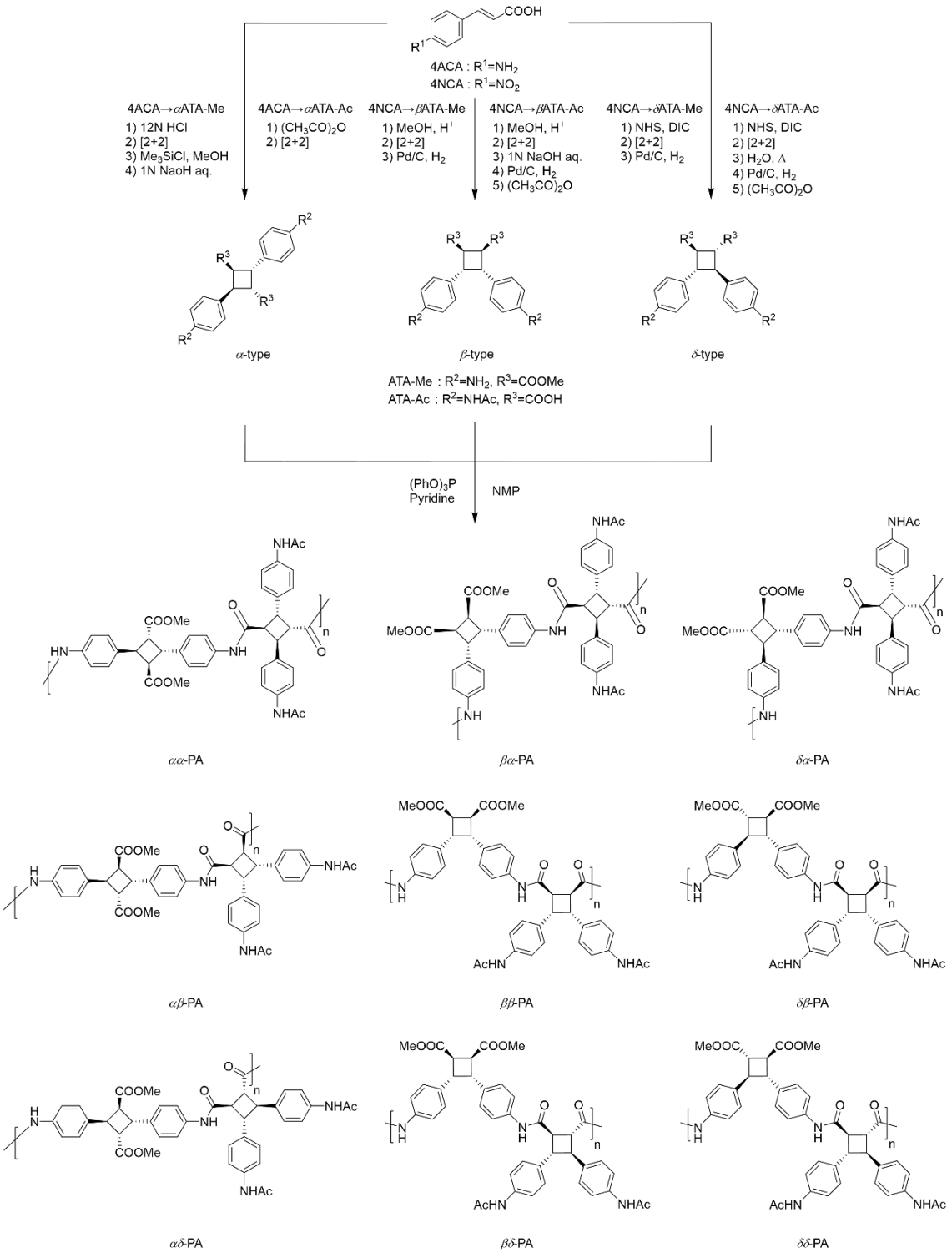

On the other hand, *δ*ATA-Me was deemed to be formed from the dimerization of molecules arranged in parallel, in which the carboxylic acid tails must be separated (Figure 3-14b). To obtain such an arrangement, 4NCA derivatives, where their carboxylic acid tails were modified by bulky functional groups that can be converted into methyl groups, were used to separate the tails based on steric hindrance. In this case, *N*-hydroxysuccinimide ester was selected because (a) the 4NCA-NHS molecule has a rigid and bulky structure, so crystals composed of alternately arranged molecules could be expected, and (b) the activated *N*-hydroxysuccinimide ester could be easily converted into other esters, such as methyl esters. Solid-state photodimerization of the 4NCA-NHS was carried out in toluene dispersion state, and the reduction of nitro groups was conducted using hydrogen gas in the present of palladium carbon after methyl esterification. From ^{1}H NMR spectrum, the olefin signals of the 4NCA-NHS disappeared at 7.24 and 8.11 ppm, while the cyclobutane signals of the objective products, *δ*NTA-NHS, appeared at 4.16–4.26 ppm. Monitored by NMR, once 99% conversion was achieved, the suspended crystals were collected. The successful formation of *δ*NTA-NHS, *δ*NTA-Me, and *δ*ATA-Me was confirmed by NMR spectroscopy. The steric structure of *δ*NTA-Me was confirmed by single-crystal X-ray diffraction analysis (Figure 3-15). The two enantiomers of *δ*NTA-Me were packed into the crystal lattice (Figure 3-16), indicating

that the *δ*-type photodimers were obtained as racemates.

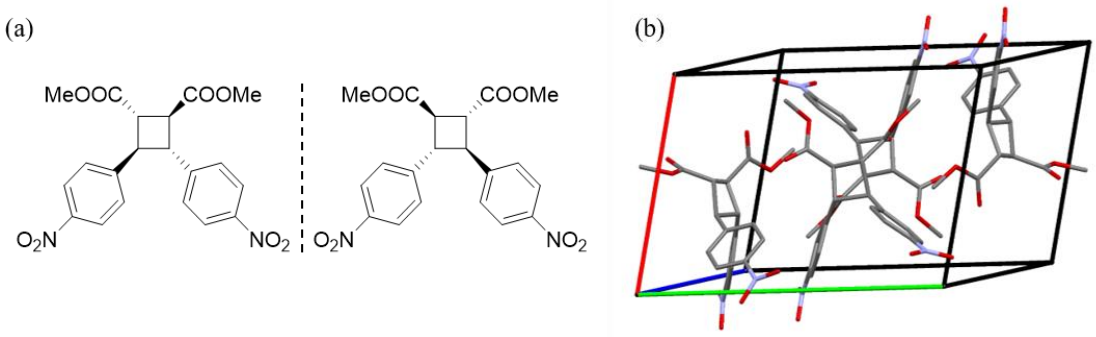

Figure 3-16. (a) Enantiomers of the *δ*NTA-Me, (b) crystal packing of *δ*NTA-Me.

In addition, to synthesize *β*-, and *δ*-type dicarboxylic acid monomers, *β*ATA-Ac and *δ*ATA-Ac, reduction of nitro groups and further acetylation were conducted after hydrolysis of *β*NTA-Me and *δ*NTA-NHS, respectively. The successful formation of *β*NTA, *δ*NTA, *β*ATA-Ac, and *δ*ATA-Ac was confirmed by NMR spectroscopy.

To clarify the bending angle of these isomeric dimers, the structures of *β*ATA-Me and *δ*ATA-Me were optimized by DFT calculations. Figure 3-17 shows the optimized dimer structures. *β*ATA-Me and *δ*ATA-Me exhibited bending angles of 70° and 101°, respectively, which could be introduced into the polymer backbone for bending structures. On the other hand, the bending angle of *α*ATA-Me was reported as 156°, indicating an almost straight building block structure.[21] Building blocks with such unique angles have not been reported yet.

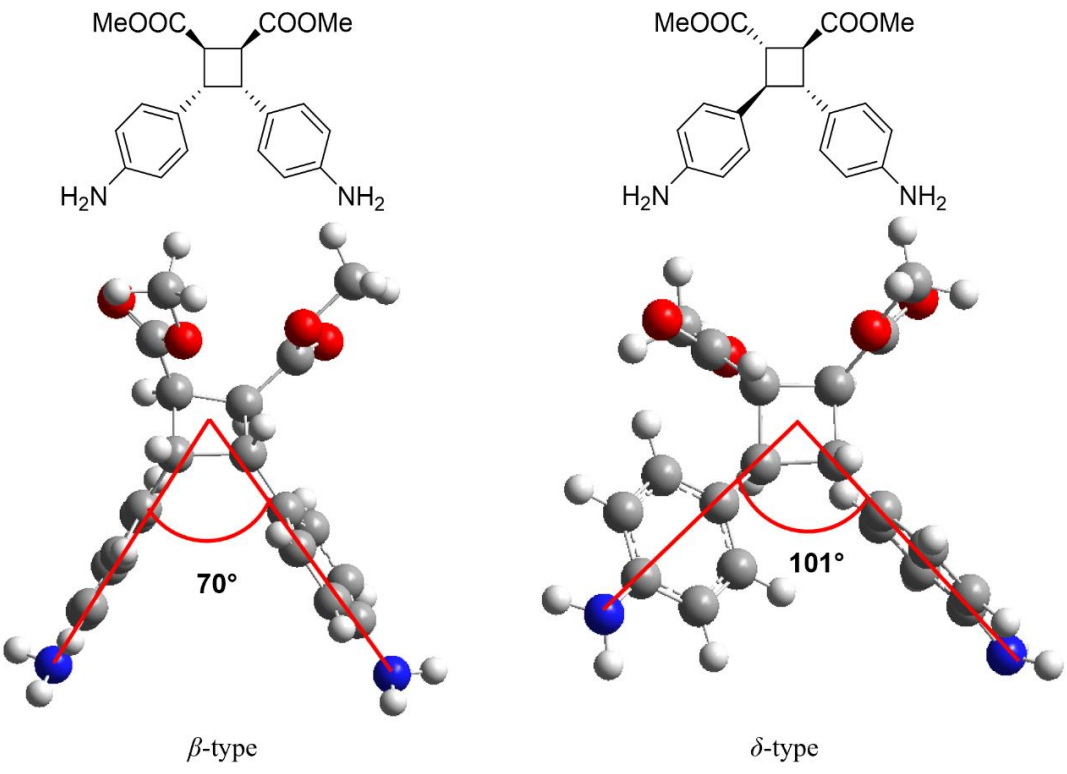

Figure 3-17. Optimized structures and bending angles of *β*ATA-Me and *δ*ATA-Me.

3.3.2 Synthesis of Polyamides from Isomeric 4-Aminocinnamoyl Dimers

Isomeric 4-aminocinnamoyl dimer-based polyamides with different bending angles, *βα*-, *δα*-, *αβ*, *ββ*-, *δβ*, *αδ*, *βδ*-, and *δδ*-PA were synthesized from corresponding diamine and dicarboxylic acid monomers using pyridine and tripheylphosphite (Scheme 3-2). The ^{1}H NMR spectrum of *βα*-PA showed the main chain proton signals for amides, aromatics and cyclobutanes at ~9.7 ppm, 7.4–6.8 ppm and 4.3–3.8 ppm, respectively (Figure 3-18). Moreover, the signals for amines and carboxylic acids in polymer chain end were not detected, indicating that the polymerization proceeded at a high efficiency. The structures of other synthesized polyamides were also confirmed by ^{1}H NMR spectroscopy. Thus, NMR spectroscopy results clearly indicated that the expected polyamides were synthesized.

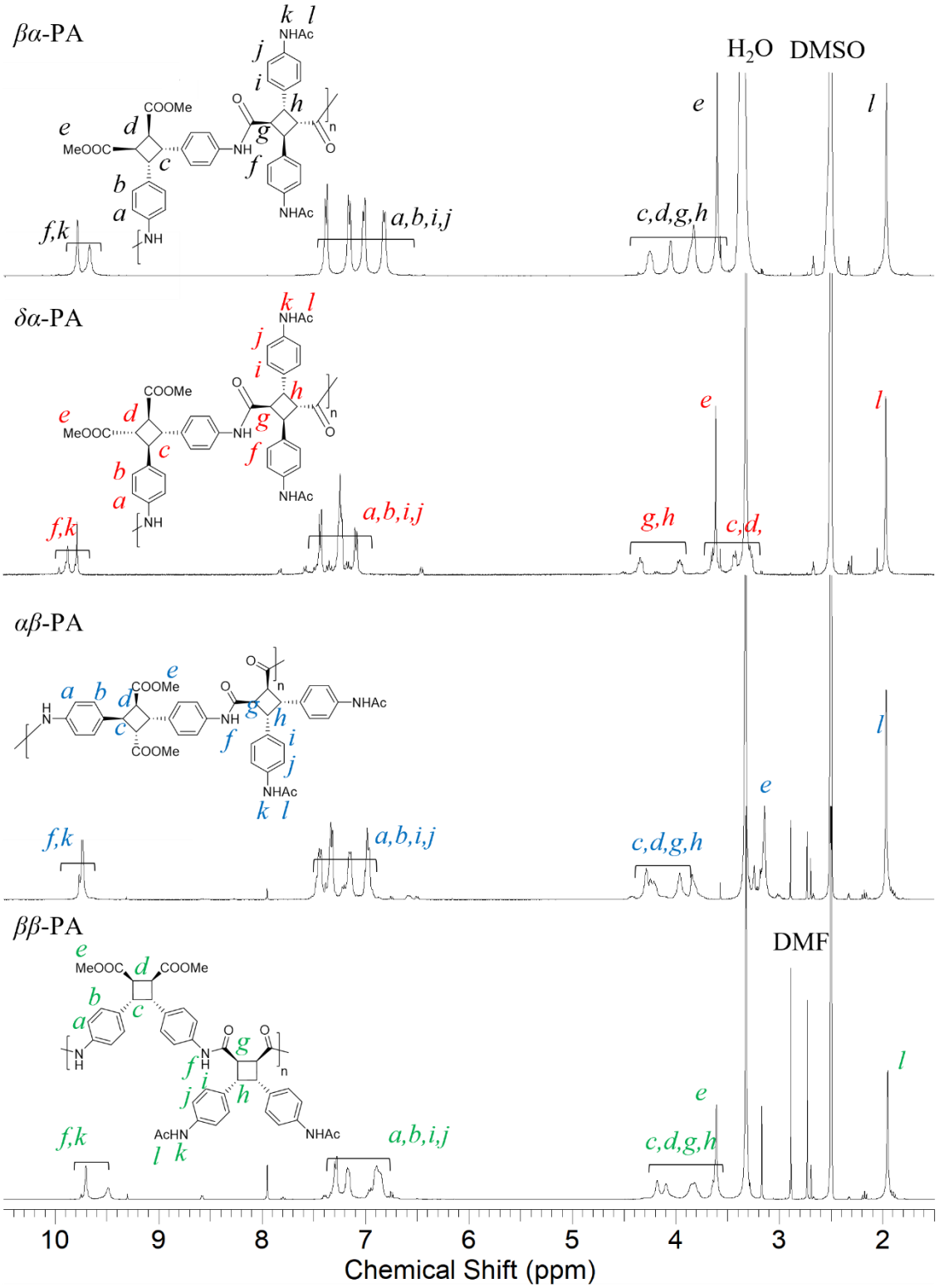
βα-PA
δα-PA
αβ-PA
ββ-PA
H2O
DMSO
DMF
COOMe
MeOOC
NHAc
NH
AcHN
a,b,i,j
c,d,g,h
f,k
g,h
c,d,
10
9
8
7
6
5
4
3
2
Chemical Shift (ppm)

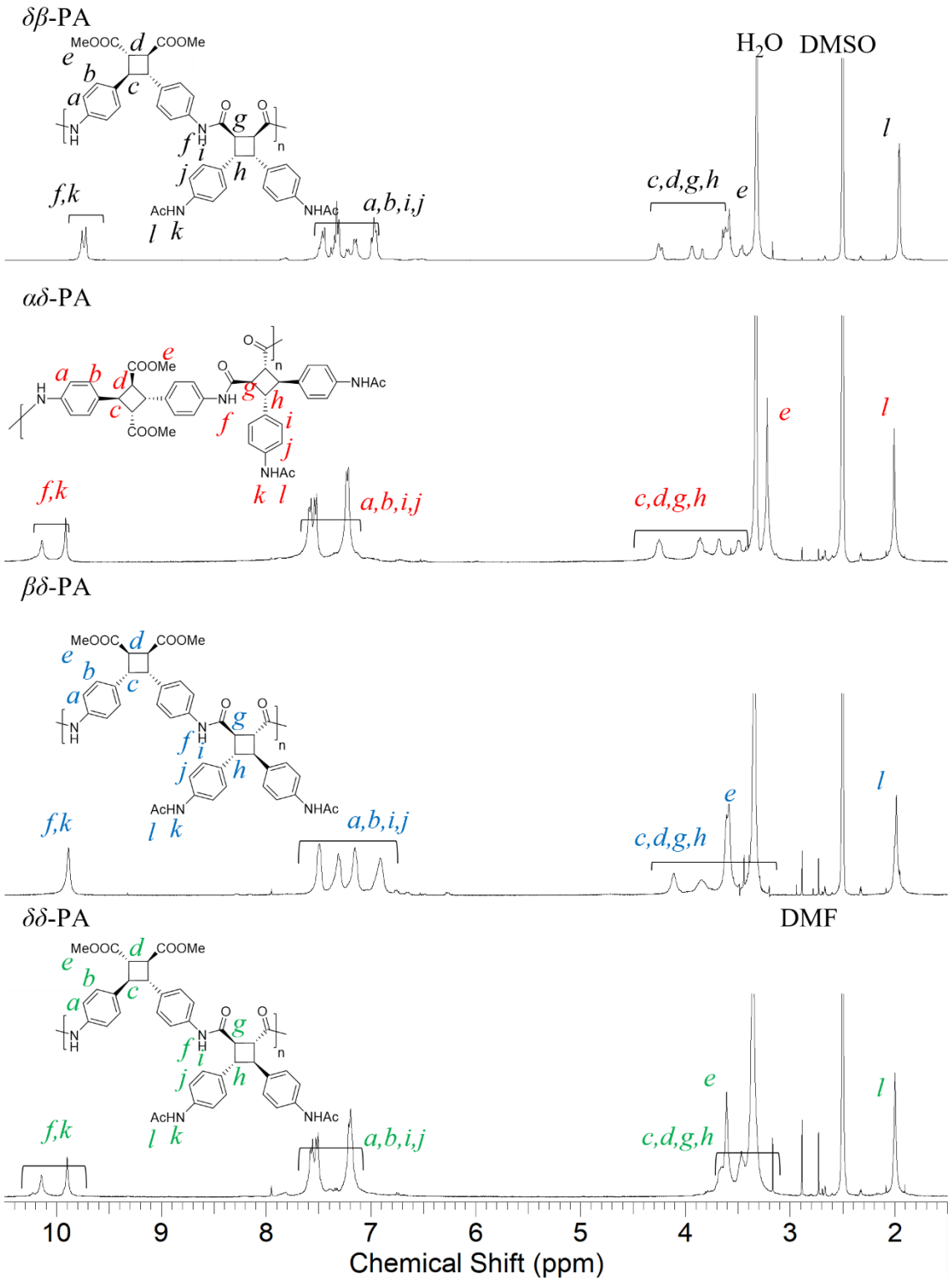

Figure 3-18. ^{1}H NMR spectra (400 MHz, DMSO-d_6) of bending polyamides.

The number-average molecular weight (M_n), weight-average molecular weight (M_w), and molecular weight distribution (M_w/M_n) of the polyamides were determined by SEC measurements (Table 3-1, SEC traces are shown in Figure 3-19). The molecular weights of the *ββ*-PA were not determined by SEC measurement because *ββ*-PA was insoluble in DMF. In addition, the *αδ*-PA exhibited higher molecular weights and wider M_w/M_n due to the gelation in polymerization process. Other polyamides showed a monomodal distribution with M_ws ranging from 10000 to 161000 and M_w/M_n ranging from 1.36 to 3,31. Even though the polymerizations of monomers with acute bending angles such as *ortho*-phenylenediamine are generally difficult, the *β*-type dimer-based diamine and dicarboxylic acid monomers, which possessed acute bending angles of 70°, were polymerized to polyamides. The *β*ATA-Ac-based polyamides, *αβ*-PA and *δβ*-PA showed lower molecular weights indicating that two carboxylic groups of *β*ATA-Ac which were located on adjacent carbon atoms in cyclobutane ring with acute bending angle, were prevent polymerization due to steric hindrance.

Table 3-1. Molecular weights of the synthesized polyamides[a]

polyamide	M_n	M_w	M_w/M_n
αα-PA	49000	161000	3.31
βα-PA	38000	66000	1.74
δα-PA	19000	33000	1.76
αβ-PA	7300	10000	1.37
ββ-PA		no data	
δβ-PA	8300	11000	1.36
αδ-PA	73000	394000	5.40
βδ-PA	18000	25000	1.38
δδ-PA	25000	42000	1.67

[a]The weight-average molecular weight, M_w, the number-average molecular weight, M_n, and the molecular weight distribution, M_w/M_n, of polyimides were determined by SEC; eluent, 0.01 M LiBr in DMF; flow rate, 1.0 mL min^{-1}; standards, PMMA standards.

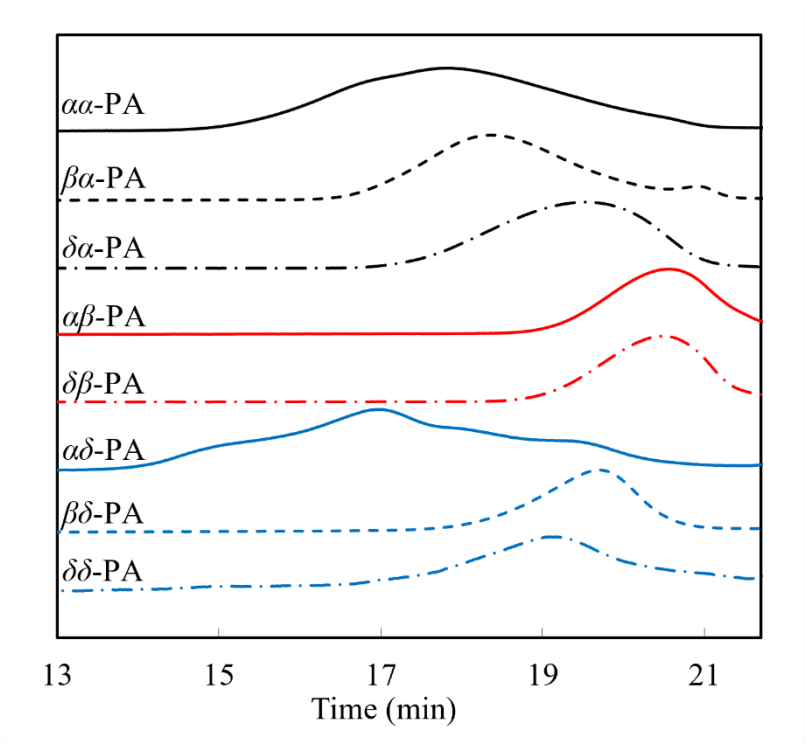

Figure 3-19. SEC traces of the bending polyamides. (solvent, 0.01 M LiBr in DMF; flow rate, 1.0 mL min^{-1}).

Solubility Test of Bending Polyamides

The solubility of the bending polyamides was evaluated by dissolving them in four groups of solvents: (1) nonpolar solvents such as hexane and toluene; (2) polar aprotic solvents such as acetone, ethyl acetate, DMF, DMAc, NMP, DMSO, THF, and chloroform; (3) polar protic solvents such as distilled water, and methanol; and (4) strong acids such as concentrated sulfuric acid (Table 3-2). The polyamides were soluble in polar solvents, such as NMP, DMAc, DMSO, and conc. sulfuric acid, at 25 °C. In addition, all the polyamides, except for *ββ*-PA, were soluble in DMF. The *ββ*-PA was composed from *β*-type diamine and dicarboxylic acid with high structural symmetry and acute bending angles, which decreased solubility of *ββ*-PA by intramolecular interactions such as π–π stacking of aromatic ring.

Table 3-2. Solubility of the synthesized polyamides[a]

solvent	*αα*-PA	*βα*-PA	*δα*-PA	*αβ*-PA	*ββ*-PA	*δβ*-PA	*αδ*-PA	*βδ*-PA	*δδ*-PA
n-hexane	–	–	–	–	–	–	–	–	–
toluene	–	–	–	–	–	–	–	–	–
chloroform	–	–	–	–	–	–	–	–	–
water	–	–	–	–	–	–	–	–	–
methanol	–	–	–	–	–	–	–	–	–
acetone	–	–	–	–	–	–	–	–	–
ethyl acetate	–	–	–	–	–	–	–	–	–
tetrahydrofuran	–	–	–	–	–	–	–	–	–
N,N-dimethylformamide	+	+	+	+	–	+	+	+	+
N,N-dimethylacetamide	+	+	+	+	+	+	+	+	+
N-methyl-2-pyrrolidone	+	+	+	+	+	+	+	+	+
dimethyl sulfoxide	+	+	+	+	+	+	+	+	+
conc. sulfuric acid	+	+	+	+	+	+	+	+	+

[a] The solubility was evaluated under the condition of 2 mg-polyamide/1 mL-solvent at 25 °C. + refers to soluble, and – refers to insoluble.

Thermal Properties of Bending Polyamides

To evaluate the thermal stability, the weight loss temperature (5% weight loss temperature, T_{d5}, and 10% weight loss temperature, T_{d10}), char yield, and glass transition temperature (T_g) were determined by TGA (Figure 3-20) and DSC (Figure 3-21), respectively. From Table 3-3, the T_{d5} and T_{d10} values of all the synthesized bending polyamides ranged from 300 to 340 °C and from 315 to 360 °C, respectively, indicating that the polyamides portrayed high thermal stability. In addition, all the polyamides exhibited similar weight loss temperatures because these polyamides were composed of similar skeletons, 4-aminocinnamoyl photodimer structures. The polyamides including *β*-type dimer units showed slightly lower weight loss temperatures due to difference of thermal stability of each isomeric 4-aminocinnamoyl dimers (Figure 3-22, TGA curves of *α*ATA-Me, *β*ATA-Me, and *δ*ATA-Me).

Table 3-3. Thermal properties of the synthesized polyamides

polyamide	T_{d5} (ºC)[a]	T_{d10} (ºC)[a]	T_g (ºC)[b]	char yield (%)
αα-PA	340	355	262	31
βα-PA	320	335	ND	45
δα-PA	325	350	ND	46
αβ-PA	305	335	ND	58
ββ-PA	300	315	ND	50
δβ-PA	310	345	ND	57
αδ-PA	340	360	ND	45
βδ-PA	315	330	ND	52
δδ-PA	335	360	ND	50

[a] 5% weight loss temperature, T_{d5}, and 10% weight loss temperature, T_{d10}, were obtained from TGA curve scanned at a heating rate of 10 °C min^{-1} under a nitrogen atmosphere. [b] Glass transition temperature, T_g, was measured by DSC thermogram scanned at a heating rate of 10 °C min^{-1} under a nitrogen atmosphere. ND refers to not determined.

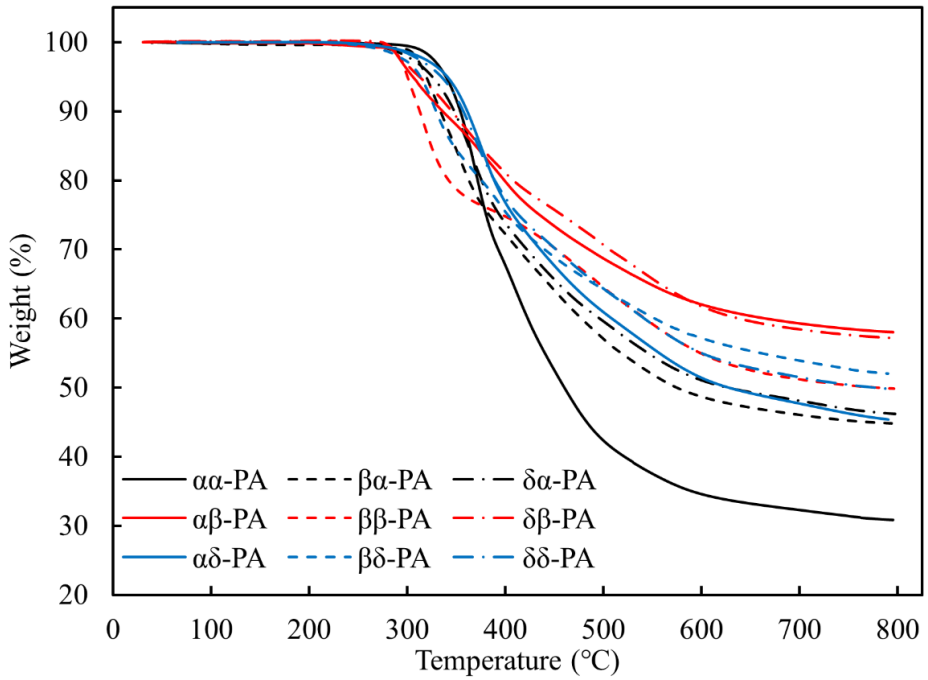

Figure 3-20. TGA curves of 4-aminocinnamoyl dimer-based polyamides.

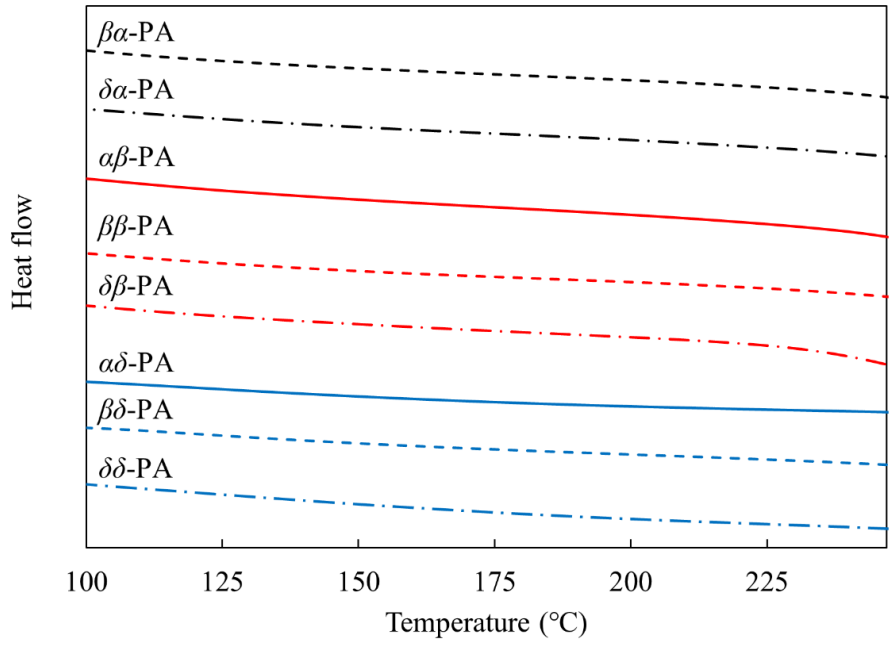

Figure 3-21. DSC curves of bending polyamides.

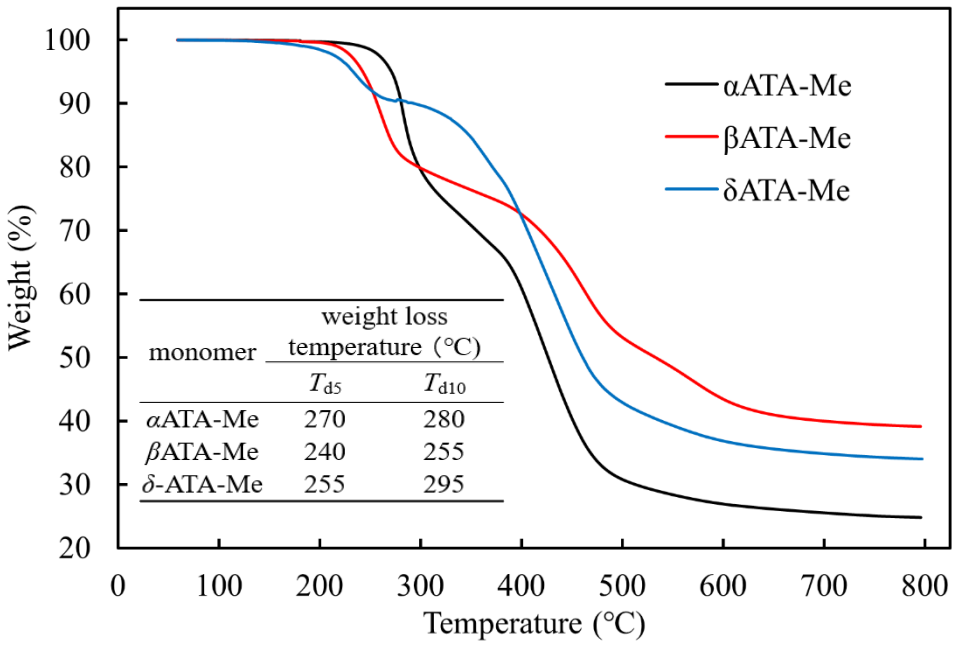

Figure 3-22. TGA curves of isomeric 4-aminocinnamoyl dimer-based diamines.

The char yield of bending polyamides was ranged from 45 to 58% although the *αα*-PA which was composed of *α*-type dimers, exhibited the char yield of 31%. Hence, the char yield was dramatically increased by introduction of bending units such as *β*-, and *δ*-type dimer structure. According to a literature regarding to thermal decomposition of cyclobutane-based polymers, possible modes of cyclobutane cleavages were proceeded competitively.[22] Therefore, truxillic acids such as *α*-type dimer, only gave cinnamic acids by thermal decomposition (Figure 3-23). On the other hand, truxinic acids such as *β*-, and *δ*-type dimer afford cinnamic acids, fumaric acid and stilbenes by thermal decomposition based on different modes of cleavage. From this hypothesis, the thermal decomposition

of *αα*-PA, which synthesized from two kinds of truxiliic acid-based monomers, induced polymer degradation by main chain scission, resulted in low char yield due to volatilization of degradation fragments. On the other hand, thermal decomposition of bending polyamides having truxinic acid components were possible to afford unsaturated polymer chains when the fumaric acids were eliminated, resulted in high char yields.

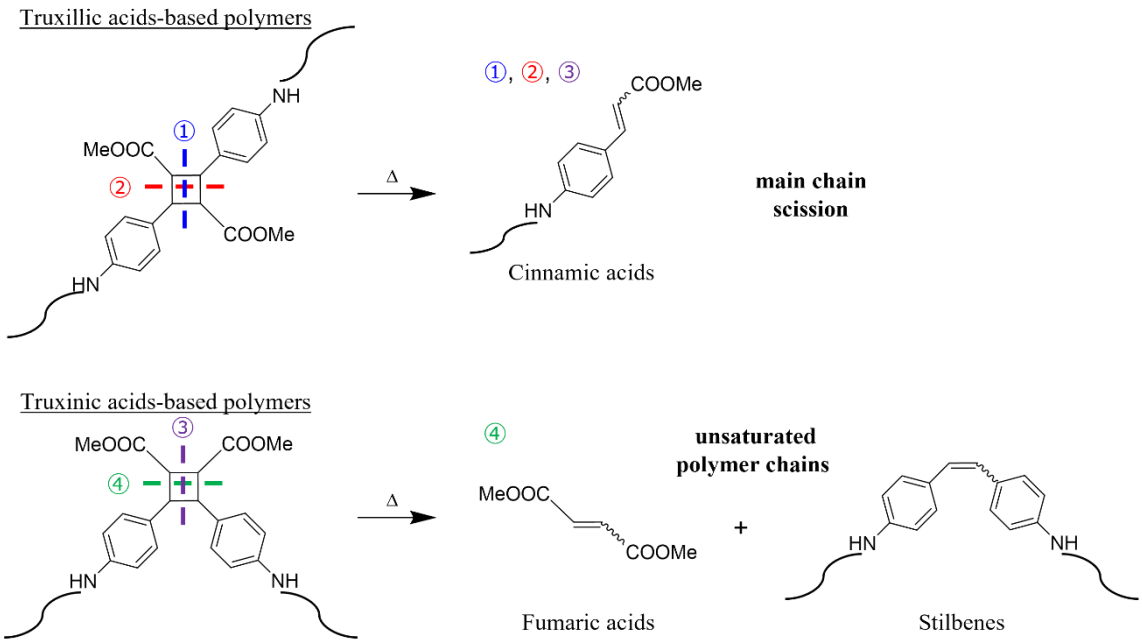

Figure 3-23 Schematic illustration of thermal decomposition of truxillic and truxinic acid-based polymers

Generally, T_g decreases when a bending structure is introduced in the backbone due to an increase in the free volume of the respective polymer chain.[2,3] However, the T_g of the bending polyamides was not observed under 250 °C, similar to that of the *αα*-PA. Hence, the T_g of the bending 4-aminocinnamyl dimer-based polyamides was not depended on its bending angles. This result is assumed that t since the backbone of these polyamides was composed by rigid ring-connected structures, the mobility of the polymer chains was inhibited resulted in maintaining T_g regardless of the bending angles.

3.4 Conclusion

Two types of isomeric 4-aminocinnamoyl photodimer-based diamine and dicarboxylic acid monomers with different bending structures were selectively synthesized and used for the synthesis of polyamides with different bending angles. DFT calculations revealed that the synthesized *β*- and *δ*-type dimers possessed unique bending angles of 70° and 101°, respectively. By polymerization of the *β*-type photodimer, the bending polyamides having acute angles with M_w >10000 were synthesized. By evaluation of solubility and molecular weights of the *β*-type-based polyamides, effects on these properties based on unique structural characteristics of cinnamoyl dimer such as acute bending angles and high axical symmetry were confirmed. In addition, all of the bending polyamides showed high heat resistance with T_{d10} of 315–360 °C. Furthermore, from the results of TGA measurement, bending polyamides showed higher char yield than almost straight-shaped *αα*-PA. In this chapter, the author has selectively prepared isomeric 4-aminocinnamoyl dimers by controlling molecular arrangements in crystals. In addition, novel polyamides were prepared that bear a unique bending angle based on the spatial arrangement around the cyclobutane rings in the polymer main chains. This research provides insights into the molecular design for synthesis of isomeric cinnamoyl dimers and their-based high-performance/functional polymers.

3.5 References and Notes

(1) Mi, Z.; Wang, S.; Hou, Z.; Liu, Z.; Jin, S.; Wang, X.; Wang, D.; Zhao, X.; Zhang, Y.; Zhou, H.; Chen, C. Soluble Polyimides Bearing (Cis, Trans)-Hydrogenated Bisphenol A and (Trans, Trans)-Hydrogenated Bisphenol A Moieties: Synthesis, Properties and the Conformational Effect. *Polymers (Basel).* **2019**, *11* (5), 854. https://doi.org/10.3390/polym11050854.

(2) Ding, M. Isomeric Polyimides. *Prog. Polym. Sci.* **2007**, *32* (6), 623–668. https://doi.org/10.1016/j.progpolymsci.2007.01.007.

(3) Hsiao, S. H.; Chen, Y. J. Structure-Property Study of Polyimides Derived from PMDA and BPDA Dianhydrides with Structurally Different Diamines. *Eur. Polym. J.* **2002**, *38* (4), 815–828. https://doi.org/10.1016/S0014-3057(01)00229-4.

(4) Kapaev, R. R.; Scherbakov, A. G.; Shestakov, A. F.; Stevenson, K. J.; Troshin, P. A. M -Phenylenediamine as a Building Block for Polyimide Battery Cathode Materials . *ACS Appl. Energy Mater.* **2021**. https://doi.org/10.1021/acsaem.1c00092.

(5) Fang, X.; Yang, Z.; Zhang, S.; Gao, L.; Ding, M. Polyimides Derived from

Mellophanic Dianhydride. *Macromolecules* **2002**, *35* (23), 8708–8717. https://doi.org/10.1021/ma0204610.

(6) Dingemans, T. J.; Mendes, E.; Hinkley, J. J.; Weiser, E. S.; StClair, T. L. Poly(Ether Imide)s from Diamines with Para-, Meta-, and Ortho-Arylene Substitutions: Synthesis, Characterization, and Liquid Crystalline Properties. *Macromolecules* **2008**, *41* (7), 2474–2483. https://doi.org/10.1021/ma8000324.

(7) Madzarevic, Z. P.; Shahid, S.; Nijmeijer, K.; Dingemans, T. J. The Role of Ortho-, Meta- and Para-Substitutions in the Main-Chain Structure of Poly(Etherimide)s and the Effects on CO2/CH4 Gas Separation Performance. *Sep. Purif. Technol.* **2019**, *210* (June 2018), 242–250. https://doi.org/10.1016/j.seppur.2018.08.006.

(8) Jassal, M.; Ghosh, S. Aramid Fibres - An Overview. *Indian J. Fibre Text. Res.* **2002**, *27* (3), 290–306.

(9) Kapaev, R. R.; Scherbakov, A. G.; Shestakov, A. F.; Stevenson, K. J.; Troshin, P. A. M-Phenylenediamine as a Building Block for Polyimide Battery Cathode Materials. *ACS Appl. Energy Mater.* **2021**, *4* (5), 4465–4472. https://doi.org/10.1021/acsaem.1c00092.

(10) Schmidt, G. M. J. Photodimerization in the Solid State. *Pure Appl. Chem.* **1971**, *27* (4), 647–678. https://doi.org/10.1351/pac197127040647.

(11) Sonoda, Y. Solid-State [2+2] Photodimerization and Photopolymerization of α,ω-Diarylpolyene Monomers: Effective Utilization of Noncovalent Intermolecular Interactions in Crystals. *Molecules* **2011**, *16* (1), 119–148. https://doi.org/10.3390/molecules16010119.

(12) Enkelmann, V.; Wegner, G.; Novak, K.; Wagener, K. B. Single-Crystal-to-Single-Crystal Photodimerization of Cinnamic Acid. *J. Am. Chem. Soc.* **1993**, *115* (22), 10390–10391. https://doi.org/10.1021/ja00075a077.

(13) Cohen, M. D.; Schmidt, G. M. J.; Sonntag, F. I. 384. Topochemistry. Part II. The Photochemistry of Trans-Cinnamic Acids. *J. Chem. Soc.* **1964**, 2000. https://doi.org/10.1039/jr9640002000.

(14) Schmidt, G. M. J. 385. Topochemistry. Part III. The Crystal Chemistry of Some Trans-Cinnamic Acids. *J. Chem. Soc.* **1964**, 2014. https://doi.org/10.1039/jr9640002014.

(15) Pattabiraman, M.; Kaanumalle, L. S.; Natarajan, A.; Ramamurthy, V. Regioselective Photodimerization of Cinnamic Acids in Water: Templation with

Cucurbiturils. *Langmuir* **2006**, *22* (18), 7605–7609. https://doi.org/10.1021/la061215a.

(16) Nakanishi, F.; Nakanishi, H.; Tsuchiya, M.; Hasegawa, M. Water-Participation in the Crystalline-State Photodimerization of Cinnamic Acid Derivatives. A New Type of Organic Photoreaction. *Bull. Chem. Soc. Jpn.* **1976**, *49* (11), 3096–3099. https://doi.org/10.1246/bcsj.49.3096.

(17) Bernstein, H. I.; Quimby, W. C. The Photochemical Dimerization of Trans-Cinnamic Acid 1. *J. Am. Chem. Soc.* **1943**, *65* (10), 1845–1846. https://doi.org/10.1021/ja01250a016.

(18) D'Agostino, S.; Taddei, P.; Boanini, E.; Braga, D.; Grepioni, F. Photo- vs Mechano-Induced Polymorphism and Single Crystal to Single Crystal [2 + 2] Photoreactivity in a Bromide Salt of 4-Amino-Cinnamic Acid. *Cryst. Growth Des.* **2017**, *17* (9), 4491–4495. https://doi.org/10.1021/acs.cgd.7b00415.

(19) Tateyama, S.; Masuo, S.; Suvannasara, P.; Oka, Y.; Miyazato, A.; Yasaki, K.; Teerawatananond, T.; Muangsin, N.; Zhou, S.; Kawasaki, Y.; Zhu, L.; Zhou, Z.; Takaya, N.; Kaneko, T. Ultrastrong, Transparent Polytruxillamides Derived from Microbial Photodimers. *Macromolecules* **2016**, *49* (9), 3336–3342.

https://doi.org/10.1021/acs.macromol.6b00220.

(20) Suvannasara, P.; Tateyama, S.; Miyasato, A.; Matsumura, K.; Shimoda, T.; Ito, T.; Yamagata, Y.; Fujita, T.; Takaya, N.; Kaneko, T. Biobased Polyimides from 4-Aminocinnamic Acid Photodimer. *Macromolecules* **2014**, *47* (5), 1586–1593. https://doi.org/10.1021/ma402499m.

(21) Dwivedi, S.; Nag, A.; Sakamoto, S.; Funahashi, Y.; Harimoto, T.; Takada, K.; Kaneko, T. High-Temperature Resistant Water-Soluble Polymers Derived from Exotic Amino Acids. *RSC Adv.* **2020**, *10* (62), 38069–38074. https://doi.org/10.1039/d0ra06620f.

(22) Hasegawa, M.; Katsumata, T.; Ito, Y.; Saigo, K.; Iitaka, Y. Topochemical Photoreactions of Unsymmetrically Substituted Diolefins. 2. Photopolymerization of 4′-(Alkoxycarbonyl)-2,5-Distyrylpyrazines. *Macromolecules* **1988**, *21* (11), 3134–3138. https://doi.org/10.1021/ma00189a002.

Chapter 4

Soluble Biobased Polyimides from Diaminotruxinic Acid with Unique Bending Angles

4.1 Introduction

Polyimides, which are well known as super engineering plastics, have been used for the production of high-performance industrial materials, such as electronic[1,2] and optical devices,[3,4] as well as materials used in space applications[5] due to their excellent thermal resistance and mechanical properties. However, their low solubility in solvents and nonthermoplastic properties lead to the poor processability of these materials. In addition, thermal imidization of poly(amic acid)s was generally used for syntheses of insoluble polyimide, which should decrease their mechanical performance for two reasons: (a) Water molecules condensed at high temperatures during the imidization process may hydrolyze the remaining poly(amic acid)s to reduce the molecular weight. (b) The voids in polyimide film were generated by the evaporation of water. To avoid such performance decreases, soluble polyimides which can be directly cast to film without thermal treatment, are required. As such, numerous studies have been conducted to design soluble and processable polyimides. One of the strategies to improve the solubility of polyimides is the introduction of bulky side chains,[6,7] flexible linkages,[8,9] and bending structures into their main chain for better flexibility of the polymer chains.[10,11] However, modifications to the chemical structures decrease the heat resistance of these materials. The introduction of isomeric bending structures to polymer chains is considered an

effective approach to improve the solubility and processability of polymers. With the polymer skeletons unchanged, the heat resistance of these polymers is maintained. In view of this, the effects of introducing isomeric bending structures such as diamines and tetracarboxylic acid dianhydrides to polymers have been widely studied.

A typical and simple example of such an approach in polyimides is the synthesis of *para*- and *meta*-phenylenediamine as bending diamines.[12,13] Polyimides with a bending dianhydride structure such as mellophanic dianhydride show good solubility in organic solvents, such as $CHCl_3$, *N,N*-dimethylacetamide, and dimethyl sulfoxide.[11] Recently developed biobased polyimides synthesized from microorganism-metabolized 4-aminocinnamic acid (4ACA) dimer and various tetracarboxylic acid dianhydrides showed high heat resistance and transparency.[14] Soluble biobased polyimides have also been synthesized from bending tetracarboxylic acid dianhydrides or by modifying the carboxylic acid side chains.[15,16] The dimers of cinnamic acid generate various structural isomers, some of which may be suitable bending structure candidates that induce high solubility.

This research focused on bending 4ACA photodimers such as β- and δ-type dimers to be used as diamine monomers for the synthesis of soluble biobased polyimides (Scheme 4-1). These soluble polyimides with bending 4ACA dimer components were

expected to exhibit excellent heat resistance and processability based on 4ACA dimer skeleton without performance degradation by thermal imidization. In addition, since 4ACA is produced from bio-derived resources, these polyimides are expected to contribute to a sustainable society as high-performance and eco-friendly materials.

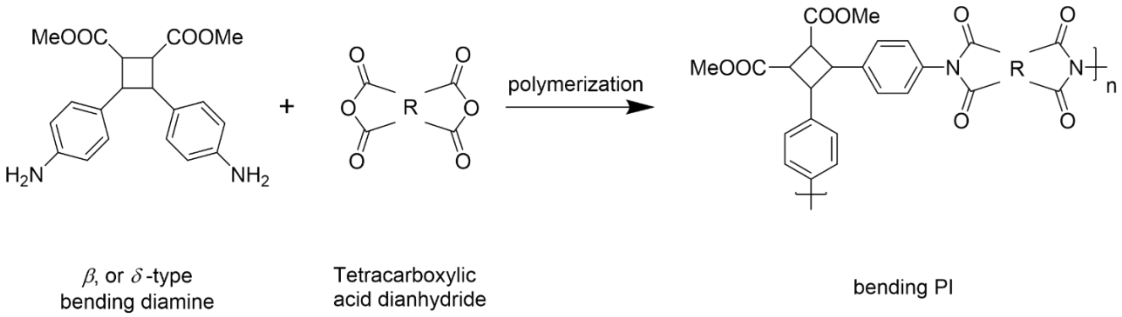

Scheme 4-1. Synthesis of Bending 4ACA Photodimer -Based Polyimides

4.2 Experimental Section

Materials. Hexane (>95.0%), toluene (>99.0%), chloroform (>99.0%), dichloromethane (>99.0%), tetrahydrofuran (THF, >99.5%), methanol (>99.8%), acetone (>99.0%), ethyl acetate (>99.5%), dimethyl sulfoxide (DMSO, >99.0%), *N*,*N*-dimethylformamide (DMF, >99.5%), *N*,*N*-dimethylacetamide (DMAc, >99.0%), sulfuric acid (96.0%), trifluoroacetic acid (>99.0%), acetic anhydride (>97.0%), and triethylamine (TEA, >99.0%) were purchased from Kanto Chemicals Co., Inc. 1,2,3,4-Cyclobutanetetracarboxylic dianhydride (CBDA, >98.0%), pyromellitic dianhydride (PMDA, >98.0%), 3,3′,4,4′-benzophenonetetracarboxylic dianhydride (BTDA, >96.0%), 4,4′-oxydiphthalic anhydride (ODPA, >98.0%), and 3,3′,4,4′-diphenylsulfonetetracarboxylic dianhydride (DSDA, >99.0%) were purchased from Tokyo Kasei Kogyo Co., Ltd. Calcium hydride (>80.0%), and 1-methyl-2-pyrrolidone (NMP, >99.0%) were purchased from FUJIFILM Wako Pure Chemical Corporation. Ethanol (95.2–95.4%) was purchased from Japan Alcohol Trading Co., Ltd. TEA and DMAc were distilled from CaH_2 prior to their use. Acetic anhydride was distilled from molecular sieve 4A prior to their use. CBDA, PMDA, BTDA, ODPA, and DSDA were sublimated prior to their use. The *β*- and *δ*-type 4-aminocinnamyl dimer-based diamine, *β*ATA-Me and *δ*ATA-Me, were synthesized by analogous to method described in chapter

3. All other chemicals were purchased from available suppliers and used without purification.

Characterization. The ^{1}H (400 MHz) and ^{13}C NMR (100 MHz) spectra were recorded on a Bruker AVANCE 400 instrument using DMSO-d_6 as the solvent. The Fourier transform infrared (FT-IR) spectra were recorded with a Perkin-Elmer Spectrum One spectrometer between 4000 and 500 cm^{-1} using a diamond-attenuated total reflection (ATR) accessory. Size exclusion chromatography (SEC) measurements of the obtained polyimides were performed at 40 °C using a JASCO GPC-101 system equipped with two Shodex OHpak SB-806M columns (linear, 8 mm × 300 mm) using 0.01 M LiBr in DMF at the flow rate of 1.0 mL min^{-1}. The number-average molecular weight (M_n) and dispersity (M_w/M_n) of the polymers were determined by the RI based on poly(methyl methacrylate) (PMMA) standards. Thermogravimetric analysis (TGA) and differential scanning calorimetry (DSC) were carried out on Hitachi High-Tech Corporation, STA7200 and Seiko Instruments SII, X-DSC7000T, respectively, at a heating rate of 10 °C min^{-1} under a nitrogen atmosphere. TGA and DSC measurements were carried out over the range of 25−800 °C, and 25−250 °C, respectively. The tensile measurements were carried out at an elongation speed of 0.5 mm min^{-1} on a tensiometer, the Instron 3365 with a load cell (5 kN), at room temperature. The ultraviolet−visible (UV−vis)

optical absorption spectra were recorded on a JASCO, V670 UV/vis spectrophotometer at room temperature over the range of 200−800 nm. The solubility of the polyimides was evaluated at room temperature in various polar (protic and aprotic) and nonpolar solvents and strong acids with a concentration 2 mg mL^{-1}.

Syntheses of Biobased Polyimides. A typical polymerization procedure is as follows. To a solution of *δ*ATA-Me (271 mg, 0.765 mmol) in DMAc (0.3 mL), CBDA (150 mg, 0.765 mmol) was added under argon atmosphere. The reaction mixture was stirred to dissolve the tetracarboxillic acid dianhydride, and then DMAc (1.00 mL), triethylamine (0.200 mL, 1.43 mmol), and acetic anhydride (0.300 mL, 3.17 mmol) were added. The reaction mixture was heated at 40 °C for 1 h and 100 °C for 10 min. After the heating, the solution was added dropwise into methanol to precipitate the polyimide. The formed precipitates were collected by filtration and thoroughly washed with methanol and then were dried at 200 °C under reduced pressure. The obtained polyimide was dissolved in small amount of DMAc then was cast onto a glass plate to obtain a polyimide film. The obtained film was heated stepwise at 100, 150, 200, and 250 °C for 1 h at each step to give a polyimide film. *δ*PI-1 (Yield, 350 mg, 65%). Other polyimides from *β*ATA-Me or *δ*ATA-Me and tetracarboxillic acid dianhydride such as CBDA, PMDA, BTDA, ODPA, and DSDA were synthesized following the above methods. Yield, *β*PI-1 (74%), *β*PI-2 (69%), *δ*PI-2 (86%),

*δ*PI-3 (83%), *δ*PI-4 (65%), *δ*PI-5 (60%). The obtained polyimides were purified several times by reprecipitation to remove low-molecular-weight fraction including triethylamine and acetic anhydride, resulting in low yields of polyimides.

4.3 Results and Discussion

4.3.1 Synthesis of Biobased Polyimides from *β*-Type and *δ*-Type Diamine Monomers

*β*ATA-Me- and *δ*ATA-Me-based biopolyimides (*β*PIs and *δ*PIs) were synthesized by a two-step chemical imidization reaction. First, the obtained *β*ATA-Me or *δ*ATA-Me was polycondensed with tetracarboxylic acid dianhydride (e.g., CBDA, PMDA, BTDA, ODPA, and DSDA), followed by the imidization of the precursor, poly(amic acid), which was conducted using triethylamine and acetic anhydride (Scheme 4-1). When CBDA and PMDA were used, *δ*ATA-Me-based polyimides with obtuse bending angles showed good solubility in DMAc along with an increase in the molecular weight during polymerization. Even though the *β*ATA-Me-based polyimides possessed smaller bending angles than *δ*ATA-Me-based polyimides, the polyimides were precipitated during the imidization process. Due to the high structural symmetry of *β*ATA-Me, intramolecular interactions were enhanced by π–π stacking of aromatic rings, resulting in a decrease in the solubility of *β*ATA-Me-based polyimides similar to the *β*-type diamine and dicarboxylic acid-based polyamide described in chapter 3. These results suggested that a diamine with an angle of 101°, similar to *δ*ATA-Me, has a suitable structure to provide solubility to the obtained polyimide, and a diamine of *β*ATA-Me bent at 70° is insufficient to produce a soluble polyimide owing to the narrow angle and

interaction. Hence, δATA-Me was used for further research on soluble biobased polyimides with other tetracarboxylic acid dianhydrides, BTDA, ODPA, and DSDA (Scheme 4-2).

Scheme 4-2. Synthetic Route of the δ-Type Dimer-Based Biopolyimides

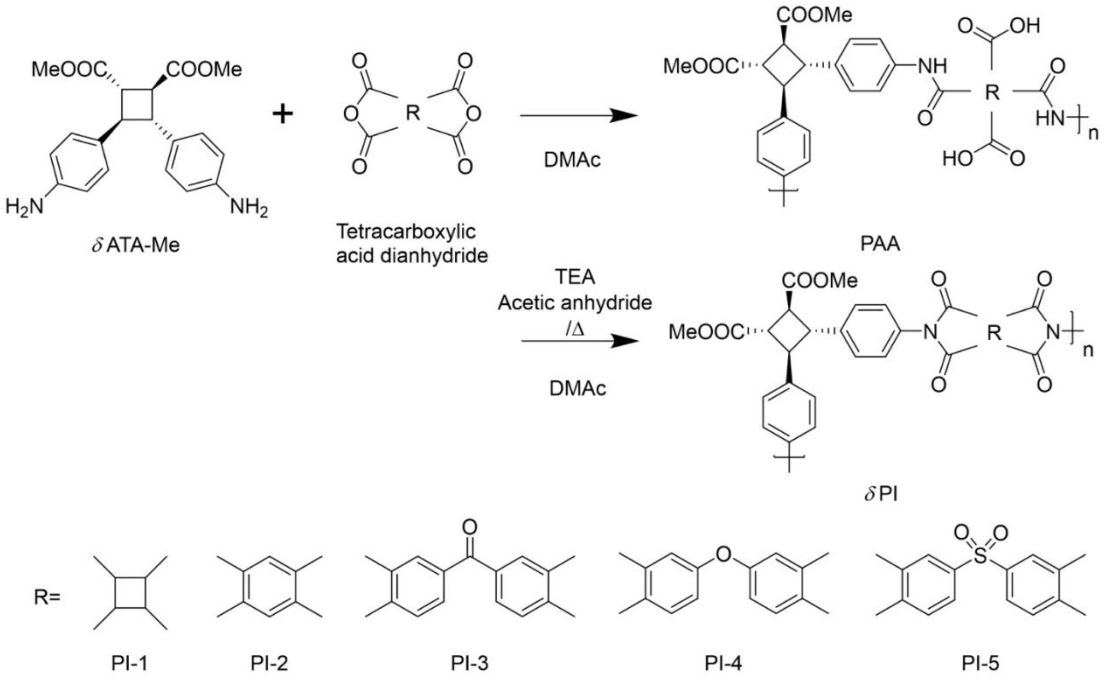

The FT-IR spectra of *δ*PI-1 showed two peaks assigned to the carbonyl group, 1364 cm^{-1} (C–N stretching) and 1776 cm^{-1} (C=O asymmetric stretching), which represented the characteristic peaks of the polyimides (Figure 4-1). The peaks at 1436 cm^{-1} and 1515 cm^{-1} were assigned to the C–C stretching of the aromatic rings due to the dianhydride and diamine moieties, respectively. In *δ*PI-4, a small peak at 1231 cm^{-1} was assigned to the C–O stretching of the ether bond. *δ*PI-5 showed peaks at 1149 cm^{-1} and 1322 cm^{-1}, which were assigned to the symmetric and asymmetric S=O stretching, respectively. Since the obtained *δ*PIs were dissolved in DMSO, ^{1}H NMR measurements of the polyimides were performed. The ^{1}H NMR spectrum of *δ*PI-1 showed the main chain proton signals for aromatics and cyclobutanes at ~7.6–7.3 ppm and 4.3–3.5 ppm, respectively (Figure 4-2). Moreover, the signals for amides and carboxylic acids were not detected, indicating that the imidization and dehydrocyclization reactions of poly(amic acid) proceeded at a high efficiency. The NMR and IR spectroscopy results clearly indicated that the expected *δ*PIs were synthesized.

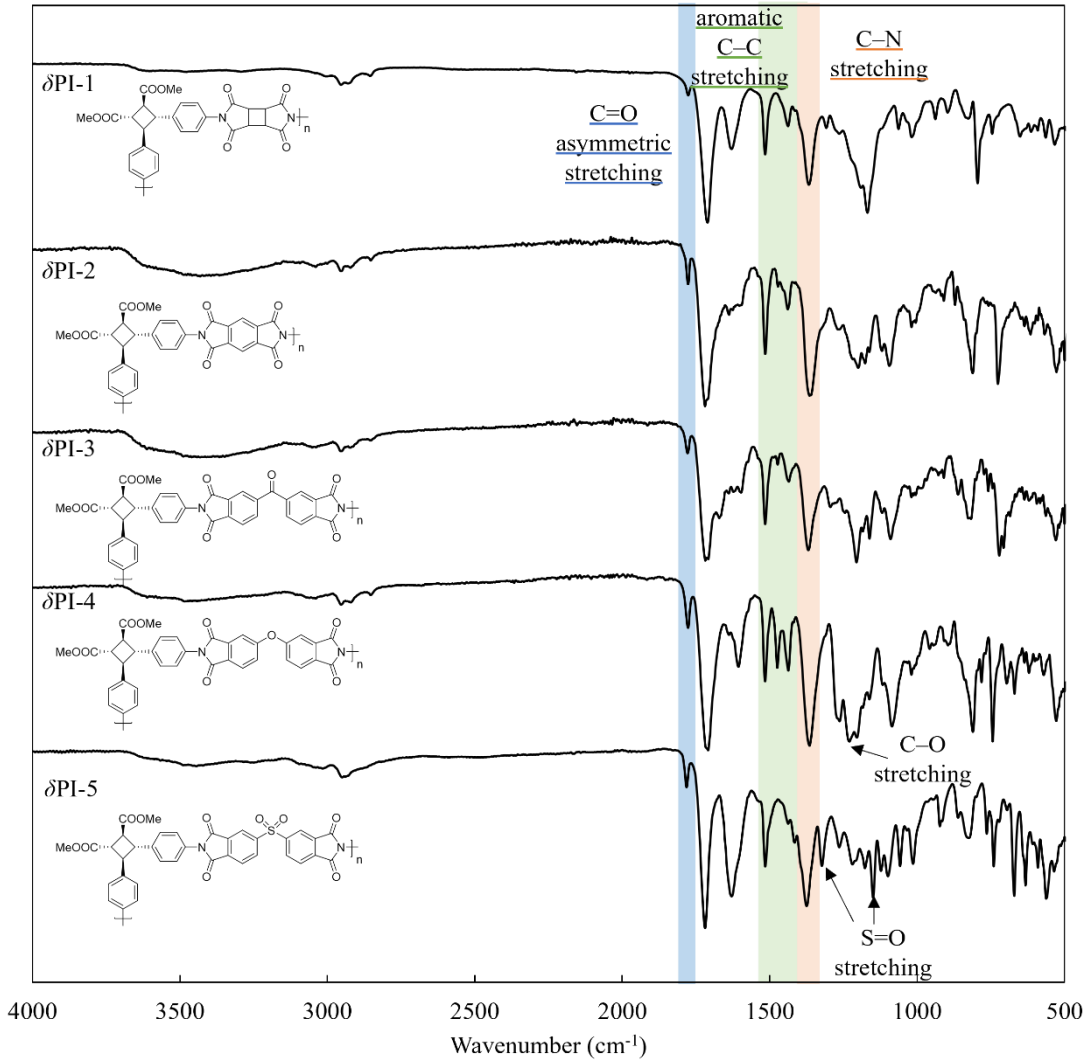

Figure 4-1. IR spectra of *δ*PIs.

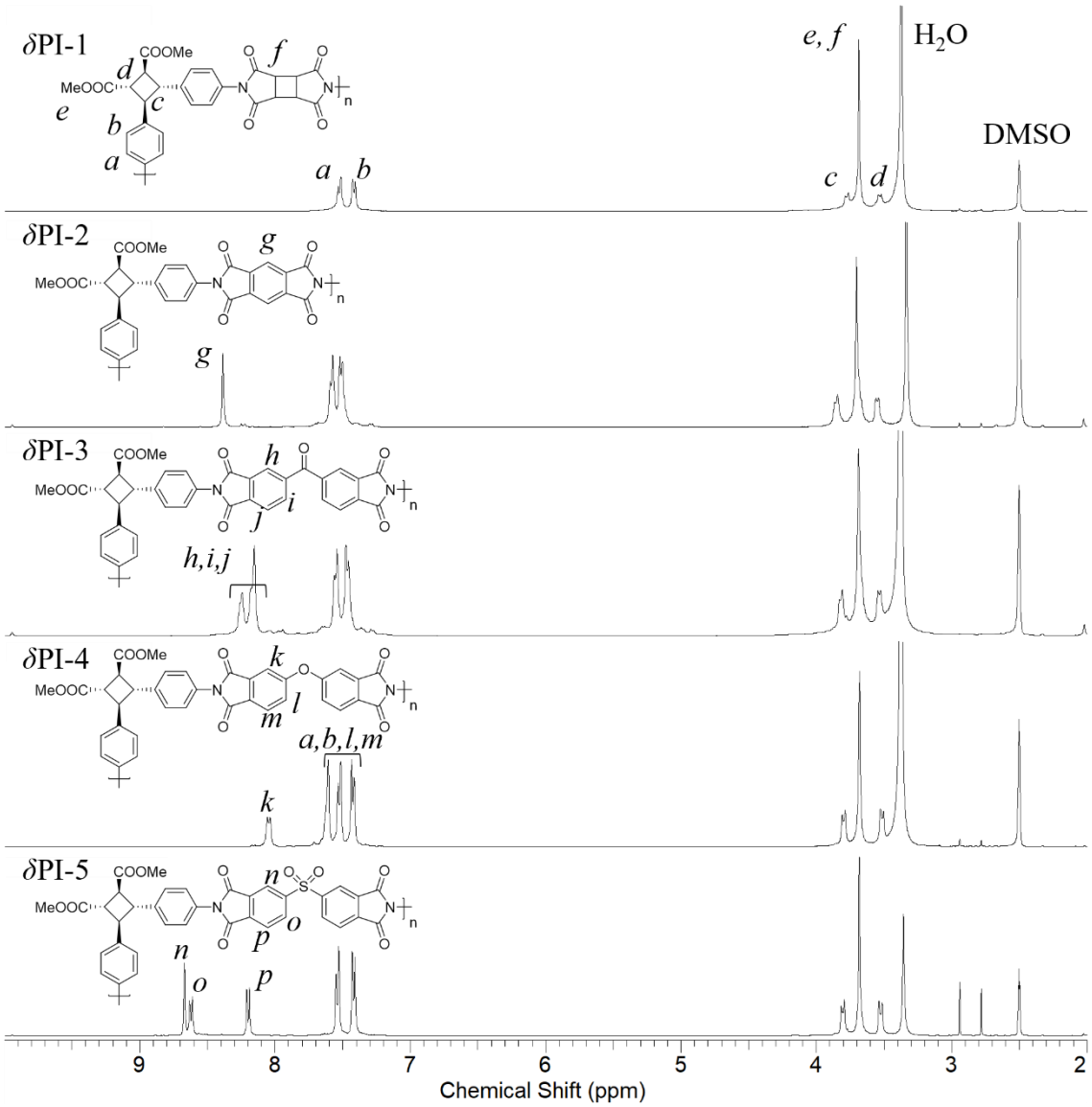

Figure 4-2. ^{1}H NMR spectra (400 MHz, DMSO-d_6) of δPIs.

The number-average molecular weight (M_n), weight-average molecular weight (M_w), and molecular weight distribution (M_w/M_n) of the *δ*PIs were determined by SEC measurements (Table 4-1, SEC traces are shown in Figure 4-3). In a previous study on *α*ATA-Me-based polyimides,[14] their molecular weights and M_w/M_n were difficult to be determined because of their insolubility in DMF. On the other hand, soluble *δ*PIs showed a monomodal distribution with M_ws ranging from 21000 to 72000 and M_w/M_n ranging from 4.20 to 6.74.

Table 4-1. Molecular weights of the synthesized polyimides[a]

polyimide (DA)	diamine	M_n	M_w	M_w/M_n
PI-1	*α*		no data	
(CBDA)	*δ*	10000	66000	6.18
PI-2	*α*		no data	
(PMDA)	*δ*	9600	65000	6.74
PI-3	*α*		no data	
(BTDA)	*δ*	13000	72000	5.69
PI-4	*α*		no data	
(ODPA)	*δ*	3000	21000	6.55
PI-5	*α*		no data	
(DSDA)	*δ*	5500	23000	4.20

[a]The weight-average molecular weight, M_w, the number-average molecular weight, M_n, and the molecular weight distribution, M_w/M_n, of polyimides were determined by SEC; eluent, 0.01 M LiBr in DMF; flow rate, 1.0 mL min^{-1}; standards, PMMA standards.

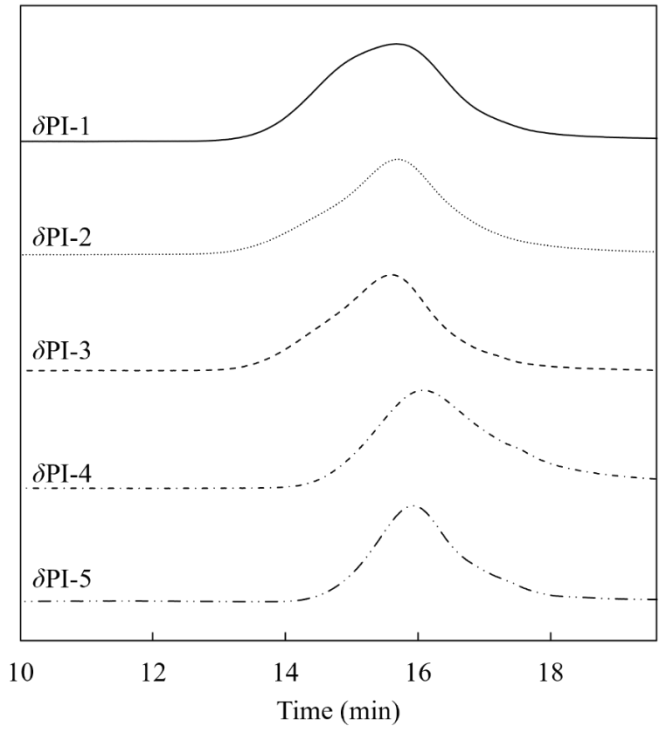

Figure 4-3. SEC traces of the *δ*PIs (solvent, 0.01 M LiBr in DMF; flow rate, 1.0 mL min^{-1}).

To evaluate the thermal stability, the weight loss temperature (5% weight loss temperature, T_{d5}, and 10% weight loss temperature, T_{d10}) and glass transition temperature (T_g) were determined by TGA (Figure 4-4) and DSC (Figure 4-5), respectively. From Table 4-2, the T_{d5} and T_{d10} values of all of the *δ*PIs ranged from 380 to 395 °C and from 400 to 415 °C, respectively, indicating that the *δ*PIs portrayed high stability against thermal decomposition. In particular, *δ*PI-3 exhibited the highest thermal stability at T_{d5} of 415 °C. In addition, all of the *δ*PIs exhibited similar or slightly lower weight loss temperatures than the *α*PIs, indicating that the *δ*PIs maintained a high resistance against thermal decomposition despite the introduction of a bending structure in the polymer backbone because these polyimides were composed of similar skeletons, cinnamoyl photodimer structures. The T_g of the *δ*PIs was above 230 °C, similar to that of the *α*PIs. Hence, the bending structure of the *δ*ATA moiety was considered to have negligible effects on enhancing the micro-Brownian motion of the polyimide chains because of the fixed bending angle, in contrast to conventional bending linkages, such as –O–, –S–, –CH_2–, S=O, and SO_2.

Table 4-2 Thermal properties of the synthesized polyimides

polyimide (DA)	diamine	T_{d5} (ºC)[a]	T_{d10} (ºC)[a]	T_g (ºC)[b]
PI-1	α	365	390	ND
(CBDA)	δ	380	400	ND
PI-2	α	410	425	ND
(PMDA)	δ	385	410	ND
PI-3	α	400	420	260
(BTDA)	δ	385	415	ND
PI-4	α	400	410	250
(ODPA)	δ	395	415	230
PI-5	α	410	425	275
(DSDA)	δ	380	405	ND

[a] 5% weight loss temperature, T_{d5}, and 10% weight loss temperature, T_{d10}, were obtained from TGA curve scanned at a heating rate of 10 °C min^{-1} under a nitrogen atmosphere.

[b] Glass transition temperature, T_g, was measured by DSC thermogram scanned at a heating rate of 10 °C min^{-1} under a nitrogen atmosphere. ND refers to not determined.

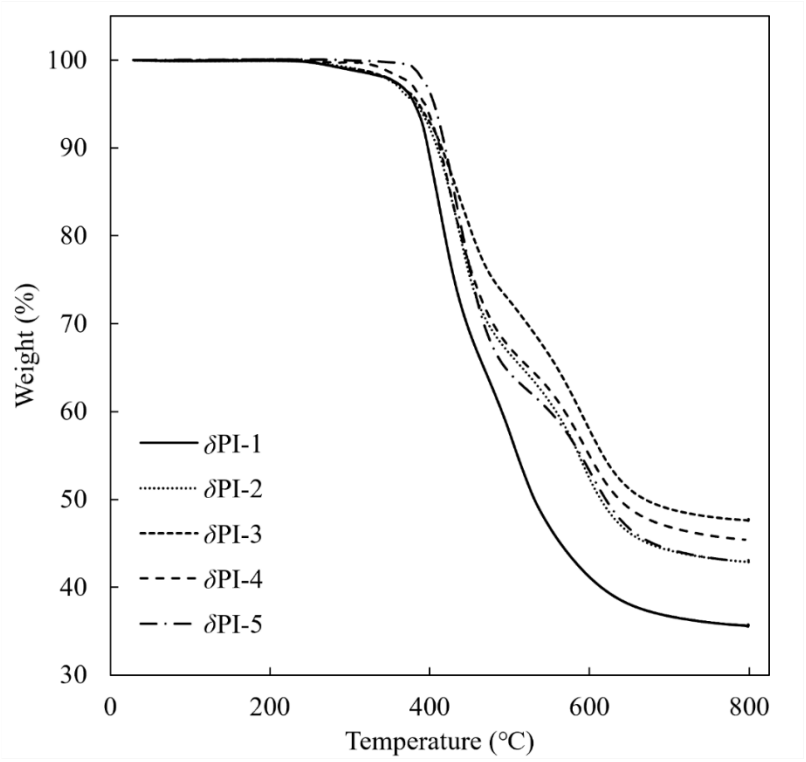

Figure 4-4. TGA curves of *δ*PIs.

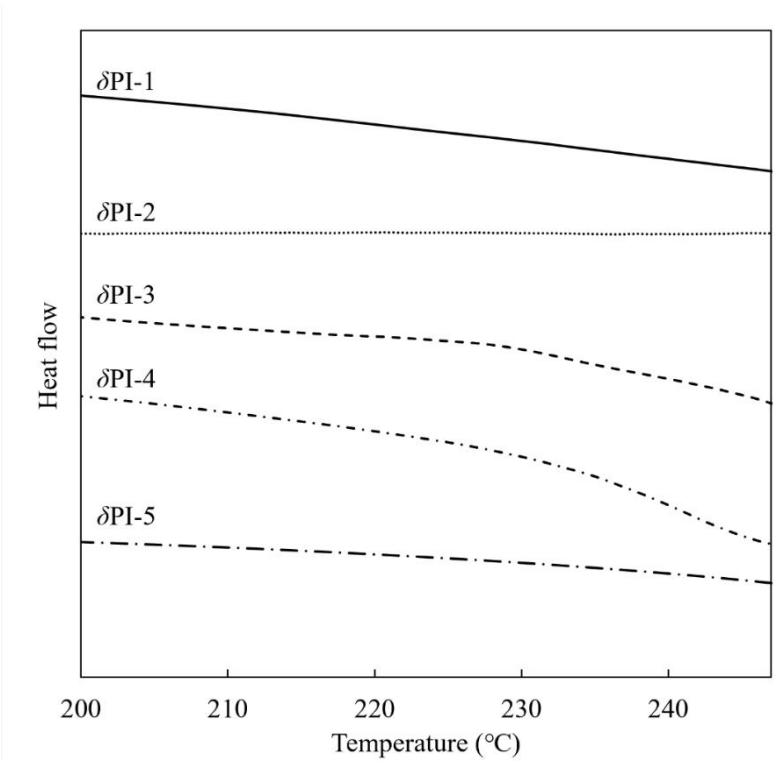

Figure 4-5. DSC curves of *δ*PIs.

4.3.2 Solubility Test of Bending Polyimides, *δ*PIs

The solubility of the *δ*PIs was further evaluated by dissolving them in four groups of solvents: (1) nonpolar solvents such as hexane and toluene; (2) polar aprotic solvents such as acetone, ethyl acetate, DMF, DMAc, NMP, DMSO, THF, dichloromethane, and chloroform; (3) polar protic solvents such as distilled water, methanol, and ethanol; and (4) strong acids such as trifluoroacetic acid and concentrated sulfuric acid (Table 4-3). Although all of the *α*PIs, which were synthesized from *α*ATA-Me with an almost straight structure, were only soluble in strong acids, the *δ*PIs were soluble in polar solvents, such as NMP, DMAc, DMF, DMSO, and strong acids, at 25 °C. In addition, all of the *δ*PIs, except for *δ*PI-1, were soluble in volatile solvents, such as dichloromethane and chloroform. Although *δ*PI-2 had a rigid dianhydride moiety, PMDA, it was also soluble in the above-mentioned solvents. The high solubility indicated that the bending structure of *δ*ATA improved the solubility of polyimides in a similar manner as bending tetracarboxylic acid dianhydrides,[15] as mentioned in previous literature. Furthermore, the racemic monomer of *δ*PI contributed to the increased solubility of the obtained *δ*PI because of the diastereomeric disordering of the polymer main chains.

Table 4-3. Solubility of the Synthesized Polyimides[a]

solvent	δPI-1	δPI-2	δPI-3	δPI-4	δPI-5	αPIs
n-hexane	−	−	−	−	−	−
toluene	−	−	−	−	−	−
dichloromethane	−	+	+	+	+	−
chloroform	−	+	+	+	+	−
water	−	−	−	−	−	−
methanol	−	−	−	−	−	−
ethanol	−	−	−	−	−	−
acetone	−	−	−	−	−	−
ethyl acetate	−	−	−	−	−	−
tetrahydrofuran	−	−	−	−	−	−
N,N-dimethylformamide	+	+	+	+	+	−
N,N-dimethylacetamide	+	+	+	+	+	−
N-methyl-2-pyrrolidone	+	+	+	+	+	−
dimethyl sulfoxide	+	+	+	+	+	−
trifluoroacetic acid	+	+	+	+	+	+
conc. sulfuric acid	+	+	+	+	+	+

[a] The solubility was evaluated under the condition of 2 mg-polyimide/1 mL-solvent at 25 °C. + refers to soluble, and − refers to insoluble.

4.3.3 Film Preparation of the *δ*PIs

Since the obtained *δ*PIs were soluble in some organic solvents, *δ*PI films were casted on glass plates after dissolution in DMAc (Figure 4-6). As a result, films for all of the *δ*PIs were fabricated, except for *δ*PI-5, which exhibited hard and brittle properties. Factors such as molecular weight and entanglement of the polymer chain are important in film preparation. As *δ*PI-1−3 exhibited a higher molecular weight than *δ*PI-5, these polyimides easily formed films. In addition, *δ*PI-4, with a molecular weight similar to that of *δ*PI-5, formed its film, suggesting that the flexible ether structure of *δ*PI-4 enhanced the entanglement of the polymer chain to support the film preparation.

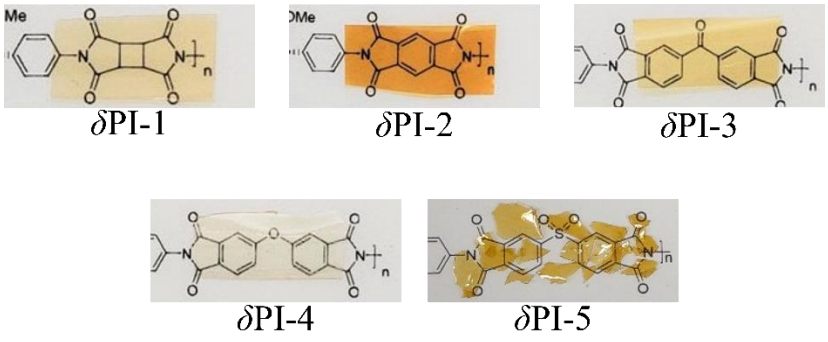

Figure 4-6. Appearance of *δ*PI films casted over DMAc in the polyimide state.

The mechanical properties of the *δ*PI films were evaluated by a tensile tester to determine their Young's modulus, tensile strength at break, and elongation at break (Table 4-4, stress−strain curves are shown in Figure 4-7). The Young's modulus of the *δ*PI films, in the range of 0.2–0.6 GPa, was lower than that of the *α*PIs films. The tensile strength of the *δ*PI films showed almost constant values, except for the *δ*PI-1 film synthesized from aliphatic tetracarboxylic acid dianhydride. The elongation at break of the *δ*PI films, in the range of 2.9–10.2%, was larger than that of the *α*PIs films. One important factor affecting mechanical properties is the interaction of the polymer chains. Since the *α*PIs have almost straight structures, they are strongly influenced by intermolecular interactions. The strong interactions caused by the aromatic rings derived from diamines and tetracarboxylic acid dianhydride moieties make the film hard and brittle. Furthermore, because of the almost straight structure of the *α*PIs, they are less likely to be influenced by the difference in the tetracarboxylic acid dianhydride moieties, resulting in the insignificant difference in the physical properties (Figure 4-8a). However, as the bending *δ*PI is composed of a bending diamine and linear tetracarboxylic acid dianhydride units that are mixed, its mechanical properties depend on the structure of the tetracarboxylic acid dianhydrides, particularly the presence or absence of an aromatic ring (Figure 4-8b).

Table 4-4. Mechanical and optical properties of the synthesized polyimide films[a]

polyimide (DA)	diamine	Young's modulus[b] (GPa)	tensile strength[b] (MPa)	elongation at break[b] (%)	T_{450}[c] (%)	λ_0[c] (nm)
PI-1	α	10 ± 3.7	75 ± 6.6	1.8 ± 0.3	88	270
(CBDA)	δ	0.4 ± 0.2	31 ± 5.4	10.2 ± 3.4	76	284
PI-2	α	8.0 ± 1.2	89 ± 9.2	2.5 ± 0.1	80	357
(PMDA)	δ	0.6 ± 0.1	15 ± 2.9	2.9 ± 0.3	6	424
PI-3	α	4.2 ± 0.2	48 ± 0.8	1.7 ± 0.3	79	326
(BTDA)	δ	0.5 ± 0.2	22 ± 1.4	5.8 ± 1.3	52	379
PI-4	α	13.4 ± 3.0	98 ± 5.7	4.5 ± 0.5	69	363
(ODPA)	δ	0.2 ± 0.1	16 ± 2.7	8.9 ± 0.4	73	378

[a] Thickness of αPIs and δPIs films was 12±3 and 19±3 μm, respectively. [b] Young's modulus, tensile strength, and elongation at break were obtained from a tensiometer at room temperature. [c] UV cutoff wavelength, λ_0, and transmittance at 450 nm, T_{450}, were measured by UV−vis spectrophotometer.

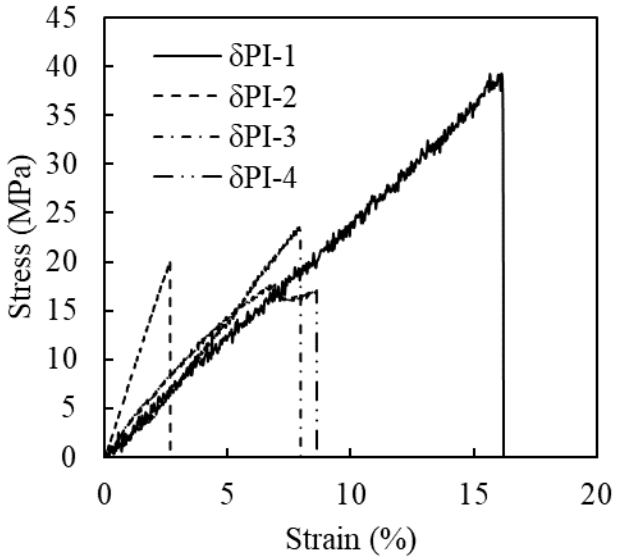

Figure 4-7. Stress-strain curves of *δ*PIs.

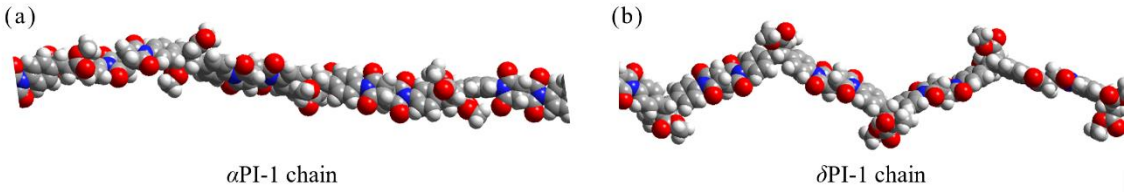

Figure 4-8. Molecular structures of the 4-aminocinnamate photodimer-based polyimides: (a) *α*PI-1 and (b) *δ*PI-1.

To support the above hypothesis, the optical transparency at 450 nm (T_{450}) and the cutoff wavelengths (λ_0) were measured by UV−Vis spectroscopy (Table 4-4, UV−Vis absorption spectra are shown in Figure 4-9). The *δ*PI films, except for *δ*PI-2, showed yellow appearances, and the T_{450} values ranged from 6 to 76%. The *α*PI in a previous work showed a lower difference in transmittance, ranging from 69 to 88%, which was attributed to the dianhydride monomers. *δ*PI-2 exhibited a transmittance of 6% because

the interaction between the PMDA units, as described above, was strongly affected, and the charge-transfer effect was observed. The difference in the yellowness between the *α*PI and the *δ*PI was derived from each monomer color; *δ*ATA-Me showed a paler red appearance compared to *α*ATA-Me. The above evaluations of the obtained PIs showed that the bending structure of the *δ*ATA-Me unit strongly affected the obtained *δ*PI. In addition, the mechanical and optical properties of the obtained *δ*PI could be modified by changing the counter dianhydride monomers.

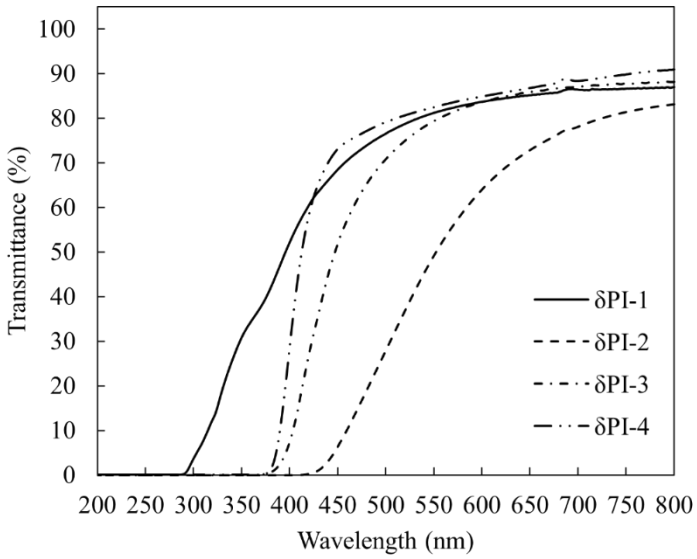

Figure 4-9. UV−Vis absorption spectra of *δ*PIs.

4.4 Conclusions

Two types of isomeric 4-aminocinnamoyl photodimer-based diamines with bending structures were polymerized with tetracarboxylic acid dianhydrides for the synthesis of soluble biobased polyimides. By chemical imidization of the *δ*-type photodimer, the *δ*PIs showed solubility in organic solvents, such as NMP, DMAc, DMF, DMSO, and strong acids. All of the *δ*PIs, except for *δ*PI-1, were soluble in dichloromethane and chloroform, in addition to the above-mentioned organic solvents. In addition, all of the *δ*PIs showed high heat resistance, with T_{d10} of ~400 °C, similar to that of the previously reported *α*PIs, which also possessed almost straight main chain structures. Furthermore, several *δ*PIs were formed into films by solution casting, taking advantage of their good solubility in organic solvents. In addition, the obtained *δ*PIs, except for *δ*PI-1, showed brittle properties, indicating that the structural properties of tetracarboxylic acid dianhydride moieties were strongly affected by the obtained polyimides. In the present study, polyimides that bear a single-component, high flexibility, and good solubility, were prepared. These properties can only be realized by truxinic acid derived from biobased cinnamic acid, which is an essential component of this study. This research provides insights into the molecular design of high-performance soluble polymers by focusing on the bending angles of the polymer chains.

4.5 References and Notes

(1) Stieglitz, T.; Beutel, H.; Schuettler, M.; Meyer, J. U. Micromachined, Polyimide-Based Devices for Flexible Neural Interfaces. *Biomed. Microdevices* **2000**, *2* (4), 283–294. https://doi.org/10.1023/A:1009955222114.

(2) Rousche, P. J.; Pellinen, D. S.; Pivin, D. P.; Williams, J. C.; Vetter, R. J.; Kipke, D. R. Flexible Polyimide-Based Intracortical Electrode Arrays with Bioactive Capability. *IEEE Trans. Biomed. Eng.* **2001**, *48* (3), 361–370. https://doi.org/10.1109/10.914800.

(3) Liaw, D. J.; Wang, K. L.; Huang, Y. C.; Lee, K. R.; Lai, J. Y.; Ha, C. S. Advanced Polyimide Materials: Syntheses, Physical Properties and Applications. *Prog. Polym. Sci.* **2012**, *37* (7), 907–974. https://doi.org/10.1016/j.progpolymsci.2012.02.005.

(4) Su, H. W.; Chen, W. C. High Refractive Index Polyimide-Nanocrystalline-Titania Hybrid Optical Materials. *J. Mater. Chem.* **2008**, *18* (10), 1139–1145. https://doi.org/10.1039/b717069f.

(5) Gouzman, I.; Grossman, E.; Verker, R.; Atar, N.; Bolker, A.; Eliaz, N. Advances in Polyimide-Based Materials for Space Applications. *Adv. Mater.* **2019**, *31* (18), 1–15. https://doi.org/10.1002/adma.201807738.

(6) Dhara, M. G.; Banerjee, S. Fluorinated High-Performance Polymers: Poly(Arylene Ether)s and Aromatic Polyimides Containing Trifluoromethyl Groups. *Prog. Polym. Sci.* **2010**, *35* (8), 1022–1077. https://doi.org/10.1016/j.progpolymsci.2010.04.003.

(7) Liaw, D.-J.; Chang, F.-C.; Leung, M.; Chou, M.; Muellen, K. High Thermal Stability and Rigid Rod of Novel Organosoluble Polyimides and Polyamides Based on Bulky and Noncoplanar Naphthalene−Biphenyldiamine. *Macromolecules* **2005**, *38* (9), 4024–4029. https://doi.org/10.1021/ma048559x.

(8) Liaw, D. J.; Liaw, B. Y.; Yu, C. W. Synthesis and Characterization of New Organosoluble Polyimides Based on Flexible Diamine. *Polymer (Guildf).* **2001**, *42* (12), 5175–5179. https://doi.org/10.1016/S0032-3861(00)00822-3.

(9) Kaya, İ.; Kamacı, M. Synthesis, Optical, and Thermal Properties of Polyimides Containing Flexible Ether Linkage. *J. Appl. Polym. Sci.* **2018**, *135* (31), 1–8. https://doi.org/10.1002/app.46573.

(10) Mi, Z.; Wang, S.; Hou, Z.; Liu, Z.; Jin, S.; Wang, X.; Wang, D.; Zhao, X.; Zhang, Y.; Zhou, H.; Chen, C. Soluble Polyimides Bearing (Cis, Trans)-Hydrogenated Bisphenol A and (Trans, Trans)-Hydrogenated Bisphenol A Moieties: Synthesis, Properties and the Conformational Effect. *Polymers (Basel).*

2019, *11* (5), 854. https://doi.org/10.3390/polym11050854.

(11) Fang, X.; Yang, Z.; Zhang, S.; Gao, L.; Ding, M. Polyimides Derived from Mellophanic Dianhydride. *Macromolecules* **2002**, *35* (23), 8708–8717. https://doi.org/10.1021/ma0204610.

(12) Ding, M. Isomeric Polyimides. *Prog. Polym. Sci.* **2007**, *32* (6), 623–668. https://doi.org/10.1016/j.progpolymsci.2007.01.007.

(13) Hsiao, S. H.; Chen, Y. J. Structure-Property Study of Polyimides Derived from PMDA and BPDA Dianhydrides with Structurally Different Diamines. *Eur. Polym. J.* **2002**, *38* (4), 815–828. https://doi.org/10.1016/S0014-3057(01)00229-4.

(14) Suvannasara, P.; Tateyama, S.; Miyasato, A.; Matsumura, K.; Shimoda, T.; Ito, T.; Yamagata, Y.; Fujita, T.; Takaya, N.; Kaneko, T. Biobased Polyimides from 4-Aminocinnamic Acid Photodimer. *Macromolecules* **2014**, *47* (5), 1586–1593. https://doi.org/10.1021/ma402499m.

(15) Dwivedi, S.; Kaneko, T. Molecular Design of Soluble Biopolyimide with High Rigidity. *Polymers (Basel).* **2018**, *10* (4), 1–8. https://doi.org/10.3390/polym10040368.

(16) Dwivedi, S.; Nag, A.; Sakamoto, S.; Funahashi, Y.; Harimoto, T.; Takada, K.;

Kaneko, T. High-Temperature Resistant Water-Soluble Polymers Derived from Exotic Amino Acids. *RSC Adv.* **2020**, *10* (62), 38069–38074. https://doi.org/10.1039/d0ra06620f.

Chapter 5

Conclusions

Chapter 5

Conclusions

Cinnamoyl photodimers have useful structural characteristics for high-performance and/or functional polymers such as rigid structure, unique bending angles, chirality, and photodegradable cyclobutane. In this thesis, the author describes effects of cinnamoyl dimer unit in polymer backbone on physicochemical properties of polymers through development of high-performance and/or functional polymers from unique cinnamoyl dimers.

A summary of this thesis is as follows:

Chapter 2 "Syntheses of Photodegradable Adhesive Polyamides from 3,4-Dihydroxycinnamoyl Dimer"

3,4-Dihydroxycinnamoyl dimer was synthesized from methyl 3,4-dihydroxycinnamate by solid-state photodimerization and further chemical modification. The obtained dimer was used as dicarboxylic acid monomer for the syntheses of adhesive polyamides. The obtained polyamides exhibited high thermal stability with 10% weight loss temperature of ~355 °C and strong adhesive property of ~7 MPa based on the rigid cinnamoyl dimer skeleton and adhesive catechol groups in the side chain, respectively. In addition, the cyclobutanes in polymer backbone were cleaved by ultraviolet light

irradiation. The results described in this chapter provides insights into the molecular design of eco-friendly, high-performance adhesive materials with photodegradability.

Chapter 3 "Syntheses and Polymerizability of Isomeric 4-Aminocinnamoyl Dimers with Different Bending Angles"

Isomeric 4-aminocinnamoyl dimers with different bending angles, *β*- and *δ*-type truxinic acids, were selectively synthesized from functionalized 4-nitrocinnamic acid derivatives by solid-state photodimerization. Density functional theory (DFT) calculations revealed that the *β*- and *δ*-type photodimers possessed unique bending angles of 70° and 101°, respectively. The obtained dimers were modified to diamine and dicarboxylic acid monomers then was used for synthesis of polyamides. Although *β*-type monomer possessed acute bending angle of 70°, *β*-type-based polyamides with high molecular weight of M_w>10000 were synthesized. In addition, the obtained polyamides exhibited a high thermostability based on the rigid cinnamoyl dimer skeleton at 10% weight loss temperature of ~360 °C. The results described in this chapter showed demonstration for the selective synthesis and polymerization of cinnamyl dimer-based monomers with unique bending angles based on the spatial arrangement around

cyclobutane ring. Building blocks with such unique angles have not been reported yet.

Chapter 4 "Soluble Biobased Polyimides from Diaminotruxinic Acid with Unique Bending Angles"

The *β*- and *δ*-type diamines with unique bending angles, which were synthesized in chapter 3, were polymerized with tetracarboxylic acid dianhydrides to produce soluble polyimides via chemical imidization. The obtained δ-type-based polyimides exhibited a high thermostability at 10% weight loss temperature of ~415 °C and good solubility in organic solvents. Most of the *δ*-type-based polyimides were soluble in chloroform and dichloromethane, as well as polar organic solvents. Tensile test results showed that biopolyimide films from cyclobutanetetracarboxylic dianhydride exhibited ~10.2% elongation at break, indicating high flexibility. In this chapter, effects of unique bending angles on solubility and thermal/mechanical properties of polyimides were investigated. As a result, the diamine with an angle of 101°, similar to *δ*ATA-Me, has a suitable structure to provide solubility to the obtained polyimides. This result provides insights into the molecular design of high-performance soluble polymers by focusing on the bending angles of the polymer chains.

Chapter 5

Conclusions

Thus, the author revealed the methodology for the synthesis of high-performance and/or functional polymers focused on cinnamoyl dimer skeleton, particularly cyclobutane rings in polymer backbone. Importantly, since the cyclobutane ring is easily obtained by [2+2] cycloaddition of olefins, these molecular design for high-performance/functional polymers are not only limited to cinnamoyl dimer-based polymers, but also other synthetic polymers bearing cyclobutane components. The author expects that these unique functions of cyclobutane ring will attract much interest by not only polymer scientists, but also the researchers in different fields.

Academic achievements

Publications:

1) Noda, T.; Iwasaki, T.; Takada, K.; Kaneko, T. Soluble Biobased Polyimides from Diaminotruxinic Acid with Unique Bending Angles. *Macromolecules* **2021**, *54* (22), 10271–10278. https://doi.org/10.1021/acs.macromol.1c01273.

2) Takada, K.; Noda, T.; Kobayashi, T.; Harimoto, T.; Singh, M.; Kaneko, T. Synthesis of PH-Responsive Polyimide Hydrogel from Bioderived Amino Acid. *Polym. J.* **2021**, *53* (11), 1223–1230. https://doi.org/10.1038/s41428-021-00509-8.

3) Yusof, F. A. A.; Noda, T.; Takada, K.; Kaneko, T.; Kawai, M.; Mitsumata, T. Critical Electric Field and Activation Energy for Electric Conductivity for Biopolyimide Using 4,4′-Diamino-α-Truxillic Acid and 1,2,3,4-Cyclobutanetetracarboxylic Dianhydride. *Chem. Lett.* **2020**, *49* (8), 929–931. https://doi.org/10.1246/cl.200232.

Patent:

1) 高田健司，野田拓海，佐藤拓実，金子達雄．ポリアミド系ポリマー．特願2021-132518.

Conferences:

1) Takumi Noda, Takuma Iwasaki, Kenji Takada, Tatsuo Kaneko “Structure-property relationships of biopolyimides from 4-aminocinnamate photodimers with unique bending structure”, *Pacifichem 2021*, 3450278 (Oral).

2) Takumi Noda, Takuma Iwasaki, Kenji Takada, Tatsuo Kaneko “Syntheses of Soluble Bio-based Polyimides from Bending-shaped Racemic 4-Aminocinnamate Photodimers” dimers” *JAIST World Conference 2020 (JWC2020) & The 7th International Symposium for Green-Innovation Polymers (GRIP2020)*,P07 (Poster).

3) Takumi Noda, Takuma Iwasaki, Kenji Takada, Tatsuo Kaneko “Syntheses of 4-Aminocinnamate Photodimer -based Soluble Biopolyimides with Unique Bending Angles” *The 48th World Polymer Congress IUPAC-MACRO2020+*, SS8-46 (Online).

4) Takumi Noda, Takuma Iwasaki, Kenji Takada, Tatsuo Kaneko “Evaluation of Structure-Property Relationships of Cinnamoyl-photodimer-based Biopolyamides Having Unique Bending Angles in Backbone” *The 7th International Conference on Bio-Based Polymer*, MFHP-O06 (Oral).

5) Takumi Noda, Kenji Takada, Amit Kumar, Tatsuo Kaneko “Synthesis of Biopolyamides from 4-Aminocinnamoyl Photodimers with Different Bending Angles”

15th IUPAC International Conference on Novel Materials and their Synthesis (NMS-XV), P4, (Poster).

6) 野田拓海, 高田健司, 金子達雄 “4,4'-ジアミノトルキシン酸をベースとした屈曲角の異なるポリアミドの合成と物性評価”, *第 68 回高分子討論会*, 2S02, (Oral).

7) Takumi Noda, Kenji Takada, Amit Kumar, Tatsuo Kaneko “Biopolyamides of cinnamoyl photodimer derivatives with abnormal bending angles” *ASIA PACIFIC SOCIETY for MATERIALS RESEARCH Annual Meeting 2019*, P20 (Poster).

8) 野田拓海, 高田健司, 金子達雄 “4,4’-ジアミノトルキシン酸誘導体を用いたバイオポリアミドの合成と物性評価”, *第68 回高分子年次大会*, 2J11 (Oral).

Awards:

1) “Best Presentation award of JWC2020 & GRIP2020”, Poster award selection committee＆JWC 2020 chair, November 2020.
2) “Award Letter to Excellent Poster Prize”, 15th IUPAC International Conference on Novel Materials and their Synthesis (NMS-XV), September 2019.